THE PROPAGATION OF SUNLIGHT AND THE SIZE DISTRIBUTION OF SUSPENDED PARTICLES IN A MUNICIPALLY POLLUTED OCEAN WATER

Thesis by

Lee Louis Peterson

In Partial Fulfillment of the Requirements

for the Degree of

Doctor of Philosophy

California Institute of Technology

Pasadena, California

1974

(Submitted January 15, 1974)

TO BLAINE

ACKNOWLEDGMENTS

This study was performed under the direction and inspiration of Professor Wheeler North. He taught me to work in the ocean, monitored my research and provided crucial guidance in writing my thesis.

Timely criticism and technical advice from Professor Sheldon Friedlander is deeply appreciated. His support and encouragement during my years at Caltech provided incentive for successful completion of my work.

Professor James Morgan reviewed my research and suggested valuable improvements in presentation of the results. I am especially grateful for his interest and participation in student life.

Professor Bruce Murray patiently served on all of my examining committees. Professor Norman Brooks encouraged my work and progress.

Professor Seibert Duntley, from the Scripps Institution of Oceanography, graciously consented to participate in the final dissertation exam.

A computer program for calculating the propagation of sunlight in ocean water was written by Dr. Warren White. Ed Myers filtered and analyzed suspended ocean particulates for carbon isotope ratios and percent organic carbon. A computer program, written by Arthur Jensen, was used to

calculate statistical parameters. Joe Devinny, Peter Kirkwood, and Ed Myers at times arranged their schedules so that their work and mine could be performed on the same field trip. Steve Heisler and George Jackson provided helpful criticism and comment.

Elton Daly and Tom Stephan were responsible for the very difficult task of maintaining the boats and other marine equipment.

I am grateful to Bob Douglas and Gerald Johnson of TRW Systems, Redondo Beach,for their hospitality in offering the use of their laboratory, Coulter Counter, transmissometer, and water sampling equipment.

It has been a privilege to be one of Marjorie Connely's "boys". A heartfelt thanks for her expert typing of the text and figures of my thesis.

Kind assistance was received from Angela Bressan in the Registrar's Office, Rod Casper in the Library, and Ruth Toy in the Graduate Office.

Whit and Judy Howland were especially kind and helpful through difficult times. Andrea Muir, a very lovely lady, provided many helpful suggestions regarding style and content of the thesis. Constant support and encouragement were received from my parents, Louis and Marie, during all of my years at Caltech.

The research and the student's livelihood were supported by grants from the United States Public Health Service and TRW Systems.

ABSTRACT

Waste discharge by the Los Angeles County Sanitation District (LACSD) affects sunlight in the ocean. Increased sunlight attenuance affects productivity and changes in ocean surface color could be useful for monitoring dispersal.

Temperature, sunlight irradiance in five colors, light beam attenuance, and particle size distributions were simultaneously measured as a function of water depth. A limited number of samples were analyzed by a co-worker for particulate percent organic carbon and particulate carbon isotope ratio. Background field stations included Catalina, Dana Point, and Rocky Point. Stations in the vicinity of the LACSD outfall at Whites Point represented a dispersing sewage field. The most significant result was that pollutants decreased the optical albedo of ocean water, increasing the extinction of sunlight irradiance as a function of optical depth.

Additional findings were that 1) pollutants decreased euphotic zone depths by as much as 60 percent (depending upon particle concentrations), 2) water surface color spectra indicated that pollutants increased light absorption at short wavelengths (violet, blue and green), 3) the average particle concentration in polluted waters was twice that of background waters, 4) the LACSD discharge caused a bimodal increase in

particle numbers as a function of particle size: there was a dramatic increase for particles less than 1.5 microns and a secondary increase at 8 microns, 5) assuming real particle refractive indices (no light absorption by particles), scattering by natural and sewage particles was maximum between particle diameters 3 and 8 microns, 6) calculations assuming complex refractive indices (absorbing particles) indicated that light absorption by sewage particles was maximum for particles less than 1.5 microns in diameter, and 7) heavy (high specific gravity) particles had lower percent organic carbon and a lower carbon isotope ratio.

TABLE OF CONTENTS

LIST OF FIGURES

LIST OF FIGURES (continued)

LIST OF FIGURES (continued)

LIST OF FIGURES (continued)

LIST OF FIGURES (continued)

LIST OF FIGURES (continued)

LIST OF FIGURES (continued)

LIST OF TABLES

LIST OF TABLES

CHAPTER 1

INTRODUCTION

One billion gallons of sewage per day are discharged into Southern California waters. Significantly altered chemical and biological conditions have been demonstrated (42). In particular, a significant decrease in the number and variety of marine plants has been reported (1, 20, 32 42).

Basic factors affecting the survivability and growth of marine plants are nutrients, tolerable temperatures, and sufficient sunlight. It has been suggested that increased turbidity in the vicinity of sewage outfalls decreases the amount of sunlight for photosynthesis (1). This study quantitatively examines the relationship between discharged sewage particulates and sunlight attenuation in coastal ocean water.

The study was conducted at selected stations near the Los Angeles County Sanitation Districts (LACSD) sewer outfall at Whites Point, Palos Verdes. Other stations in relatively natural areas represented background conditions.

About one third of Southern California's ocean discharge is managed by the LACSD facility (370 million gallons per day in 1971). Treatment is primary (settleable and floatable solids are removed in retention tanks). About 300 ppm of particulate matter remain in suspension. This

amounts to a suspended solids discharge rate of 500 tons per day at Whites Point. This rate is comparable to natural coastal transport of sediments in some areas (42).

The majority of the material is transported through two large pipes (90 and 120 inches in diameter) to diffuser sections (lengths of pipe with discharge ports along the vertical portion of the pipe wall). The diffusers lie on the sea floor at water depths ranging between 165 and 195 feet. During most of the year, the ocean is thermally stratified. Surface waters are often 3 to 5^{o}C warmer than sea floor temperatures. This retards vertical mixing and prevents the discharged wastes from reaching the ocean surface.

During the winter months, however, the surface waters cool off and winter swells increase vertical mixing. At times the thermal stratification is too weak to prevent the buoyant (warmer) sewage effluents from reaching the surface. Driven by winds or currents, the polluted waters are then able to reach the shoreline (Figure 1-1). Several miles of coastline can be affected. The polluted water does not always reach the shore. Wind driven surface currents may transport the sewage field seaward (Figure 1-2).

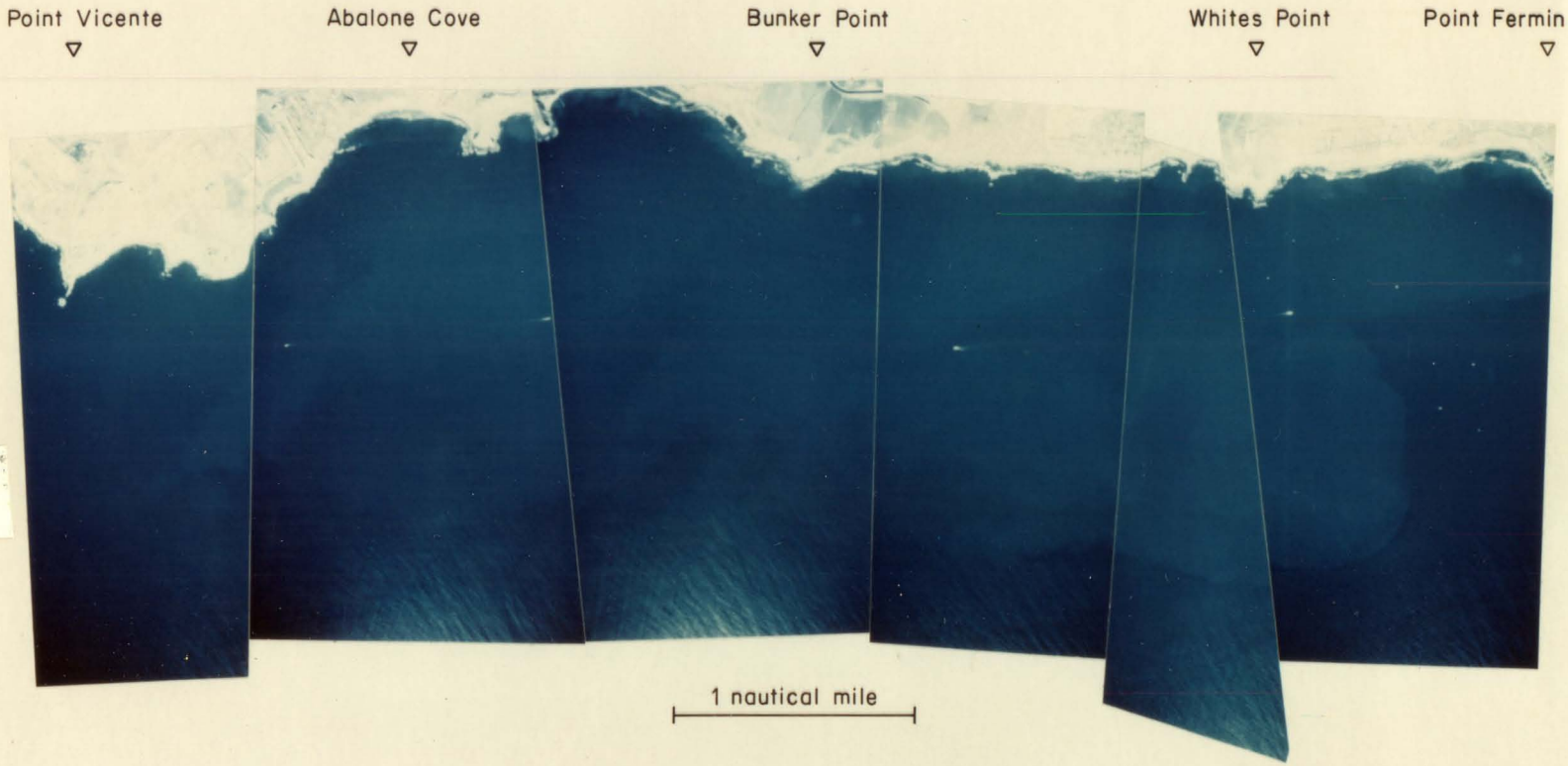

Figure I-1. Photo-mosaic of sewage field from the Los Angeles County outfall. Alongshore drift. Infrared color by Wheeler North. December 30, 1972

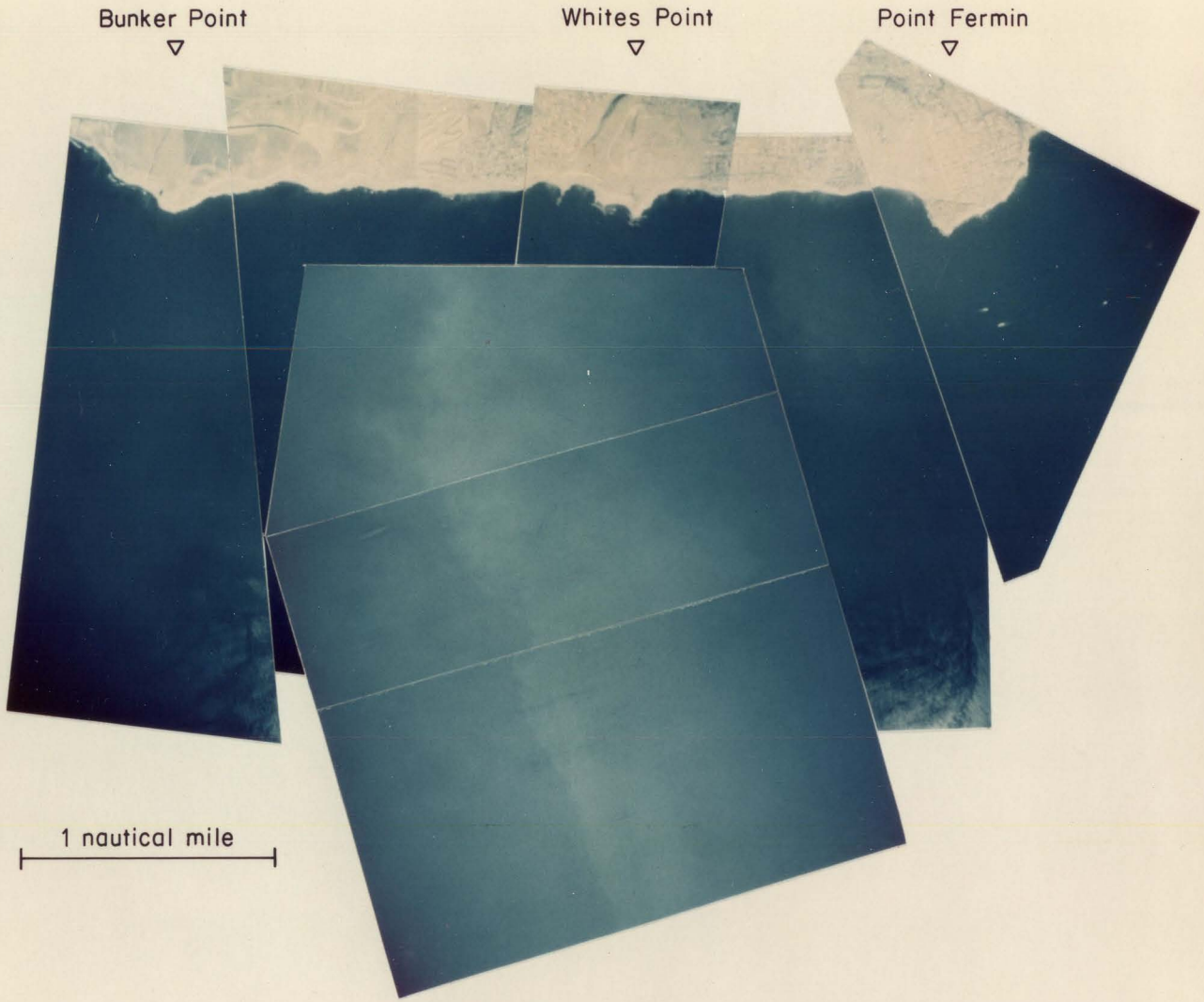

Figure I-2. Photo-mosaic of sewage field from the Los Angeles County outfall. Seaward drift. Infrared color by Wheeler North. January 6, 1973

Sewage discharge began in 1934 at the rate of 17 million gallons per day (MGD). Prior to that time aerial photographs show that large beds of kelp (Macrocystis) were growing along the Palos Verdes Peninsula (Figure 1-3). This plant, harvested for chemicals, animal foods, and fertilizer, is commercially valuable. It is also an important habitat for fishes and shellfish.

Between the years 1934 and 1958, the sewage discharge rate tripled each decade. Disappearance of the beds began around 1940 and continued steadily until 1955 when all of the major beds near the outfall had disappeared. During that year the sewage discharge rate was half of that reported in 1971.

Deterioration of plant communities near sewer outfalls has been attributed to various causes. Grigg and Kiwala (20) suggested that sedimentation upon normally rocky surfaces prevents settling by microscopic planktonic larvae. North (1) has demonstrated large populations of grazing sea urchins in the vicinity of destroyed kelp plants. It has been hypothesized that dissolved organics near the LACSD outfall are utilized by absorption through the sea urchin dermis, resulting in large urchin populations (42). Deterioration of the Point Loma kelp bed near San Diego was halted and reversed after urchin populations were brought under control (42).

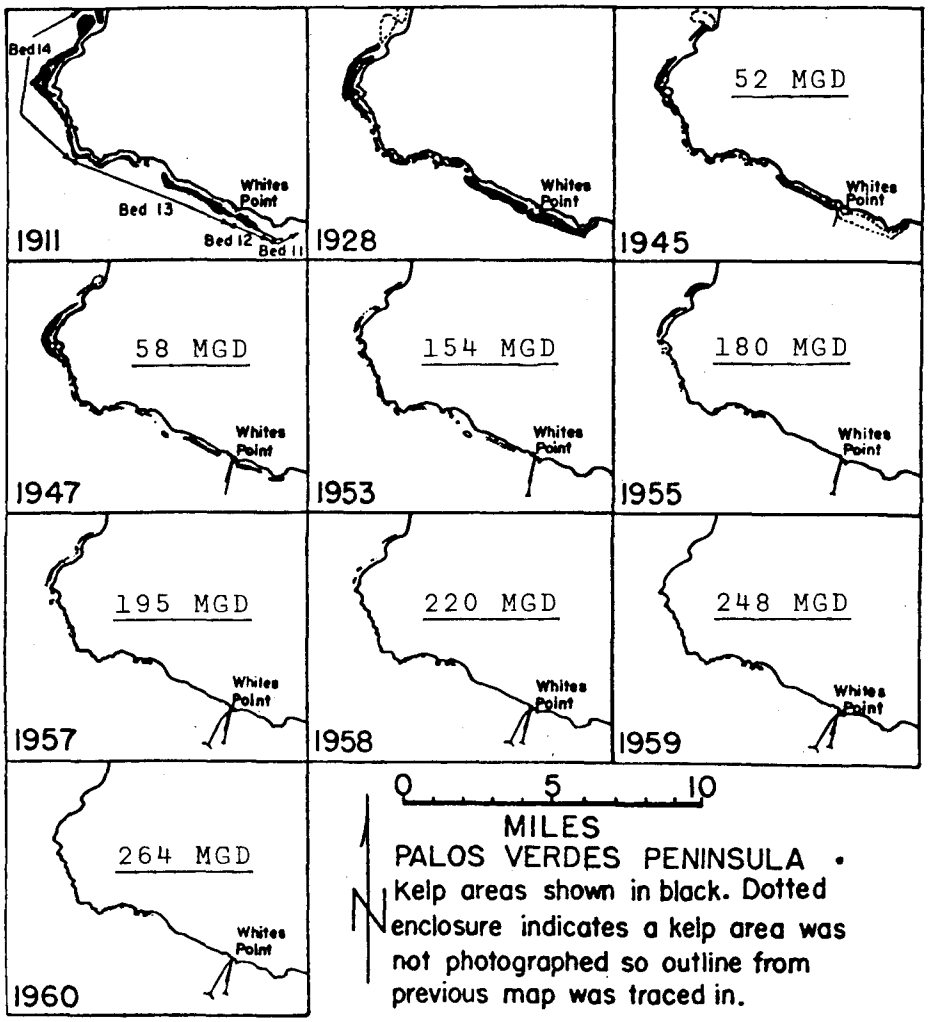

Figure 1-3. Historical charts of the Palos Verdes coastline, showing gradual disappearance of kelp beds. Kelp areas drawn in black. Only two adult plants could be found here in summer, 1967. Average sewage discharge rate for each year given in MGD (32, 42).

The observed scarcity of attached algae in the deeper areas near outfalls suggests that light incident on the bottom may be insufficient for plant growth to keep pace with grazing (1). Thus the combined effects of decreased light and artificially supported urchin predation is a possible explanation for the inability of kelp beds to return to their natural state.

The 1928 kelp beds extended to water depths of 60 feet. The seaward edge of the beds was smooth, extending farthest from shore where the bottom slope was least at Rocky Point and Whites Point. This indicates that the outer edge generally followed a constant depth contour or relatively constant sea floor illumination level. Hence, penetration of juvenile plants into deeper waters might have been limited by insufficient light. If light was a limiting factor in kelp bed size in 1928, attenuation of sunlight by pollutants after 1934 would have been a factor in the receding of kelp beds to shallower waters in 1945 and 1947 (Figure 1-3).

This study investigates the effects of pollutants upon sunlight penetration by simultaneously measuring sunlight irradiance, light beam attenuance, and particle size distribution as a function of water depth. Temperature depth profiles were also measured to assess thermal stratification effects. A small boat was used to acquire the data. Sunlight

irradiance in five colors was measured using SCUBA diving gear and a hand held bank of light meters with color filters. A transmissometer and temperature probe were lowered from the boat. Light beam attenuance and temperature were recorded on deck. Water samples were taken to a laboratory. A Coulter Counter was used to measure size distributions.

The most significant result was that pollutants decreased the optical albedo of ocean water, increasing the extinction of sunlight irradiance as a function of optical depth. The contrast between polluted water and natural water particle concentrations, the effects of pollutants upon particle size distribution, and the dependence of euphotic zone depth upon particle concentration were also determined. Scattering and absorption by particles were calculated for real and complex particle refractive indices.

Water surface color spectra were measured just below the water surface. The dependence of color spectrum upon particle concentration was noted. In addition, a limited number of samples were analyzed by a co-worker, E. Myers (41), for particulate percent organic carbon and particulate carbon isotope ratio. The organic carbon data indicated the fraction of material resulting from organic processes.

The isotopic composition indicated whether the material was *primarily of marine or terrestrial origin.*

Chapter 2 presents theory and background information necessary for interpreting the experimental results presented in Chapter 4. Chapter 3 describes the procedures and apparatus. Chapter 5 summarizes the results.

There are two appendices. Appendix A contains the preliminary results of a sunlight propagation model. Appendix B tabularizes the particle size spectrum data.

CHAPTER 2

BACKGROUND AND THEORETICAL DEVELOPMENT

2.1 Introduction

This chapter is grouped into two sections (2.2 and 2.3). The first involves measurement and mathematical modeling of sunlight propagation in the ocean. The second involves physical, optical and chemical properties of suspended ocean particles. These sections provide relationships for interpreting the sunlight and particle measurements in polluted and natural waters (Chapter 4).

Section 2.2 is divided into three parts:

1) downwelling irradiance data--exponential decrease of sunlight with depth for different ocean water types, thermal stratification effects, changes in color ratios and rate of attenuance due to varying chlorophyll concentrations,
2) the euphotic zone--dependence of photosynthesis upon wavelength and sunlight intensity, and
3) surface ocean color--dependence upon particle types and concentrations.

Section 2.3 summarizes theory and measurements of particle properties and has three parts:

1) scattering and absorption by particles--dependence upon particle size and index of refraction, calculations of extinction and absorption efficiences for three complex refractive indices based upon the van de Hulst (70) "anomalous diffraction" theory,
2) size distributions--discussion of the optically important size range, contrasting examples of open ocean and coastal particle size distributions, and
3) carbon isotope composition--carbon isotope ratios (C^{13}/C^{12}) as indicative of terrestrial or marine origin of suspended particles.

The experimental results, Chapter 4, are similarly grouped into two main sections (4.2 Sunlight Propagation in Polluted and Natural Waters, and 4.3 Particle Properties in Polluted and Natural Waters) for efficient cross reference between the two chapters.

2.2 Sunlight Propagation

2.2.1 Downwelling Irradiance Data

A number of investigators have studied the penetration of sunlight in natural waters (4, 14, 24, 25, 29, 43, 59, 68). Figure 2-1 depicts the penetration range for oceanic and coastal waters. Of special interest is the energy level needed for positive net photosynthesis (compensation point). Photosynthetic carbon fixation exceeds respiration requirements at this light intensity and plants can grow. It is generally accepted (14, 25) that one percent of the sunlight irradiance at the ocean surface fulfills compensation point requirements. The region in a specific body of water for which irradiance exceeds compensation is termed the euphotic zone.

The maximum depth of the euphotic zone ranges from 5 meters in turbid coastal waters (river plumes, estuaries, harbors) to several hundred meters in the clearest ocean waters (Figure 2-1). The clearest coastal waters display euphotic depths of 30 to 40 meters. Since this study is primarily concerned with the coastal environment, euphotic zone depths of 5 to 40 meters represent the appropriate range of natural conditions. However, these values should not be used as criteria for water quality management. The ultimate goal should be a minimum effect by man upon existing conditions.

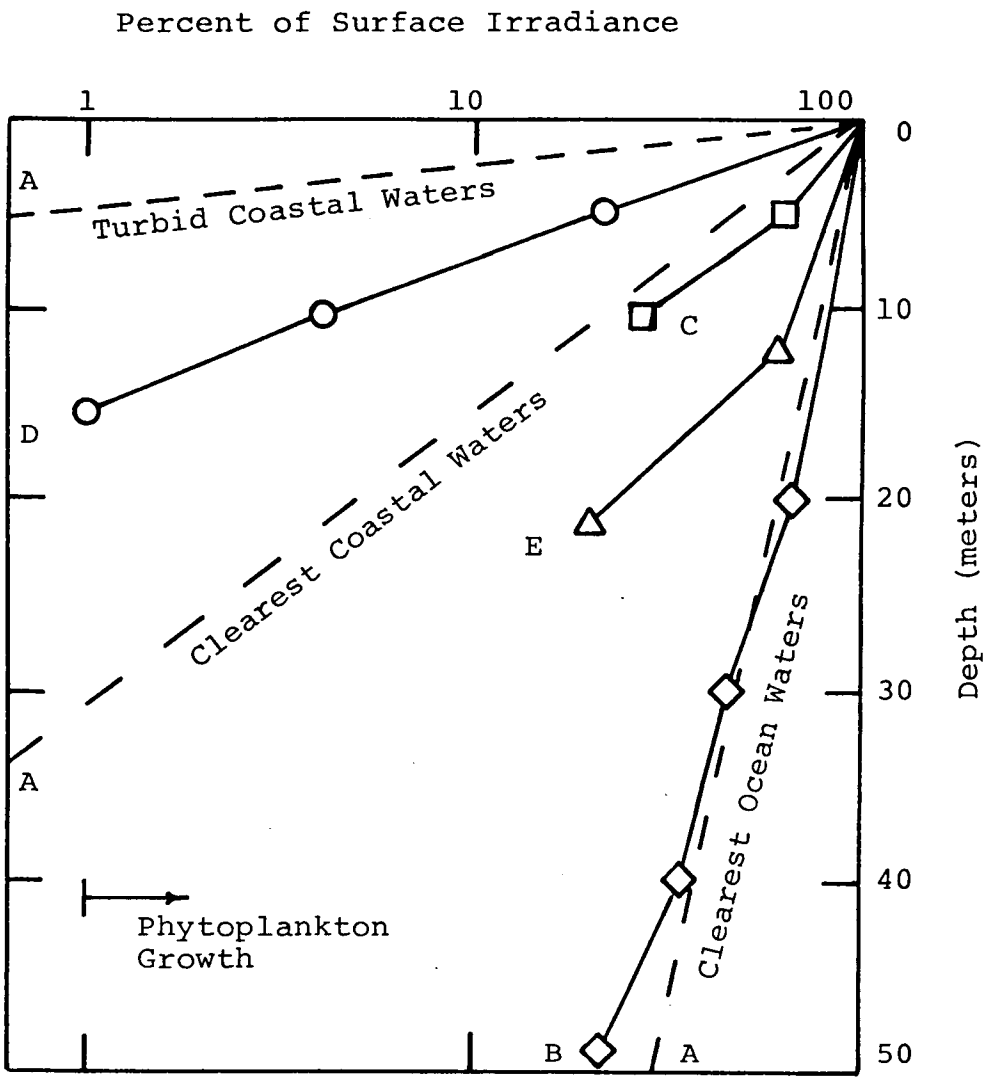

Figure 2-1. Downwelling Irradiance Profiles

A. Environmental Range, 465 nm (wavelength), Jerlov, 1963
B. Sargasso Sea, 465 nm, Ivanoff et al., 1961
C. Castle Harbour, 465 nm, Ivanoff et al., 1961
D. Woods Hole Harbor, 540 nm, Oster and Clark, 1935
E. San Diego Coast, 465 nm, Tyler and Smith, 1967

In Chapter 4 the effects of the Los Angeles County sewer outfall upon the natural environment at Whites Point are estimated by comparing sunlight levels in the outfall area with levels at selected natural background sites. In this regard, two parameters are of interest; compensation point depth, z_c (meters), and the diffuse irradiance attenuance, k (m^{-1}). Since the actual data plots in Figure 2-1 are nearly linear, the propagation of downwelling irradiance (diffuse light flux penetrating a horizontal plane in the earthward direction) can be approximated by a first order exponential:

$$E_d = E_s \exp(-kz) \qquad (2\text{-}1)$$

where z = depth in the water (meters)

E_d = downwelling irradiance at depth z (watts/m^2)

E_s = downwelling irradiance just beneath the water surface (watts/m^2)

Using one percent of E_s as a criterion for effective photosynthesis, the compensation depth is then related to the diffuse irradiance attenuance by

$$z_c = -\ln(.01)/k \approx 4.6/k \text{ (meters)}. \tag{2-2}$$

Using this relationship, the diffuse attenuance values for clear and turbid coastal waters are approximately $0.1m^{-1}$ and $1.0m^{-1}$ respectively.

Qualitatively k is a function of absorption due to water, dissolved material and suspended particulates, and a function of the directional character of water molecule and particle scattering. In the more turbid coastal zone, the effect of water molecule scattering is negligible. The directional scattering character of ocean water is similar over a wide range of turbidities (17). Therefore in the Southern California coastal zone the controlling factors are the concentrations and the spectral absorption character of suspended particulates and dissolved material.

With respect to dissolved substances, the important species are natural dissolved organic substances ("yellow substance") and pollutants. Jerlov (25) summarizes the work by Kalle (30, 31) concerning the origin and nature of yellow substance. Briefly it is a product formed in the presence of carbohydrates and amino acids and has both terrestrial

and marine origins. It is usually associated with large river runoffs and some coastal upwelling regions. It strongly absorbs in the ultraviolet and blue wavelengths. None of the natural water data in Chapter 4 exhibit these properties and the special case of yellow substance will not be discussed further.

The literature yielded little information regarding sunlight attenuation due to dissolved pollutants in the marine environment. Losses due to scattering and absorption by pollutants are assessed in the data analysis sections of Chapter 4.

There are four prominent sources of suspended particulates. These are entrained bottom sediments, terrestrial runoff, plankton (living creatures and products of decay), and pollutants. Only a minor portion of this study dealt with terrestrial runoff. The major work was devoted to pollution particulates and natural particulates, mainly originating from plankton or bottom sediments.

Boden, Kampa and Snodgrass (4) studied effects of phytoplankton upon sunlight propagation in the Bay of Biscay (Figures 2-2 and 2-3). The depth of the euphotic zone was

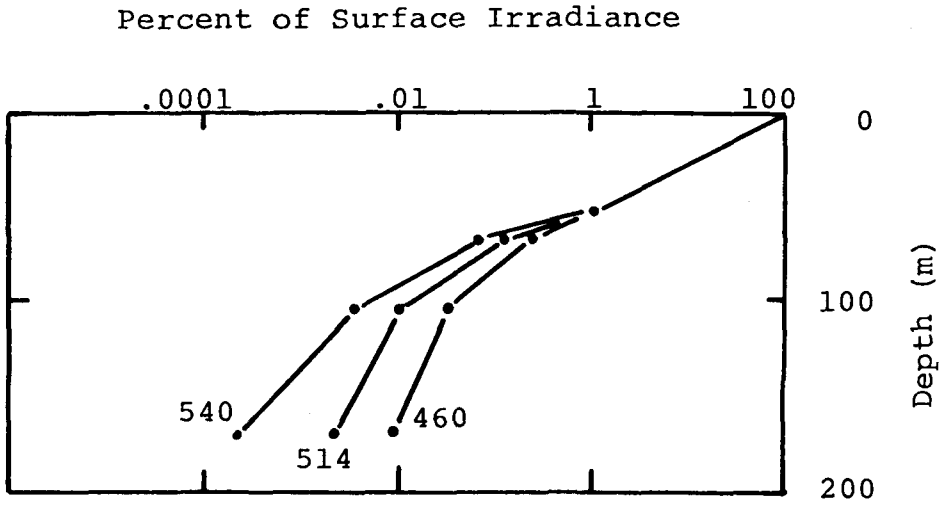

Figure 2-2. Downwelling Irradiance in the Bay of Biscay for Three Wavelengths (numbers in nm.) Boden, Kampa and Snodgrass (4).

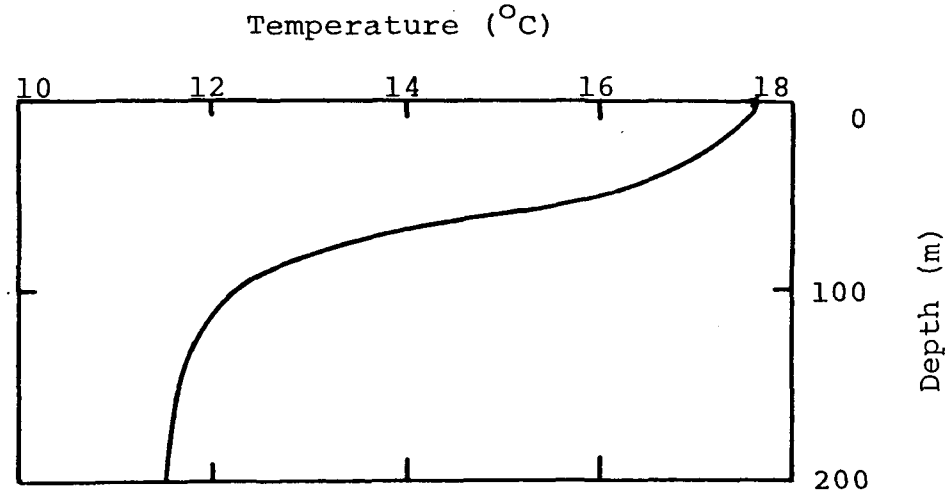

Figure 2-3. Temperature Profile for Bay of Biscay Station (Figure 2-2).

approximately 50 meters and there was a strong 6°C thermocline (a sharp temperature gradient that restricts vertical mixing). The diffuse attenuance coefficient, k, was approximately $0.08m^{-1}$ above the thermocline and 0.02^{-1} below the thermocline. A "turbid micro-layer" of phytoplankton above the thermocline accounted for the different attenuance.

This illustrates effects of a thermocline on stabilizing layers of contrasting water masses. Stratification is important for interpreting the pollution data in Chapter 4. The sewer outfall system at Whites Point was designed to utilize stability of the thermocline to prevent effluents from reaching the water surface, thus eliminating transport to the shoreline. Chapter 4 analyzes measurements of turbidity and suspended load to determine capacity of a thermocline to prevent vertical transport of the sewage field.

The irradiance data (Figure 2-2) also show an enhancement of the green wavelength (540 nm.) relative to the blue (460 nm.) as light passed through the upper layer. This is most probably due to the blue absorption band of the chlorophyll pigments in phytoplankton. Measurements of scattering and absorption by algae as a function of wavelenth show that the scattering minima nearly coincides with the absorption peaks (Figure 2-4). The absorption data by Yentsch (73) was

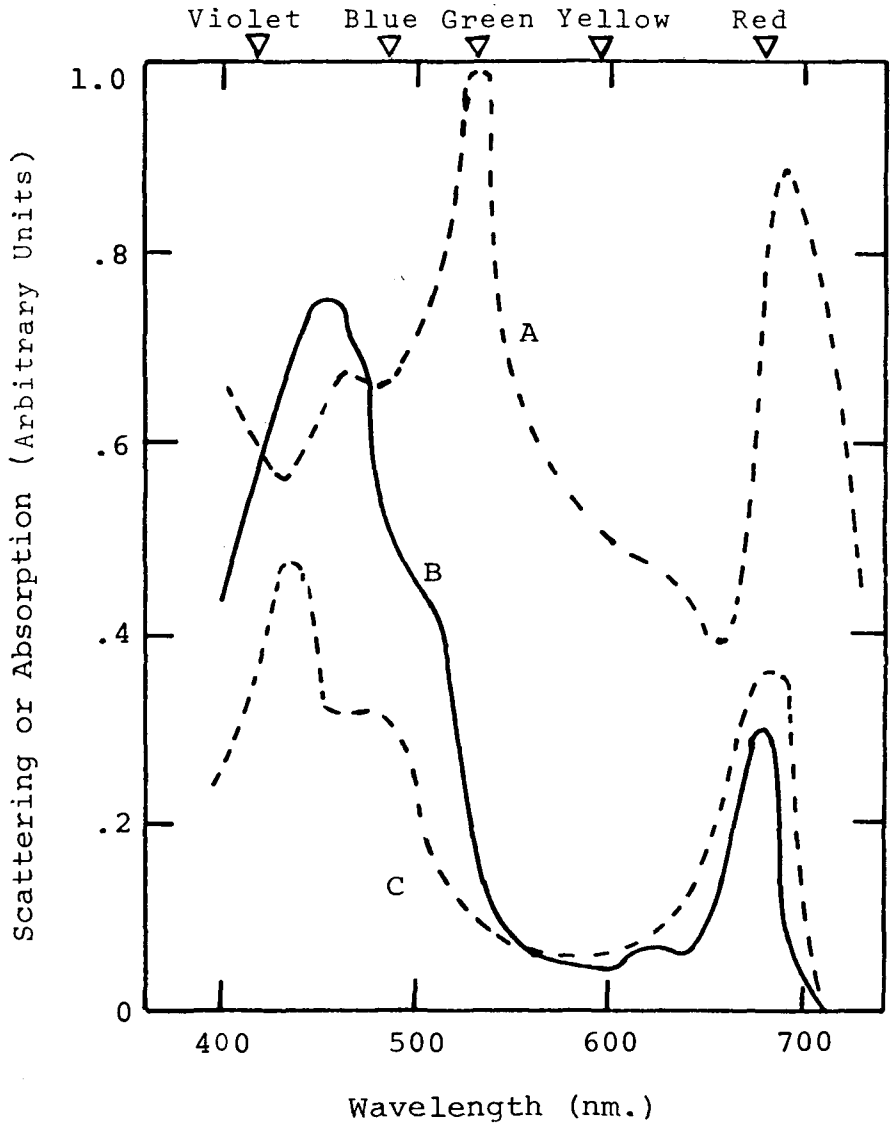

Figure 2-4. Spectral effects of chlorophyll pigments

A. Scattering, Green Alga, Chlorella, Latimer and Rabinowitch, 1957
B. Absorption, Green Alga, Chlorella, Latimer and Rabinowitch, 1957
C. Absorption, Natural Population Woods Hole, Yentch, 1960

taken by filtering samples of sea water and scanning the residue with a spectrometer. Latimer and Rabinowitch (35) analyzed spectrometrically a light beam after transmission through a suspension of green algae. Scattering was measured at 90^{o} and the gross attenuation upbeam measured absorption.

In coastal waters, light irradiance at depths greater than a few meters primarily results from previous scattering by suspended particles. Hence spectral dependence of particulate scattering largely determines the color of underwater irradiance. Chlorophyll pigmented particles have a sharp scattering maximum in the green and a minimum in the blue (Figure 2-4), so enhancement of green light relative to blue light indicates an abundance of phytoplankton. This property is used in Chapter 4 to distinguish phytoplankton particulates from pollution and entrained bottom particulates.

Johnson, Burbank and Pyke (29) established a correlation between downwelling color and chlorophyll concentration as determined by spectrophotometric absorption measurements (Figure 2-5). In the upper water layers, the blue wavelength (480 nm.) was enhanced at low chlorophyll concentrations. The green wavelength (520 nm.) dominated when chlorophyll concentrations exceeded 1 mg/m^3. The experimental results presented in Chapter 4 show similar color alterations.

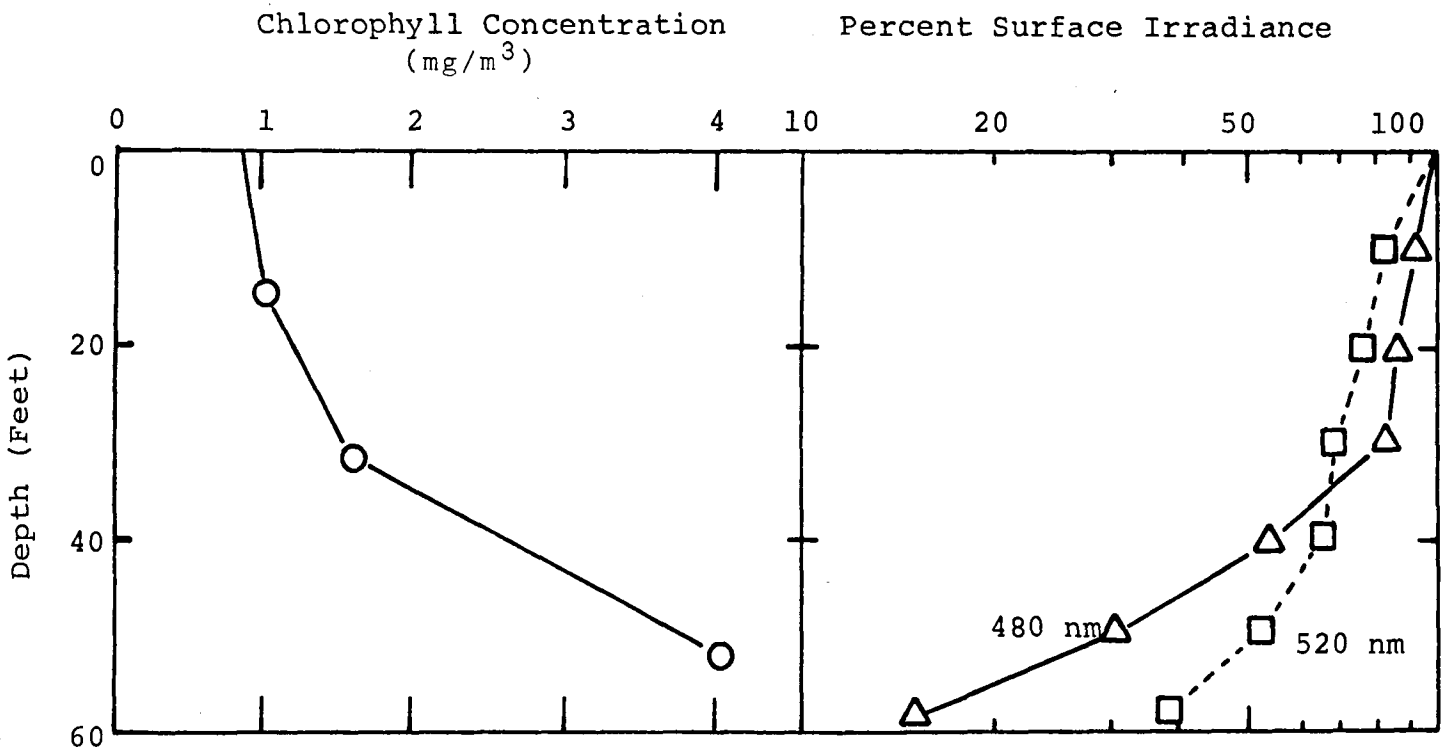

Figure 2-5. Effect of Chlorophyll Concentration On Color of Downwelling Irradiance (Santa Monica Bay), Johnson, Burbank and Pyke (1969)

2.2.2 The Euphotic Zone

As discussed in the previous section, one percent of surface irradiance is generally accepted as a reasonable value for defining the depth of the euphotic zone. A more detailed discussion of photosynthesis requirements is given here. The basic reference is an introductory review of requirements by Strickland (62).

Light between the wavelengths of 380 nm. and 720 nm. is effective for photosynthetic production. Wavelengths smaller than 300 nm. can be damaging and wavelengths larger than 700 nm. are strongly attenuated by water. The total amount of sunlight energy is as important as the spectral distribution.

Chlorophyll must be present for photosynthesis to occur and spectral efficiency closely follows the absorption curve (data plot B, Figure 2-4). For plants such as the green algae whose predominant pigment is chlorophyll, some of the sun's energy is not absorbed and is wasted. However, marine plants may also contain carotene, fucoxanthin, and phycobilins which together extend photosynthetic activity to wavelenths outside the chlorophyll absorption band. Light energy is absorbed by these accessory photosynthetic pigments and transferred to the chlorophyll for photosynthesis. The red and blue-green algae contain pigments (phycoerythrin phycocyanin and chromoprotein phycobilins)

which absorb and support photosynthesis throughout most of the visible spectrum (400 to 700 nm.). Due to the variety of pigments present, the total radiant energy in the visible spectrum must be considered in photosynthetic studies.

At low light levels, phytoplankton demonstrate a constant quantum efficiency (Figure 2-6). Beyond a certain intensity (0.05 to 0.25 langleys/min., depending upon the class of phytoplankton), increasing intensities inhibit photosynthesis. Except for dinoflagellates, the growth rate at 0.5 langleys/min. falls to only a few percent of the maximum. For a mixed phytoplankton population, 0.15 langleys/min. is a practical value for maximum photosynthesis.

The solar radiation constant (energy flux above the atmosphere normal to the earth's surface) is approximately 1.9 langleys/minute. On a clear day in the summer at 50 degrees latitude, radiation at the ocean surface rarely exceeds 1.5 langleys/min. Atmospheric conditions may reduce this by 70 percent. Effects due to season and latitude variations may reduce the intensity by one order of magnitude. Losses at the air-sea interface vary from a few percent to over 30 percent depending upon sun zenith angle, cloud cover and sea state (ocean surface condition).

Considering all these effects, the range of 0 to 1.5 langleys/min. is realistic for expected energy flux in the

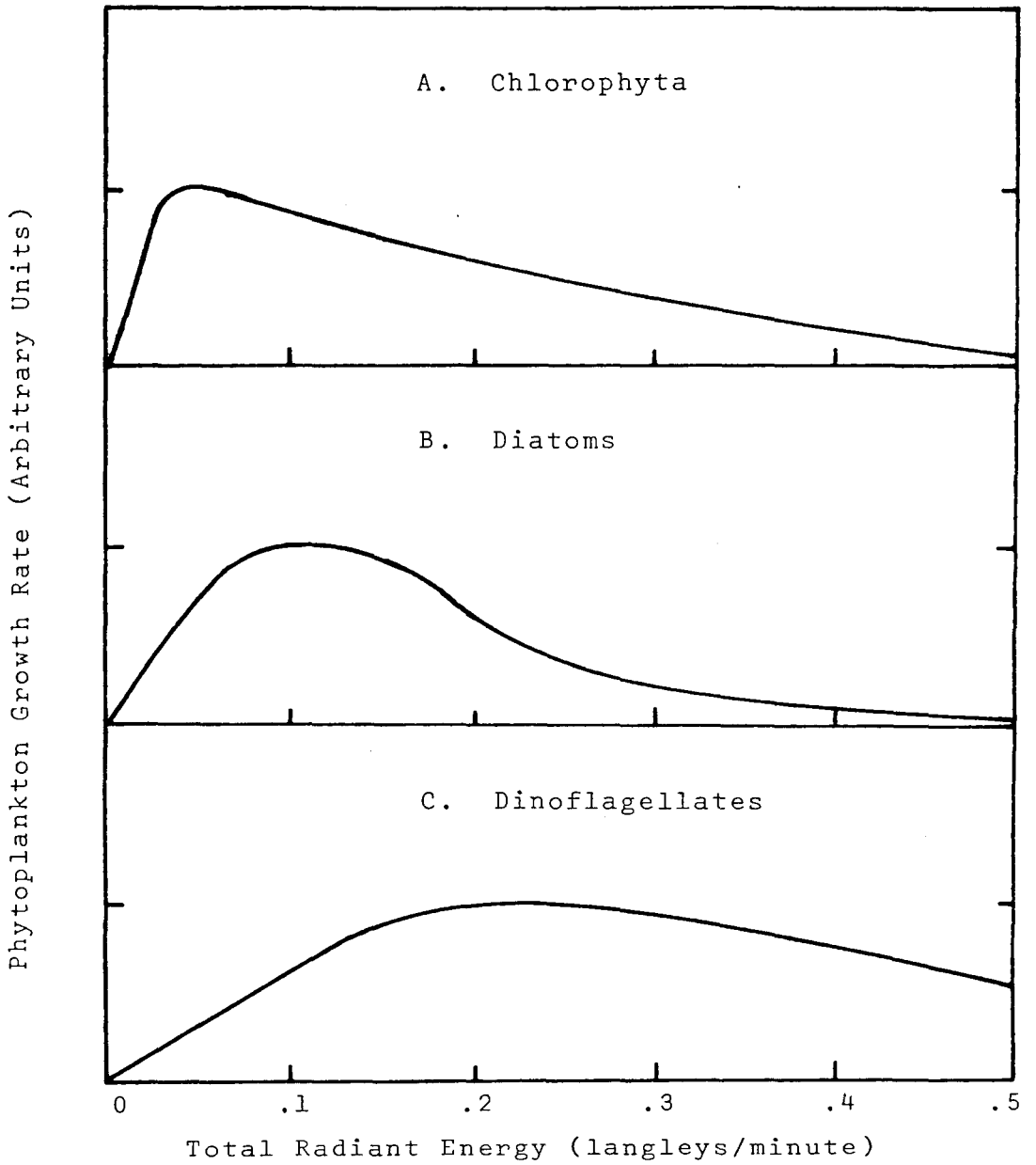

Figure 2-6. Photosynthesis vs Light Intensity for Three Classes of Phytoplankton. For more details see Ryther (1956) (1 langley/min. = 0.07 watt/cm^2)

upper layers of the ocean. The optimum depth for phytoplankton production (corresponding to the maximum growth rate intensities depicted in Figure 2-6) will vary with turbidity. Intense stratification by plankton occurs (Figure 2-7). The depth at which the maximum phytoplankton population occurs, however, is not simply a function of light intensity. It is most usually a complex function of light, temperature, nutrients and predators.

The determination of the depth of the euphotic zone is less complex because by definition the limiting factor is light energy. This study will examine the "photic health" of polluted areas by assuming that one percent of surface illumination represents the lower limit of the euphotic zone. Figure 2-8 shows depths at which irradiance levels are one percent of the surface levels as a function of wavelength for different water types. This same format will be used in Chapter 4 to compare euphotic depths of areas affected by the Los Angeles County Sanitation Districts (LACSD) sewer outfall with those of the natural southern California waters.

The one percent criterion for compensation intensity is approximate and not always valid. Since photosynthesis competes with respiration on a diurnal cycle, the appropriate specification for the compensation intensity should

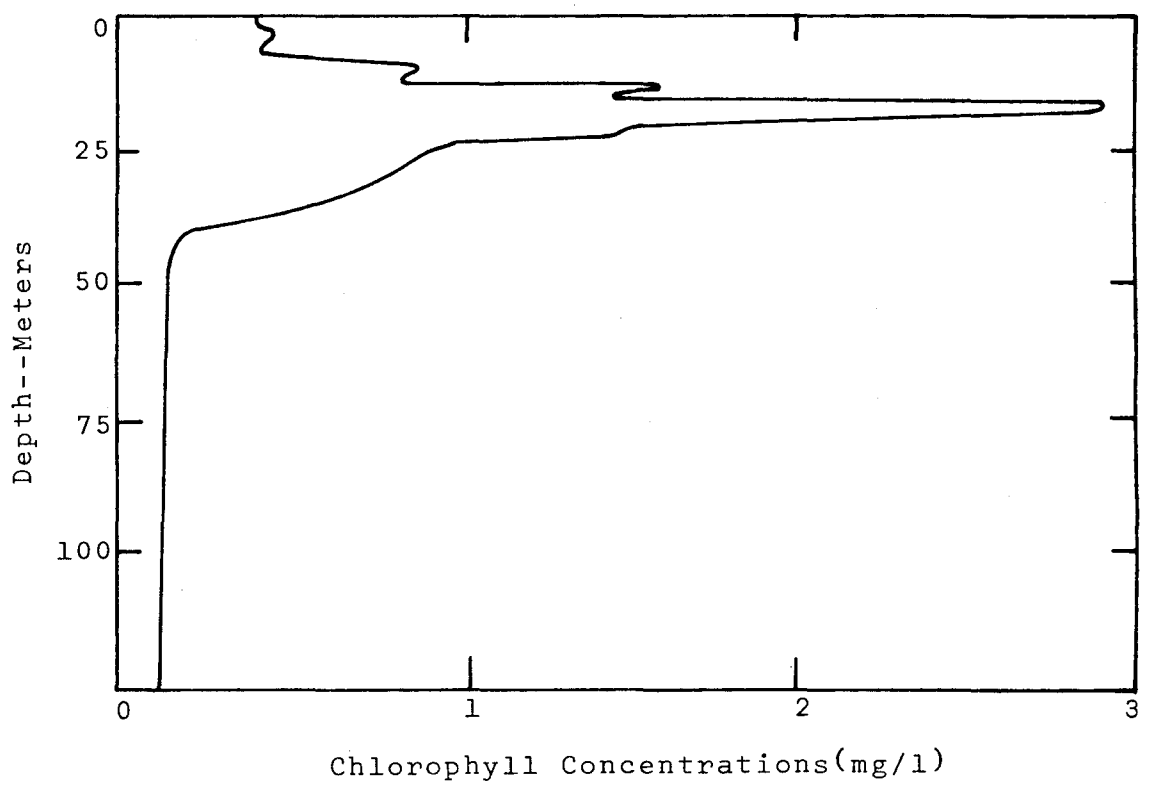

Figure 2-7. Stratification of Chlorophyll as Reported by Strickland (1968) La Jolla, California (summer)

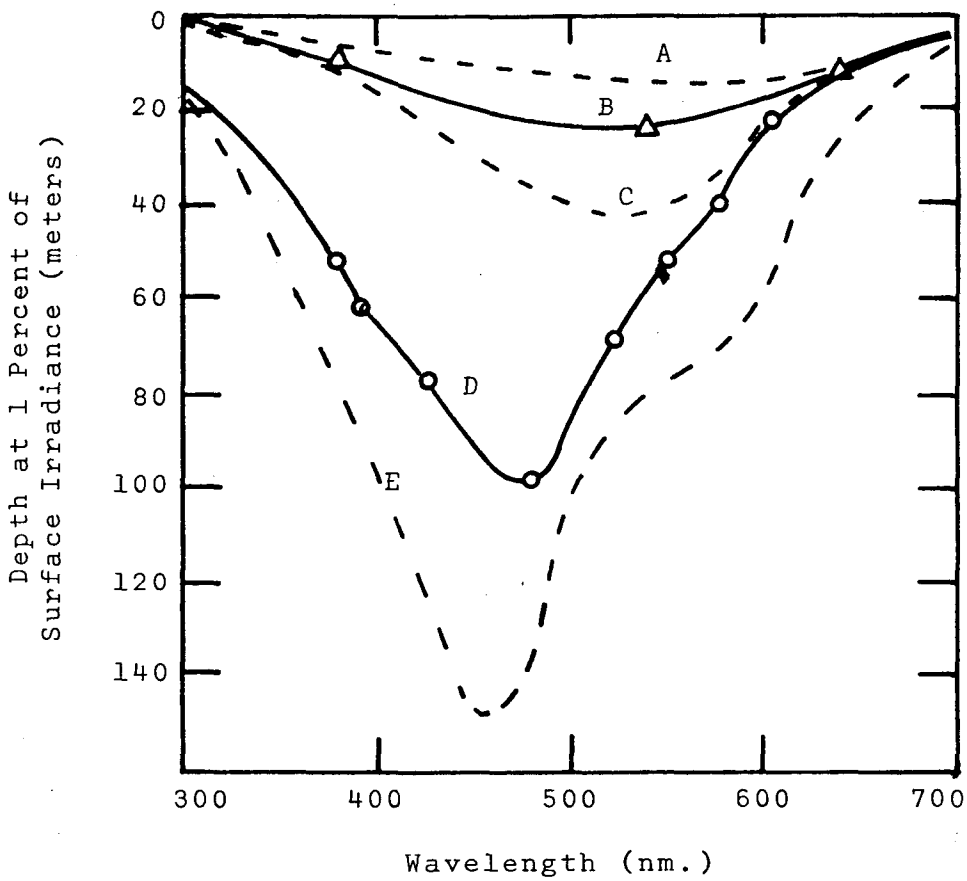

Figure 2-8. Euphotic Depth (1 percent of surface irradiance) as a Function of Wavelength.

A. Turbid Coastal Waters, Jerlov (1968)
B. Vineyard Sound, Oster and Clarke(1935)
C. Clearest Coastal Waters, Jerlov (1968)
D. Caribbean Sea, Jerlov (1968)
E. Clearest Ocean Waters, Jerlov (1968)

be in terms of langleys per day. Strickland (62) concludes that a practical value for temperate seas (regions between the tropic of Cancer and the arctic circle or between the tropic of Capricorn and the antarctic circle) is 5 langleys/day.

At latitude 50°N, the 24-hour mean figure for solar radiation at the ocean surface has an average value of 0.28 langleys/min. in June and 0.04 langleys/min. in December (62). This corresponds to 400 langleys/day in June and 60 langleys/day in December. Considering effects due to longer days in the winter and increased solar elevation angles, Southern California average surface irradiance (latitude 34°N) is 450 langleys/day in the summer and 100 langleys/day in the winter. Comparing these surface intensity values with the required compensation intensity of 5 langleys/day, one percent of surface light for the lower limit of the euphotic zone is valid in the summer (5/450), while 5 percent of surface light is appropriate in the winter months (5/100).

2.2.3 Surface Ocean Color

The potential for contributions by aircraft and satellites in detection of oceanic pollution and for understanding sources of nutrition in the sea has been a

motivation for current research in remote sensing of water quality. Point measurements or transects over an ocean area by buoys or ships are often inadequate to gather necessary synoptic information. Aircraft or satellite earth resources observations may coordinate surface measurements so that large scale dynamics are described more accurately. Remote measurements observe only upper layer phenomena, but deep water processes sometimes produce surface effects. Furthermore, basic productivity is confined to the upper layer since photosynthesis requires sunlight. "Ground truth" measurements or quantitative correlations of remote measurements with shipboard determinations are presently necessary.

There are four major spectral regions employed for remote sensing with various applications (Table 2-1). These information possibilities indicate how several spectral regions may work in tandem to observe the same phenomenon or process. Remote sensing of subsurface water quality is possible only in the visible region. Blue wavelengths in clear waters may reveal features at depths up to 30 meters. In turbid waters the resolution limit may be only a few meters. In the visible region, color shifts due to changes in water depth and quantitative correlations of color spectrum with chlorophyll concentrations have yielded best results to date.

Table 2-1. Spectral regions and associated applications for remote sensing of water quality.

Spectral regions	Information Possibilities
Visible (400-700 nm.)	Pollution Turbidity Chlorophyll Water depth Sea state Surface slicks
Near infrared (700-2500 nm.)	Surface plant growth Surface slicks
Infrared (3-5 and 8-14 microns)	Surface temperature
Microwave (1-100 centimeters)	Surface temperature Surface salinity Sea state

Light reaching an aircraft or spacecraft comes from several sources: atmospheric scattering, reflection at the surface of the sea, scattering by particles and water molecules in the ocean and reflection from the bottom of the sea. The initial step in remotely measuring water quality involves measuring effects upon the spectrum of upwelling light at the ocean surface. Downwelling and upwelling spectral irradiance should be measured as a function of depth. Water quality parameters such as chlorophyll concentration, turbidity or pollutants are simultaneously measured to correlate with color. General models of light propagation in the ocean-atmosphere system can then be developed to predict information available for remote detection and instrumentation sensitivity requirements.

This study represents an initial step toward remotely sensing distributions of sewage fields from municipal outfalls. Measured parameters of water quality included turbidity (light beam attenuation per meter for a single wavelength), total particulate suspended load (parts per million by volume), particle size distribution, temperature (for determining effects due to the thermocline) and depth. Upwelling and downwelling irradiance were measured in five color bands covering the visible spectrum from violet to orange (see Figure 3-2).

There is a continuing interest in spectral measurements of upwelling irradiance (13, 14, 15, 17, 23, 25, 26, 36, 38, 47, 51, 61, 71). The remainder of this section presents a summary of water color for a range of ocean water types and an example of remotely acquired spectral data for contrasting chlorophyll concentrations.

Apparent color of ocean water is related to the beam attenuation coefficient (Figure 2-9). Beam attenuance, c (not to be confused with the previously discussed diffuse sunlight attenuance, k) is the rate of exponential decay of a collimated beam (parallel rays of light) as a function of distance from the light source. Beam attenuance (the sum of absorption and scattering coefficients) is measured with a transmissometer (Section 3.1) which has a light source and a light detector separated by a known distance. The detector is located in the path of the light beam and produces a signal proportional to light intensity.

The instrument is lowered into the water with a cable that supplies power and transmits the detector output to the vessel. Ocean water passes freely between the detector and light source. The detector is shielded from stray sunlight so that the detector signal is proportional to the amount of the light beam that is not scattered or absorbed. The relationship between light beam intensity at the detector, I (watts), and light beam attenuation coefficient, c(m^{-1}), is

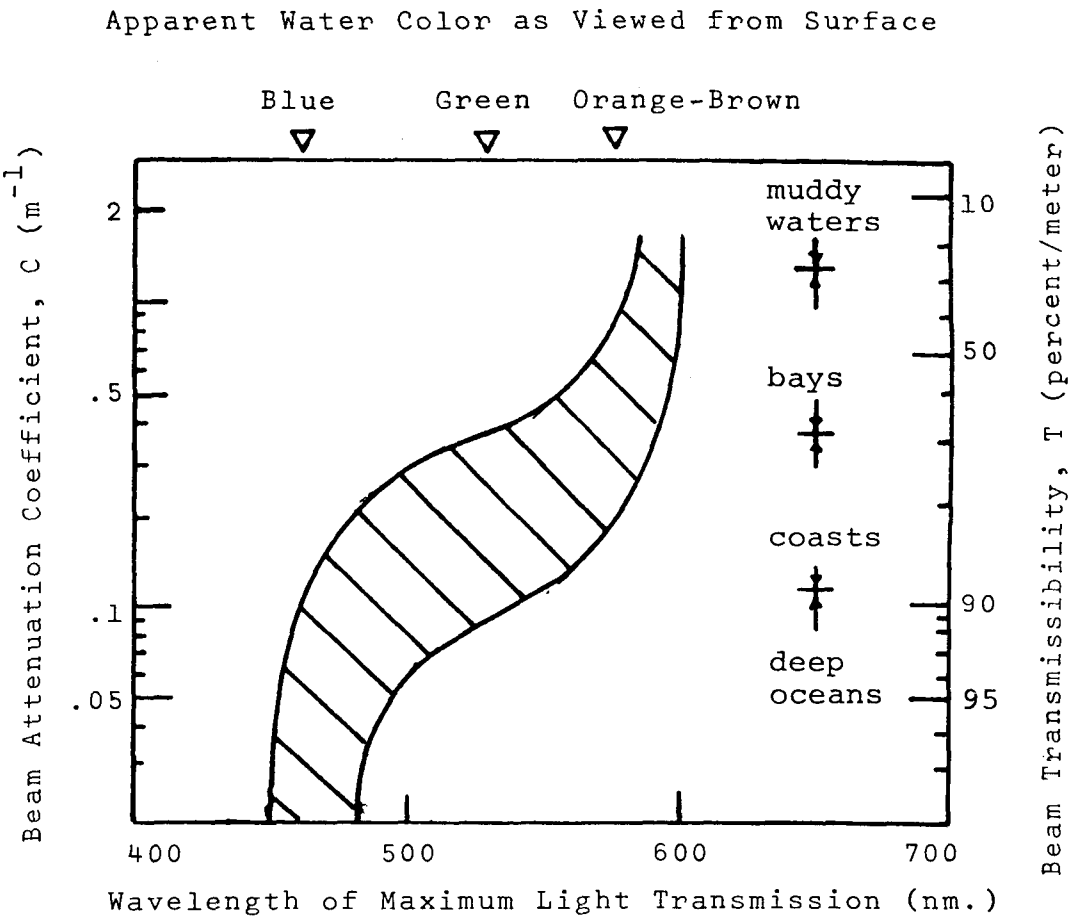

Figure 2-9. Relationship between beam attenuation per meter, wavelength of maximum light transmission and apparent water color. Derived by Lepley (1968) according to data by Clarke (1939), Jerlov (1964), Kinney (1967) and Moore (1947).

$$(2\text{-}3) \qquad I = I_o e^{-cd} = I_o e^{-(a+b)d}$$

where I_o = light beam intensity at the source(watts),

d = distance between source and detector (meters),

a = absorption coefficient (m^{-1}), and

b = scattering coefficient (m^{-1}).

The beam transmissibility, T (percent/meter), is the percent of light that is not scattered or absorbed in a one meter distance.

$$(2\text{-}4) \qquad T = 100(I/I_o) = 100e^{-c}.$$

The beam attenuance is a function of the concentration of dissolved or suspended material. At low concentrations ($c < 0.05$) the color of the ocean is blue and independent of concentration (Figure 2-9). At intermediate concentrations ($0.05 < c < 0.5$) color changes rapidly with concentration from blue to green. At high concentrations ($c > 0.5$) color is again independent of concentration and reflects the actual color of the suspended or dissolved material. Remote sensing of ocean color to determine concentrations of pollutants or natural materials may therefore be limited to intermediate concentrations.

In natural waters this can be explained by comparing the optical effects of pure water with the optical effects of suspended material (Figure 2-10). At very low concentrations of suspended material (in deep oceans such as the Sargasso Sea), scattering by water molecules is a significant source of upwelling light flux at the ocean surface. Molecular scattering increases with decreasing wavelength (inverse fourth power with wavelength according to Rayleigh small particle scattering theory). The transmission of pure water is maximum at 475 nm. This accounts for the blue color of the deep oceans.

Scattering by suspended ocean particles is relatively independent of wavelength. Scattering by chlorophyll pigmented phytoplankton is minimal in the blue. The blue color of ocean water, therefore, shifts to green when scattering by plankton or particles exceeds the blue enhanced scattering by water molecules.

Molecular scattering by water is an order of magnitude less than pure water attenuation. The shift from blue to green, therefore, occurs at small additions of suspended matter with small increases in total ocean water attenuation. This accounts for the rapid shift in ocean color with small changes in beam attenuance at $c = 0.05\ m^{-1}$.

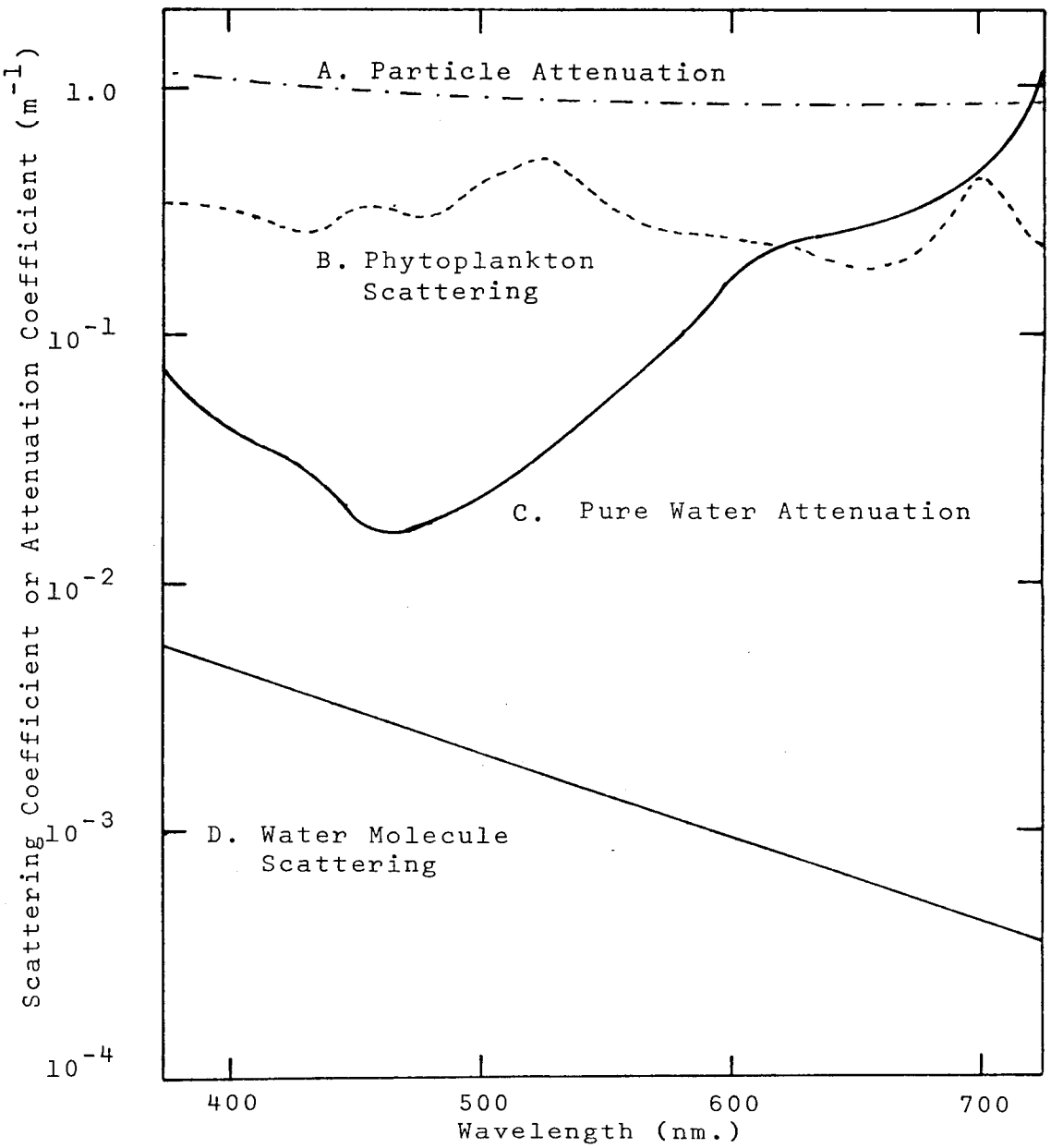

Figure 2-10. Comparison between optical effects of water and optical effects of suspended material.
A. Particle attenuation, concentration unknown, Burt (1958)
B. Scattering by green alga, Chlorella, arbitrary concentration, Latimer and Rabinowitch (1957)
C. Water attenuation, Clark and James (1939)
D. Water molecule scattering, Jerlov (1968)

The Woods Hole C-54 research aircraft data provide an example of a large shift in color spectrum with a small change in chlorophyll concentration (Figure 2-11). Using a spectrometer designed by TRW Systems (15), ocean color spectra were acquired at low altitude (305 m.) on a flight path from low chlorophyll waters in the Sargasso Sea to waters of high productivity over George's Shoals. The chlorophyll measurements, performed by the Woods Hole vessel Crawford, were taken within one day of the aircraft overflight. Unfortunately time did not permit the ship to reach the Sargasso Sea. The chlorophyll concentration there was estimated to be less than 0.1 mg/m^3. Chlorophyll concentrations varied from 0.1 to 3.0 mg/m^3, but most of the color shift occurred between 0.3 and 0.6 mg/m^3.

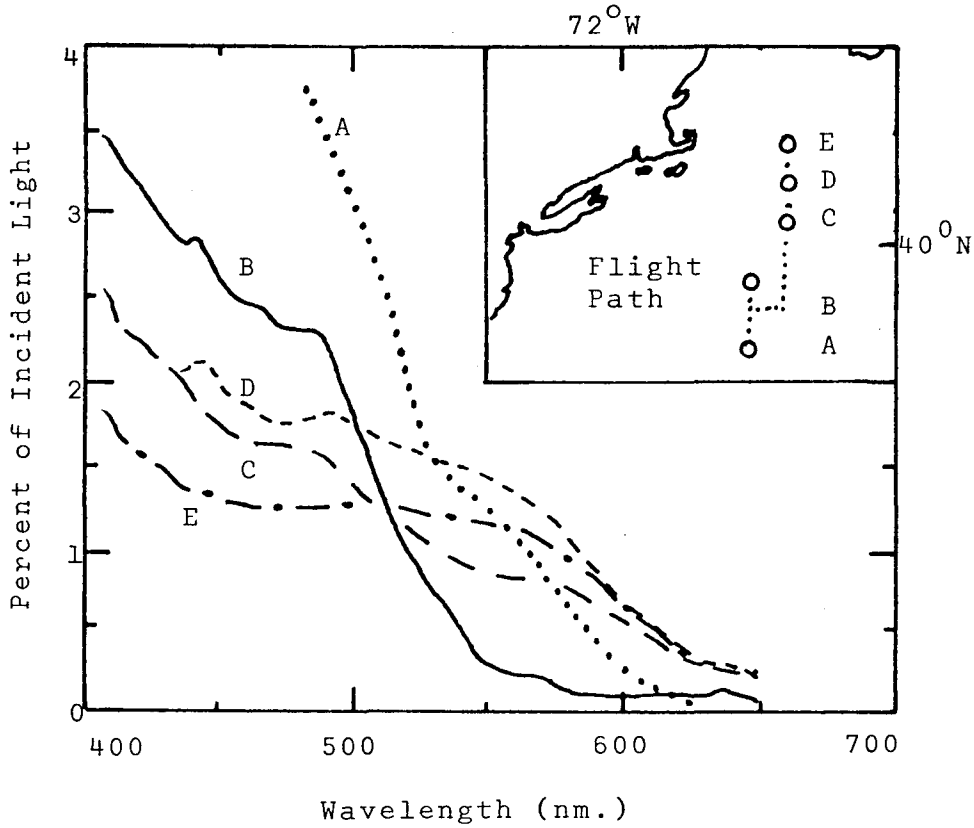

Figure 2-11. Spectra of backscattered light measured from an aircraft at an altitude of 305 meters. Clarke, Ewing and Lorenzen (1970).

Station	Location	Chlorophyll mg./m^3
A	Sargasso Sea	<0.1
B	Continental Slope	0.3
C	Transition to George's Bank	0.6
D	George's Bank	1.3
E	George's Shoals	3.0

2.3 Particle Properties

2.3.1 Scattering and Absorption

The general Mie theory predicts light scattering by large and small particles. Based upon classical electromagnetics, the theory describes the perturbation of a plane monochromatic wave by spherical nonabsorbing particles. The particle scattering coefficient, b_p, is given by (28):

$$b_p = \Sigma b_i = \sum_i N_i \left(\tfrac{1}{4}\pi s_i^2\right) K_{sca}(s_i, \lambda, n) \qquad (2\text{-}5)$$

where

s_i = particle diameter

b_i = scattering by all the particles of diameter s_i

N_i = number of particles per unit volume with diameter s_i

n = particle refractive index (relative to water)

λ = wavelength of scattered light

K_{sca} = scattering efficiency

The scattering efficiency (effective area coefficient) increases rapidly with particle diameter at diameters below two microns (Figure 2-12). Hard refractive indices (high n values) greatly enhance small particle scattering. Maximum

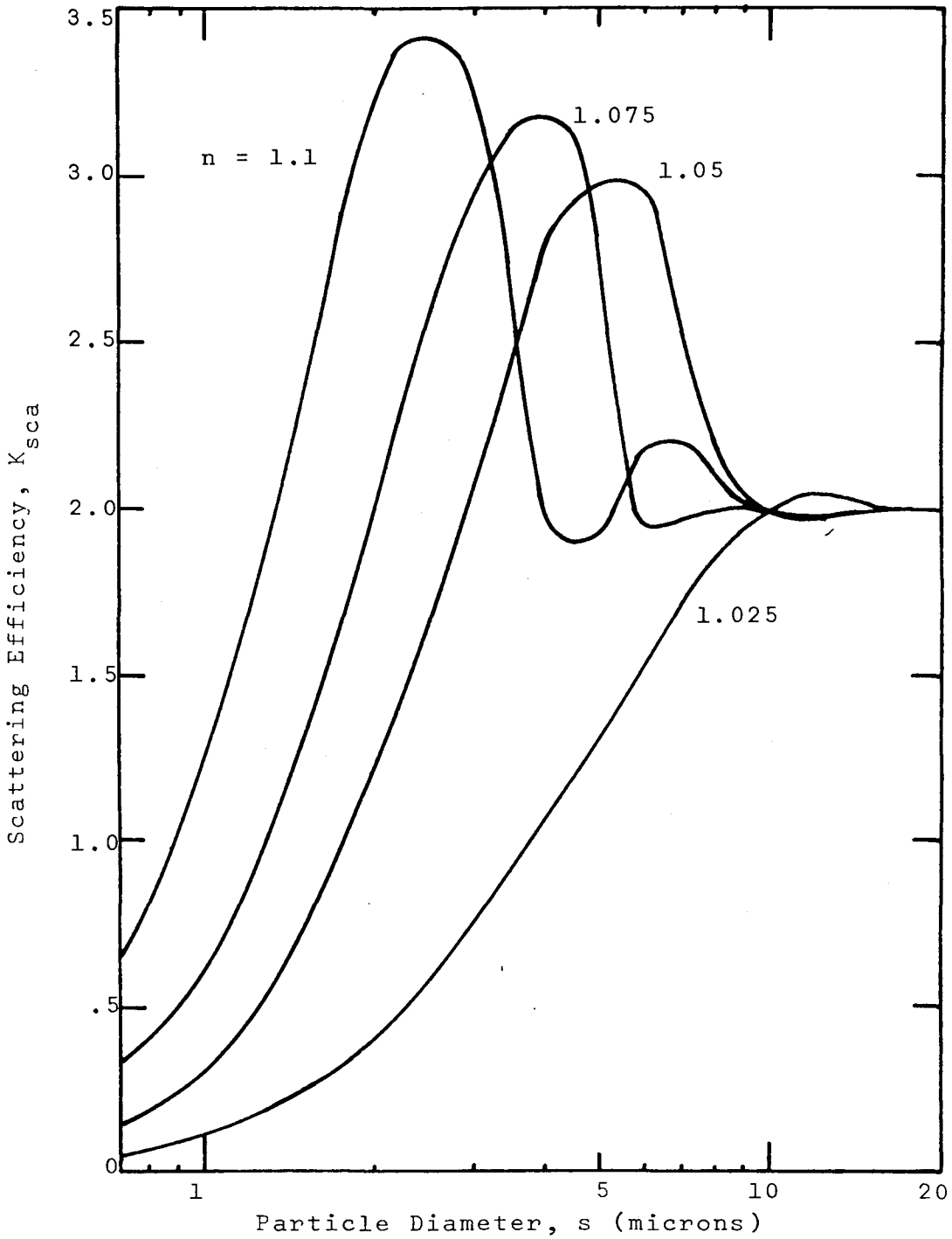

Figure 2-12. Scattering efficiency vs. particle diameter for four values of refractive index, n. (Green light, λ = 500 nm.) After Burt (1956).

K values can exceed 3 for particles the same order of size as the wavelength. After some fluctuations, K_{sca} approaches a constant value of 2 for large particle sizes, regardless of refractive index or light wavelength. Hence, a large particle scatters twice the amount of light intercepted by its geometric cross-section.

Burt (7) and Jerlov (28) indicate that refractive indices for ocean particles range from 1.0 to 1.4. Bacteria and animal and plant material have low values while hard materials (minerals, oxides, carbonates) have high values. In a phytoplankton culture (Isochrysis galbana) Carder, Tomlinson, and Beardsley (11) found that refractive indices varied from 1.026 to 1.036 over a 12 day sampling period using green and yellow wavelengths.

Absorption by particles is treated by introducing a complex refractive index, m, into the Mie theory calculations (28, 70):

$$m = n - in' \tag{2-6}$$

where $n' = a'\lambda/4\pi$

$i = (-1)^{\frac{1}{2}}$

a' = absorption coefficient of the particle material

Gordon and Brown (19) compared light scattering measurements with particle size distributions (acquired by different investigators) for the Sargasso Sea and found an average index $m = 1.05 - (0.01)i$ at $\lambda = 632.8$ nm. Using this value the Mie calculations predicted scattering with an average error of about 20 percent.

Introducing a complex refractive index results in three efficiency factors (33, 37):

$$K_{ext} = K_{abs} + K_{sca} \tag{2-7}$$

where

K_{ext} = extinction efficiency

K_{abs} = absorption efficiency

K_{sca} = scattering efficiency.

Equation 2-5 is still valid for calculating the particle scattering coefficient, b_p (replacing n by m). The particle absorption coefficient, a_p, and the particle extinction coefficient, c_p, ($c_p = a_p + b_p$) have similar expressions:

$$a_p = \sum_i N_i(\tfrac{1}{4}\pi s_i^2)K_{abs}(s_i,\lambda,m) \tag{2-8}$$

$$c_p = \sum_i N_i(\tfrac{1}{4}\pi s_i^2)K_{ext}(s_i,\lambda,m) \tag{2-9}$$

where N_i, s_i and λ are the same as before (equation 2-5).

Van de Hulst (70) simplified the Mie equations for the limiting case $(m-1)\to 0$ and $\pi s >> \lambda$ (m = refractive index, s = particle diameter, λ = light wavelength). Termed anomalous diffraction, the resulting expressions for K_{ext} (70) and K_{abs} (33) are

(2-10)
$$K_{ext} = 2 - 4\exp(-R\tan B)\,\frac{\cos B}{R}\sin(R-B) - 4\exp(-R\tan B)\left(\frac{\cos B}{R}\right)^2\cos(R-2B) + 4\left(\frac{\cos B}{R}\right)^2\cos 2B$$

(2-11)
$$K_{abs} = 1 + \frac{\exp(-2R\tan B)}{R\tan B} + \frac{\exp(-2R\tan B) - 1}{2R^2\tan^2 B}$$

where
$$m = n - in'$$

$$R = 2\alpha(n-1)$$

$$\alpha = \pi s/\lambda = \text{classical size parameter}$$

$$\tan B = \frac{n'}{n-1}$$

Moore, Bryant and Latimer (37) compared the accuracies of these expressions with the exact Mie calculations. K_{abs} was accurate to within 20 percent over the following parameter values: $1.0<n<1.1$, $0.001<n'<0.1$, $0.1< \pi s/\lambda <100$. K_{ext} was accurate to within 10 percent for $1.0<n<1.1$, $0<n'<0.1$, and $5<\pi s/\lambda <100$. Correction factors were given that improved accuracies to within a few percent.

Using equations 2-10, 2-11 and the correction factors (37), K_{abs} and K_{ext} were calculated for $m = 1.05 - (0.001)i$, $1.05 - (0.01)i$ and $1.05 - (0.1)i$ at $\lambda = 500$ nm. (Figure 2-13). Increasing n' from 0.01 to 0.1 greatly enhanced particle extinction for $s<3$ microns and particle absorption for $s <10$ microns.

For $n' \leq .001$, K_{abs} is less than 15 percent of K_{ext} for the particle size range in Figure 2-13. For $n' \geq 0.1$, K_{abs} is $\geq 0.5K_{ext}$. From equations 2-8 and 2-9, particle albedos, A_p ($= 1 - a_p/c_p$) would therefore be greater than 0.85 for $n' \leq 0.001$ and less than 0.5 for $n' \geq 0.1$. If particle attenuance was greater than attenuance due to water or dissolved materials, changes in particle albedo would significantly affect downwelling irradiance (See Appendix A for effects of albedo upon extinction of downwelling irradiance).

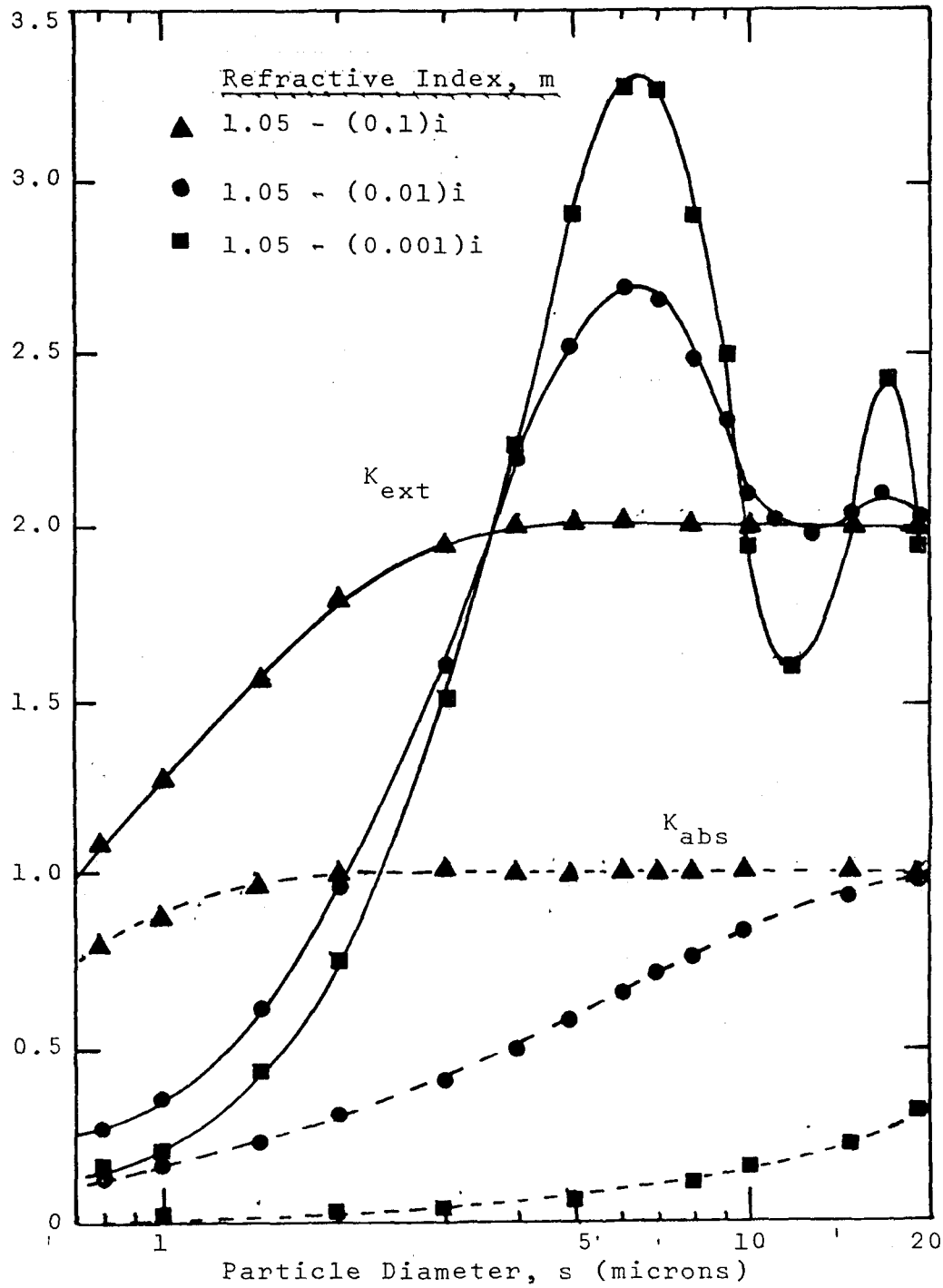

Figure 2-13. Extinction efficiency (K_{ext}) and absorption efficiency (K_{abs}) for three values of complex refractive index, m = n + in'. (Green light, λ = 500 nm.)

2.3.2. Size Distributions

Using a Coulter Counter, Sheldon and Parsons (56) measured the size distribution of particulate matter in Saanich Inlet, British Columbia (Figure 2-14). The resulting curve represented a mixture of inorganic and organic (both living and dead) particulates. The maxima indicated blooms of various planktonic species, confirmed by microscopic examination.

Plankton are traditionally grouped into three size categories, nanno-, micro-, and macroplankton (56). The greatest biomass in the Saanich Inlet sample occurred among the nannoplankton (unidentified). The microplankton consisted mainly of copepod eggs and two diatoms, Chaetoceros socialis and Chaetoceros debilis. A portion of the macroplankton were represented by the copepod Pseudocalanus minutus.

The Coulter Counter actually measures particle volume (Section 3.2). Particle diameters determined by Coulter counting refers to that of a sphere with the same volume. For example, microscopic measurements of the two diatoms (56) showed that C. socialis consisted of 30-cell chains, each cell 10 microns in diameter (or 16,000μ^3 per chain). C.debilis had about 20 cells per chain, each cell 20 microns in diameter (84,000μ^3 per chain). The calculated chain volumes correspond to equivalent sphere diameters of 31 and 54 microns,

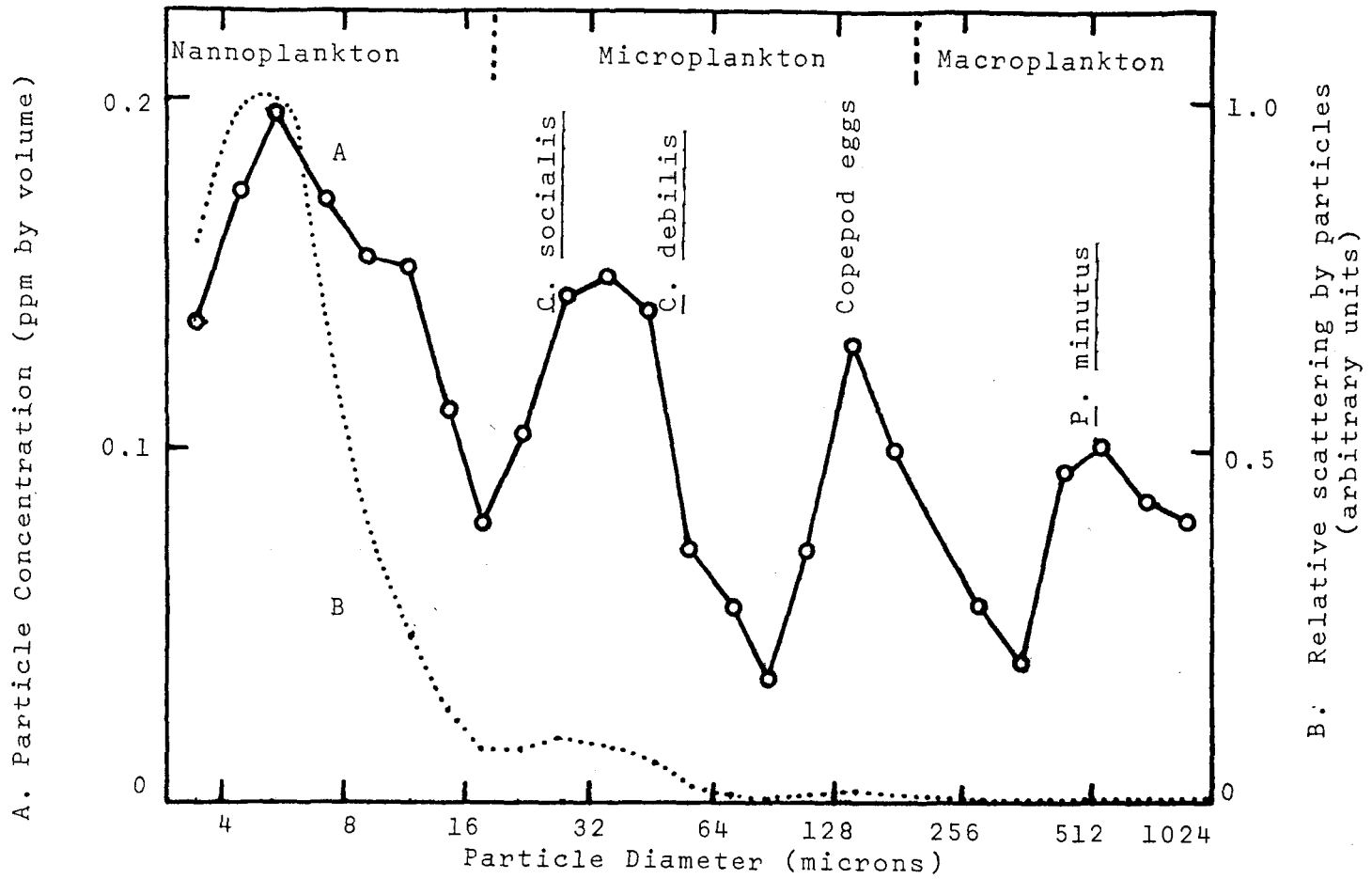

Figure 2-14. Particle size distribution (A) and relative particle scattering (B) for an ocean water sample from Saanich Inlet taken in June 1966. Size distribution data from Sheldon and Parsons (1967) Assumptions for scattering calculations: n = 1.05, λ = 500 nm.

comparing favorably with the Coulter determined diameters (Figure 2-14).

Particle scattering as a function of diameter, b_i (equation 2-5), was calculated for the Saanich Inlet particles using n = 1.05 and λ = 500 nm.. (curve B, Figure 2-14). Particles larger than 16 microns in diameter do not significantly contribute to total scattering. Gordon and Brown (19) concluded that the number of particles with diameters greater than 20 microns in the Sargasso Sea were optically insignificant. Calculations in Chapter 4 show that 20 microns also represents an upper limit of optical significance for California coastal waters.

In the optically important size range, coastal water and open ocean water particle concentrations differ by one to two orders of magnitude (Figure 2-15). Terrestrial runoff, wave action,entrained bottom sediments, nutrient-stimulated phytoplankton production and municipal waste discharges represent possible causes of coastal turbidity. For example, the discharge of untreated sewage by the cities of Halifax and Dartmouth enriched the waters inside Bedford Basin relative to waters outside the channel entrance (48). Nannoplankton-size particle concentrations were 3 to 4 times greater inside the basin (Figure 2-15).

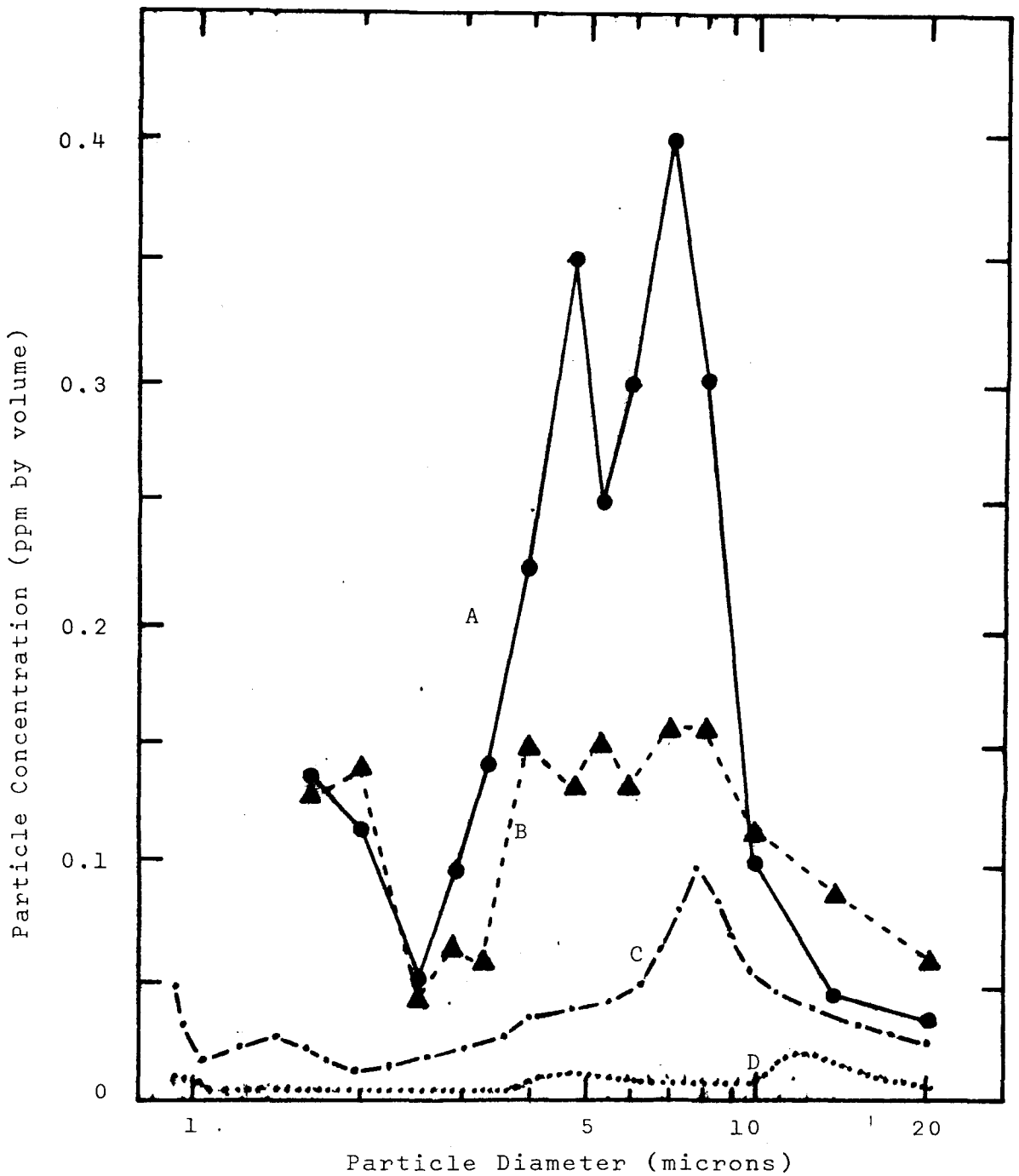

Figure 2-15 . Contrasting ocean particle size distributions.
A. Inside Bedford Basin, Nova Scotia
B. Outside channel entrance to Bedford Basin (A/B,samples from 5 m. deep, Poulet,1973)
C. Chilean coast, 35°S, 73°W
D. Equatorial Pacific, 10°S, 150°W (C/D, near surface samples, Sheldon, Prakash, and Sutcliffe, 1972)

Particle concentrations in the nutrient-poor open ocean waters of the Equatoral Pacific (Figure 2-15) and the Sargasso Sea (55) can be less than 0.02 ppm throughout the nannoplankton size range. This compares with peak values of 0.1 and 0.4 ppm for the Chilean coast and Bedford Basin (Figure 2-15). Values for polluted waters greater than 4 ppm are reported in Chapter 4.

2.3.3 Carbon Isotope Composition

Carbon isotopic composition indicates the origin of marine particulates. Terrestrial plants are in constant equilibrium with atmospheric CO_2. The dissolved CO_2 utilized by marine plants is partially supplied by air-sea exchange. When the exchange rate is insufficient, however, the CO_2 demand is satisfied by the reaction

(2-12) $$HCO_3^- \rightarrow CO_2 + OH^-$$

according to carbon dioxide-bicarbonate-carbonate (dissolved CO_2 - HCO_3^- - $CO_3^=$) equilibrium requirements. Bicarbonate in sea water has a higher carbon isotope ratio (C^{13}/C^{12}) than atmospheric CO_2. Accordingly, it has been shown that carbon photosynthetically fixed in the ocean has a higher C^{13}/C^{12} ratio than terrestrially fixed carbon (41).

Differences in C^{13}/C^{12} ratio are used in Chapter 4 to indicate a terrestrial influence on suspended particles (e.g., land runoff, waste discharge or airborne fallout). Isotopic data of this type are typically reported as δ_{PDB}-values (41):

(2-13) $$\delta_{PDB} = 1000 \left(\frac{R_s}{R_o} - 1\right)$$

where $R_s = C^{13}/C^{12}$ of the filtered ocean particulates

$R_o = C^{13}/C^{12}$ of a reference sample prepared from a Cretaceous belemnite, Belemnitella americana, found in the Peedee formation of South Carolina (hence the subscript, "PDB")

Typical values for δ_{PDB} vary from -25 for recent fresh water deposits to 0 for marine limestones (Table 2-2). Land organic carbon ($\delta_{PDB} \simeq -25$) is five units lighter than marine organic carbon ($\delta_{PDB} \simeq -20$). This difference is consistent with the 7 unit difference between atmospheric CO_2 and bicarbonate in sea water.

Table 2-2. Dependence of δ_{PDB} upon carbon reservoir (41)

Carbon Reservoir	Typical δ_{PDB} Values
Marine Limestones	0%
Bicarbonate in Sea Water	0
Atmospheric CO_2	- 7
Marine Organic Carbon	-20
Recent Marine Sediments	-20
Land Organic Carbon	-25
Recent Fresh Water Deposits	-25

CHAPTER 3

PROCEDURES AND APPARATUS

3.1 Field Work

Field data were acquired using small open vessels (primarily 18 foot and 22 foot boats manufactured by Thunderbird Products, Inc., Paso Robles, California). For the work at Palos Verdes, a boat was trailered from Pasadena and launched at San Pedro, a 15 minute boat ride from the LACSD sewer outfall. For work at the various background stations, other arrangements were made. At Corona Del Mar and Dana Point stations, the Caltech Marine Laboratory boats were used (moored in Newport Harbor). For work in distant areas (such as Morro Bay and Humboldt Bay) a commercial fishing vessel was chartered.

Once on station, the boat was anchored (water depth permitting) and water depth was determined by sounding or the use of various fathometer systems (manufactured by either Bendix or Seafarer). A transmissometer and water sampler (both manufactured by Hydro Products, San Diego) were lowered into the water to measure light beam attenuance and to acquire water samples for laboratory analysis. The depth of the measurement and sampling was monitored by length of line payout (the transmissometer had 200 feet of cable), accounting for plumb angle(angle from vertical) errors. Occasionally

the length of line payout was monitored on the fathometer.

The mean spectral response of the transmissometer (Model 612 S) is at 514 nm (Figure 3-1). Functionally described in Section 2.2.3, the instrument has a collimated light beam and a detector that measures the attenuation of light per meter of ocean path length. The spectral response represents a convolution of the light source power spectrum and the detector response spectrum. This would be measured in air (i.e. without the spectral absorption effects of water) by placing a series of narrow bandwidth filters of known transmittance in the beam path and measuring the instrument output as a function of filter wavelength. The spectral response curve was supplied by the manufacturer.

Field trips were scheduled such that data were acquired during high sun angles (between 11 a.m. and 1 p.m.). Weather permitting (cloud free skies and safe sea conditions) a dive was performed to acquire sunlight irradiance data as a function of water depth. Standard SCUBA diving gear was used. A line with loops was lowered into the water. By placing an arm into a loop a constant depth was maintained while measuring the downwelling (earthward) and upwelling (skyward) irradiance. The depth was determined by knowing the distance between loops. Depth values were occasionally compared with diver depth gauge measurements.

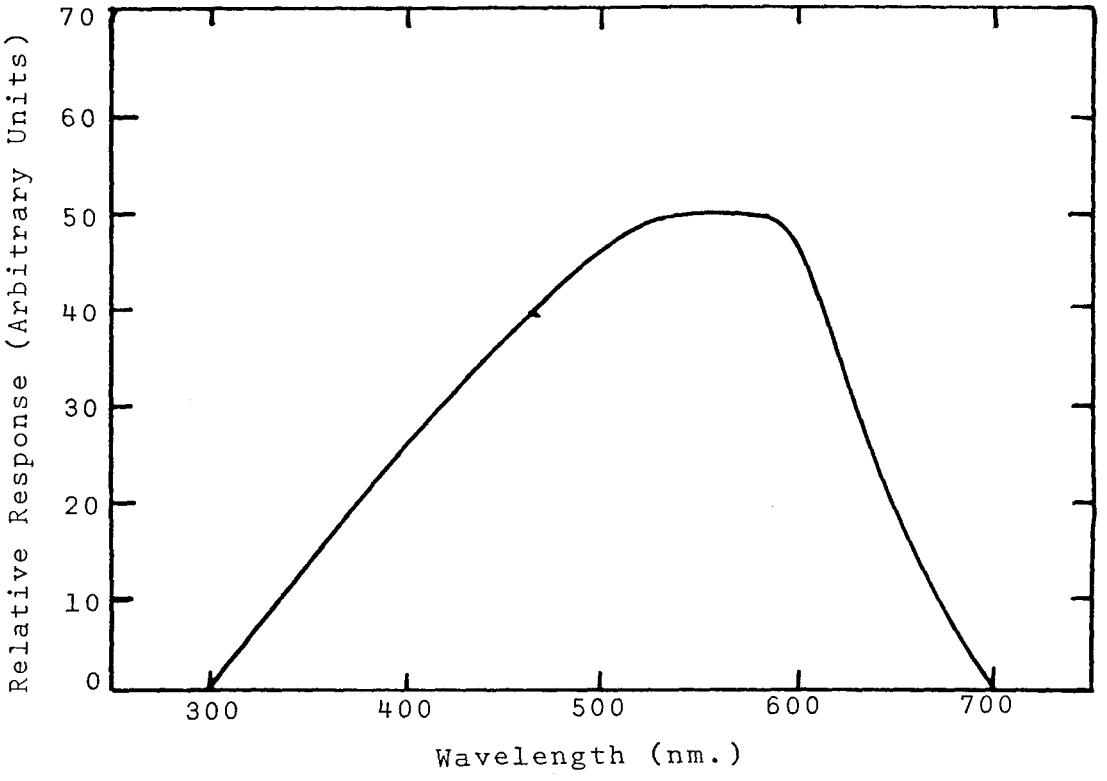

Figure 3-1. Transmissometer spectral response. Mean wavelength = 514 nm.

The device for measuring irradiance was designed and described by North (32). It incorporated a series of Weston Master V light meters as sensors. Each was fitted with a combination of interference filters designed to transmit a narrow portion of the visible spectrum (Figure 3-2). A thin sheet of opalescent plastic was affixed to the outside of the watertight case to serve as a diffuser. The system was calculated for response as a function of percent of full scale irradiance using a series of neutral density filters. A porous plastic sheet served as a writing surface for recording meter values and was affixed to the reading side of the instrument.

Temperature as a function of depth was measured either with a mercury thermometer during the dive or, when available, a temperature probe was lowered with the transmissometer and temperature was recorded on deck.

3.2 Laboratory Work

Samples from three field trips were analyzed by E. Myers for particulate percent organic carbon and particulate carbon isotope ratio. Procedures and apparatus are described in his thesis (41).

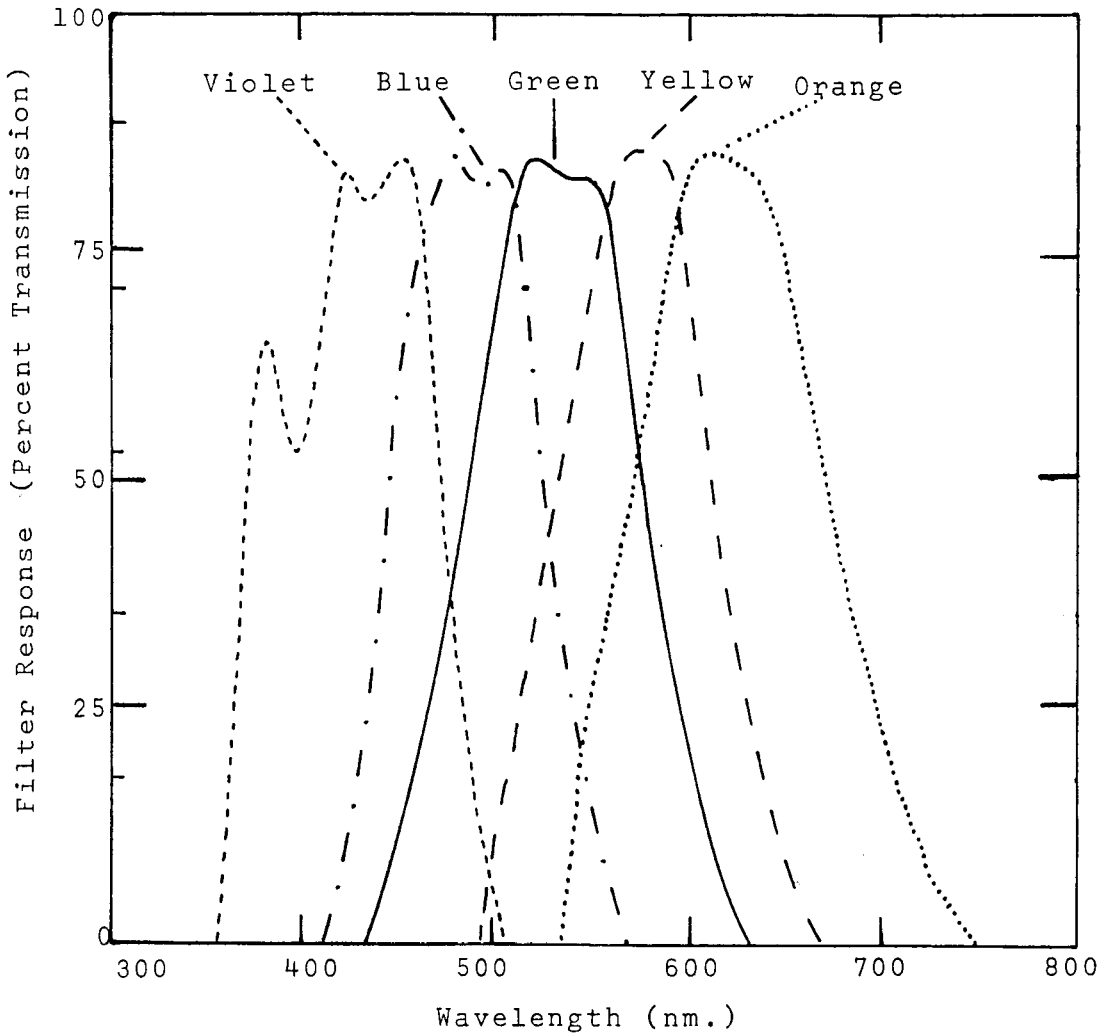

Figure 3-2. Spectral response of irradiance meter filters.

Water samples were routinely analyzed for suspended particle concentration in the Ocean Systems Department Laboratory, TRW Systems, Redondo Beach. During transmittal from the ocean station, samples were stored in a light tight box at 10 to 15°C. Typical travel time from the LACSD outfall stations to the laboratory was 1-2 hours. Water sample collection was the final task performed at each station to minimize storage time before analysis. In general, only one station was visited per field trip. Travel time was one hour longer from the Orange County stations (Corona Del Mar and Dana Point). From more distant stations (Morro Bay and Humboldt Bay water samples were flown to the Los Angeles area by light aircraft. Travel time to the laboratory for distant stations was 6-8 hours.

Changes in particle size distribution as a function of sample storage time were analyzed. Water samples were collected off the Hermosa Beach Pier and driven to the laboratory. Analysis began 30 minutes after collection. Measurements were repeated at 1, 2, 4, 8, 12, and 24 hours. Significant changes (15 to 20 percent) occurred in the number of 1 to 5 micron diameter particles after 24 hours. Measurement errors were 5 to 10 percent after 8 hours.

These additional particles were presumably due to aggregates of bacteria. In a sample of well filtered ocean water from Departure Bay, British Columbia, (0.22 micron

filters), Sheldon, Evelyn, and Parsons (58) demonstrated a growth of 1.5 to 4 micron particles after 24 hours. They attributed the phenomenon to growth of bacterial aggregates. The growth amounted to a total particle volume concentration change of 0.02 ppm in 24 hours. This amount is small compared to the concentrations encountered in this study (0.3 to 4.0 ppm).

Particle size distributions were measured using a particle counter manufactured by Coulter Electronics Corporation, Hialeah, Florida. Operation of the instrument is described by Sheldon and Parsons (57). Seawater and suspended particles are caused to pass through a glass aperture (very small round hole). Simultaneously an electrical current is driven through the aperture by two electrodes. Changes in resistivity at the aperture are caused by particles passing through the aperture. The change in resistivity is proportional to the particle volume and results in a proportional change in voltage at the constant current source. An electrical pulse height analyzer counts the number and size of particles. The instrument is designed to stop counting after a known volume of fluid has passed through the aperture.

The instrument was recently purchased by TRW Systems. It is a new model (Model 2Z) especially designed for marine work. Automatic compensation provides for changes in salinity.

The size distribution was measured over the diameter range 0.5 to 20 microns. Particle diameters greater than 20 microns were assumed to be optically insignificant (Section 2.3.1). Instrument noise prohibited measurement of smaller diameters. Since the Coulter Counter actually measures particle volume, particle diameter refers to that of a sphere with the same volume.

The use of three different aperture sizes was required. Coulter specifies that the noise free diameter range for each aperture should be 2 to 40 percent of the aperture diameter. This specification evidently fails for the very small aperture. Aperture diameters used and corresponding noise free diameter ranges were as follows:

1) 11 micron aperture, diameter range 0.5 - 4 microns
2) 30 microns aperture, diameter range 0.8 - 10 microns
3) 100 micron aperture, diameter range 2 - 40 microns

The 11 micron aperture was the smallest manufactured by Coulter. It clogged easily and was not used routinely. It was especially useful, however, in determining whether there was a maximum in the particle size spectrum between 0.5 and 1 micron (there wasn't, see Figure 4-19). Routine measurements were made over the diameter range 0.8 to 20 microns.

Polystyrene latex particles of known size were used to calibrate the output of the pulse height analyzer. The

instrument incorporated a logerithmic scale for the particle size determination. Therefore, only two calibration particle sizes were required for each aperture calibration. A third size was added to test the accuracy of the log scale. The determination of the third size agreed to within 5 percent of the particle manufacturer's determination. The three calibration particle diameters used for each aperture were as follows:

1) 11 micron aperture; 0.71, 1.1, and 1.3 microns

2) 30 micron aperture; 1.3, 3.5, and 5.7 microns

3) 100 micron aperture; 3.5, 5.7, and 9.5 microns

Before each run a sample was filtered with a 0.22 micron millipore filter to test for noise levels due to electrical or possible physical sources (such as bubbles). The measurement of especially turbid samples required dilution with the filtered seawater. All three apertures had overlapping size ranges. Results were compared for the 30 and 100 micron apertures in the overlapping diameter range, 2-10 microns. The standard error of estimate using results from both apertures was 0.08 ppm over 76 measurements.

CHAPTER 4

EXPERIMENTAL RESULTS

4.1 Introduction

The experimental results presented in this chapter are grouped into two main sections. The first (Section 4.2) deals with sunlight propagation. The second (Section 4.3) is concerned with optical and physical properties of particles.

Section 4.2 presents multi-color measurements of sunlight propagation into municipally polluted and into relatively clean coastal waters. In each case correlative data are presented depicting vertical temperature profiles, transmissometer readings and suspended particulate load. Comparisons are made between natural and polluted water environments as related to sunlight penetration, depth of the euphotic zone, and color information at the water surface that might be utilized for remote sensing of pollutants. To determine if natural and polluted waters differ with respect to optical albedo (ratio of scattering to total attenuation), sunlight irradiance measurements are plotted as a function of optical ocean depth.

Section 4.3, treating particle properties, is divided into five parts:

1) particle size distributions--environmental background data showing the range of particle sizes and numbers sampled by this investigation including differences between polluted and natural samples,
2) vertical distributions of particulate concentrations--differences between polluted and natural waters,
3) particulate optical densities--correlations between concentrations of particulates and total attenuation coefficients,
4) particle scattering and absorption--estimates of particle refractive index, calculation of particle scattering and absorption assuming real and complex refractive indices, and
5) physical-chemical investigations--correlations between particle density (mass per volume) and two chemical parameters (percent organic carbon and carbon isotope ratio).

4.2 Sunlight Propagation in Polluted and Natural Waters

4.2.1 Field Station Locations

Six field stations were selected along the Los Angeles and Orange County coastline to study sunlight propagation in natural and polluted coastal waters (Figure 4-1). Station 1 at Whites Landing on Catalina Island and Station 2, about four miles off Dana Point in Orange County, represented background conditions. Both sites are more than ten miles from a major sewer outlet. The bottom at Catalina was a mixture of rock and sand. Depth at the Dana Point station exceeded 600 feet so surface waters were not affected by the bottom. The site was off a submarine canyon that experiences a moderate amount of natural terrestrial runoff.

Station 3, at Rocky Point, was eight nautical miles westerly from the LACSD sewer outfall. The site was sufficiently far from the outfall to be relatively clean yet close enough to have a similar bottom and coastal structure. Station 3 and the outfall area usually experience similar currents and waves. Thus suspended load and sunlight conditions at Station 3 should represent Whites Point without the outfall installation.

The remaining three stations were strongly influenced by the LACSD outfall. Station 4 was at Bunker Point, about a mile westerly from Whites Point. Stations 5 and 6 were

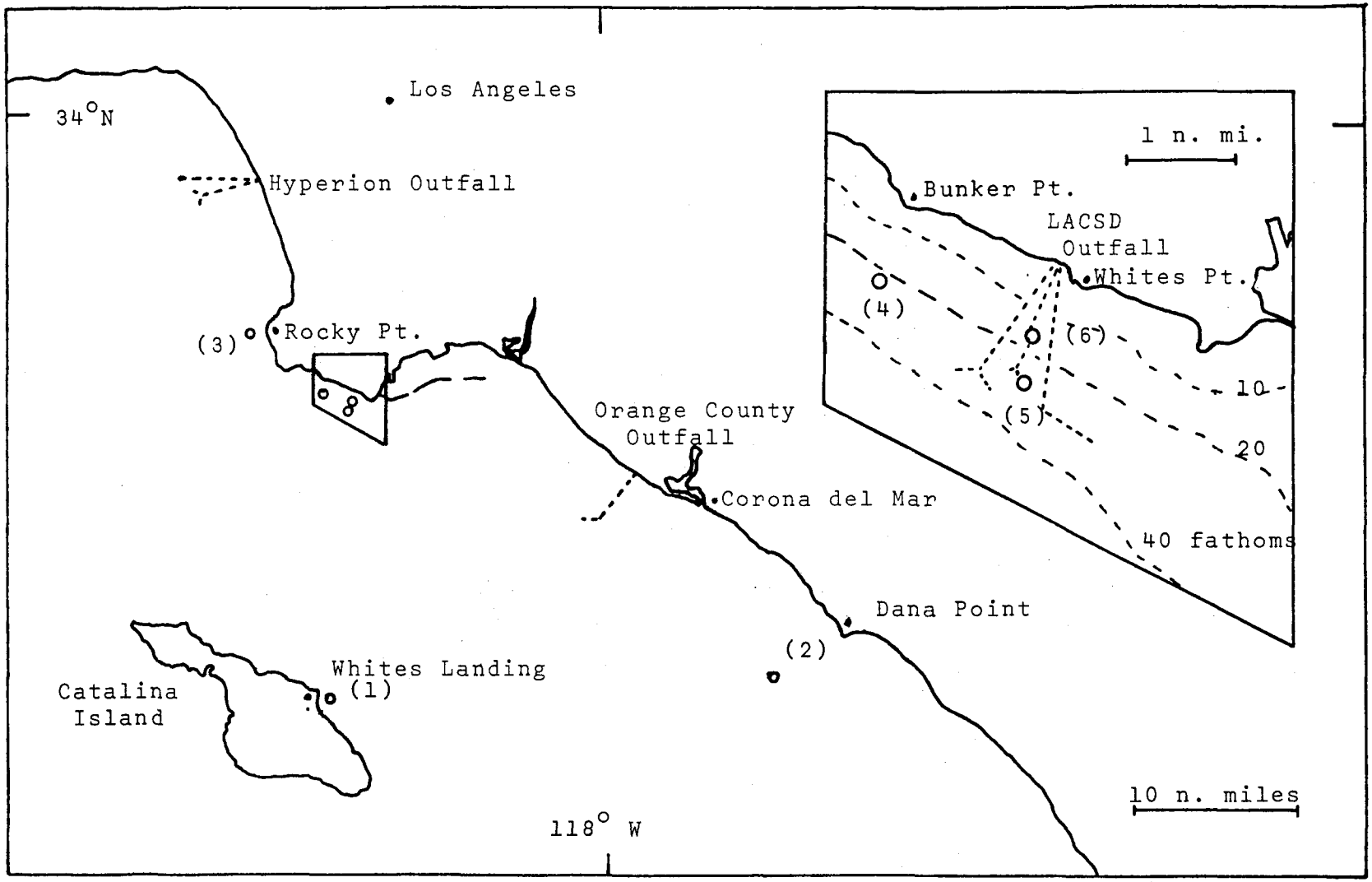

Figure 4-1. Data Station Locations

at Whites Point midway between the two main diffuser pipes, approximately 1 1/4 and 3/4 miles from the shoreline.

4.2.2 Sunlight Irradiance Data

Results of the field measurements were divided into two groups, the three natural background stations and the three sites near the outfall (Figures 4-2 through 4-13). Each station yielded the following data:

1) Date and time of day to nearest hour
2) Corresponding sun zenith angle to nearest 5 degrees
3) Bottom depth and distance from shore (feet and miles)
4) Vertical temperature profile (^{o}C)
5) Vertical transmissibility profile (percent/meter)
6) Vertical profile of the suspended particulate load (ppm by volume for particles ranging in diameter from 0.8 microns to 20 microns)
7) Vertical profiles of downwelling and upwelling sunlight irradiance in four colors, presented as percent of downwelling irradiance at the ocean surface (as measured just below the surface).

Particle size spectra are presented in tabular form in Appendix B.

Station 1: Whites Landing, Catalina, 1/19/73, bottom depth: 130 feet (natural background site, weak thermocline, uniform turbidity), Figures 4-2 and 4-3.

The temperature profile depicted a shallow winter thermocline of low intensity while the transmissometer indicated a vertically homogeneous suspended particulate load at a level of turbidity moderate for natural coastal conditions. A single water sample was taken at 50 feet. Coulter Counter measurements indicated a suspended load of 0.71 ppm.

Optically, this represents a simple, non-stratified case. Visibility observations during the dive (a dive was required for measuring irradiance using the hand held photometer package described in Chapter 3) indicated a green ocean with no detectable stratification. The irradiance data confirmed these observations. All colors showed a relatively constant diffuse attenuation coefficient (constant slope on the semi-log irradiance plot) for both downwelling and upwelling light, except for reduced values in the upwelling data near the surface. The downwelling color was predominately green. Green and blue decayed with depth at equal rates. Decay rate for yellow wavelengths exceeded blue, green and violet at all depths.

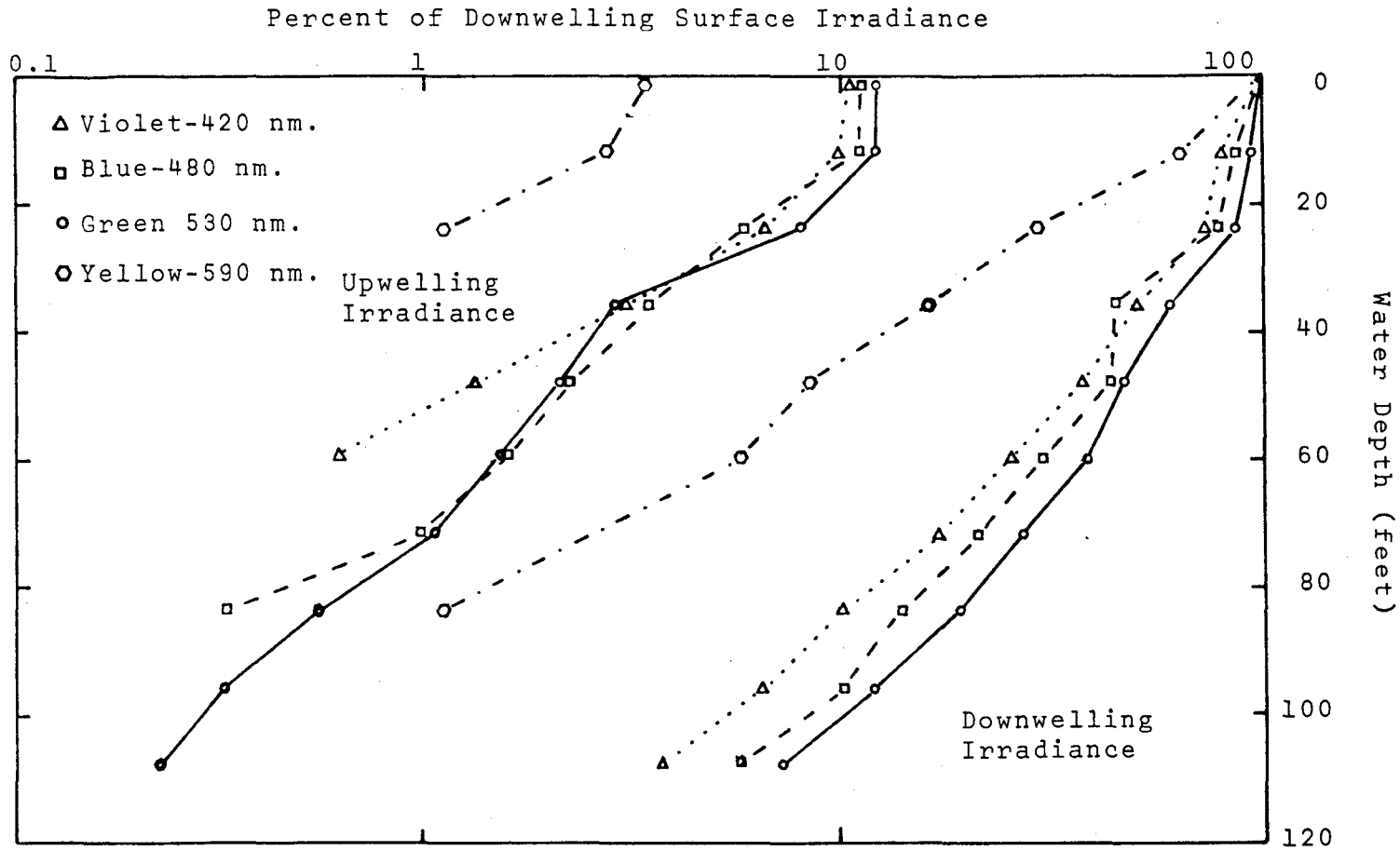

Figure 4-2. Downwelling and Upwelling Irradiance Profiles (Station 1)

Whites Landing, Catalina (¼ mile offshore, 1/19/73, 11 a.m.)
Bottom Depth: 130 feet
Sun Zenith Angle: 50°

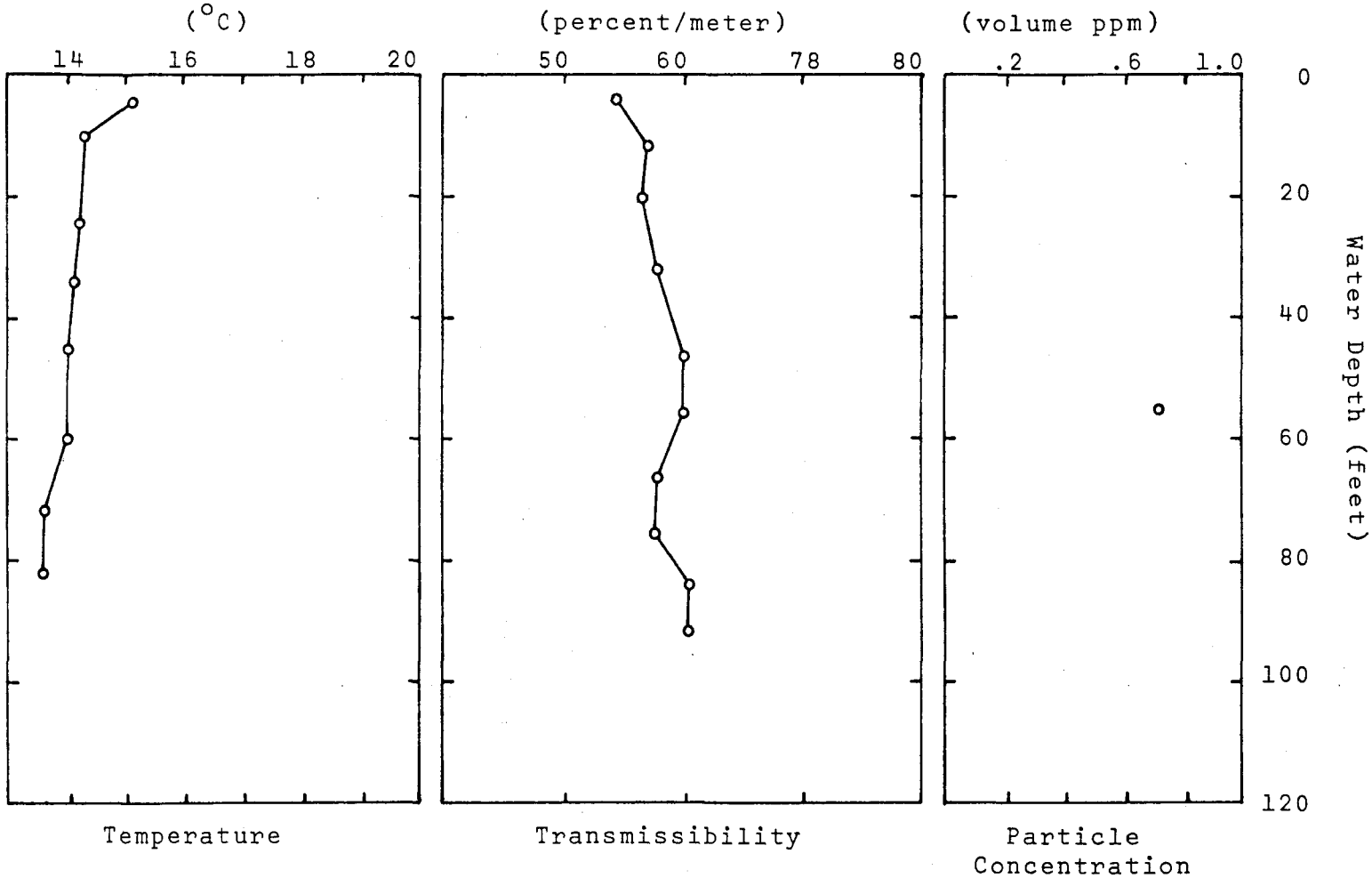

Figure 4-3. Temperature, Transmissibility and Particulate Volume Profiles. Station 1, Whites Landing, Catalina, 9/19/73.

Station 2: Dana Point, 5/15/73, bottom depth: >600 feet (natural background site, strong thermocline, productive surface waters, clear deep waters) Figures 4-4 and 4-5.

The early summer data showed a strong four degree thermocline. The transmissometer and suspended load measurements showed stratifications that correlated with the thermocline depth. Profiles were typical for a moderate phytoplankton bloom. Suspended load and turbidity peaked in the depth range 10 to 30 feet. Waters below the thermocline were very clear for coastal environments. The sea floor depth was too deep for entrained bottom sediments to affect transmissibilities at 150 feet. The 75 percent/meter transmissibility measured beneath the thermocline was the highest value obtained during this study. This compares with values greater than 90 percent/meter in the Sargasso Sea (25). The suspended particulate load off Dana Point was 0.2 ppm. This was the lowest value encountered in this coastal survey. Values as low as 0.02 ppm occur in the Sargasso Sea (55).

The irradiance profiles showed strong enhancement for green wavelengths in the surface layers, presumably due to chlorophyll absorption. Below the thermocline, blue and green were attenuated equally. Diving observations indicated

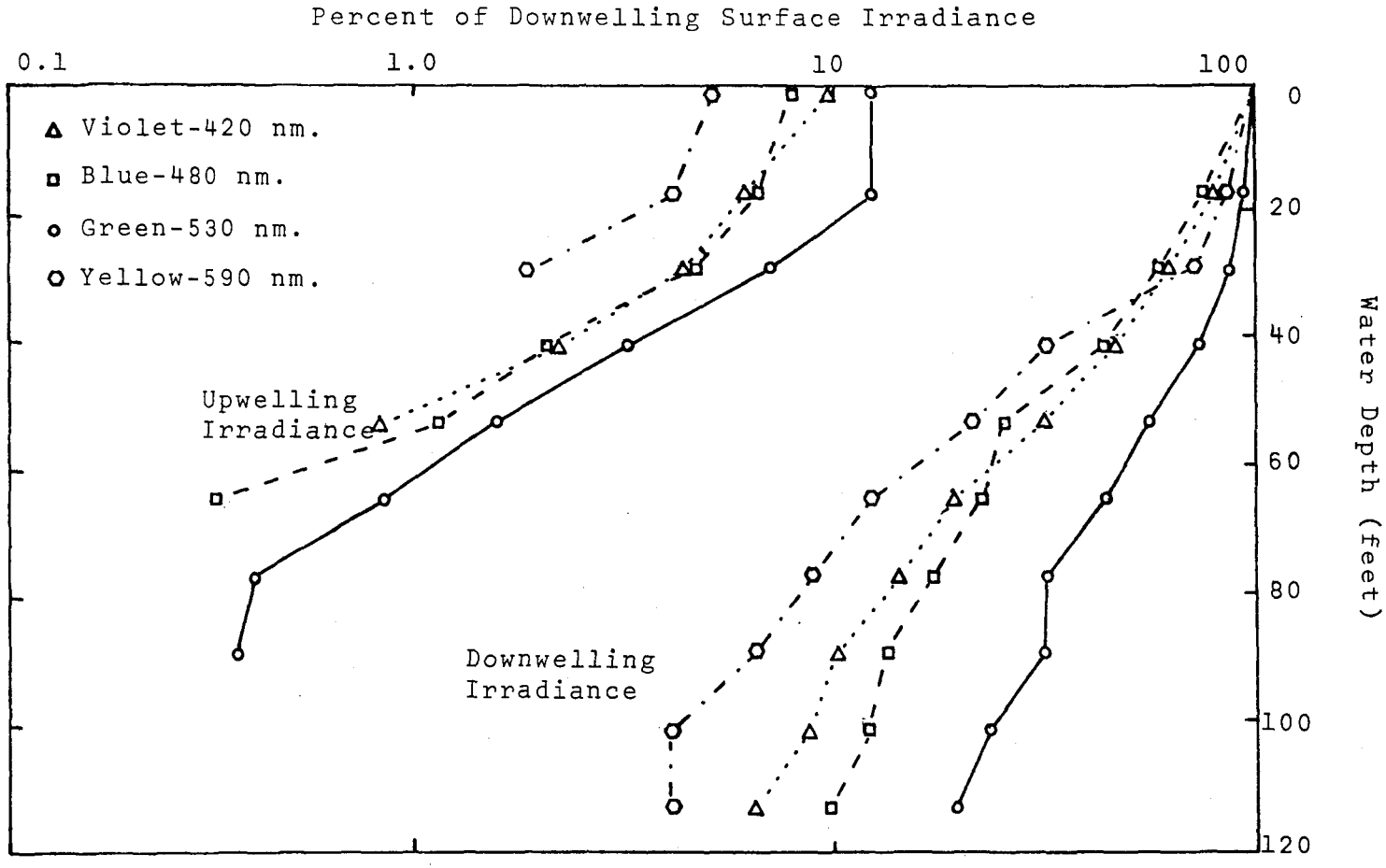

Figure 4-4. Downwelling and Upwelling Irradiance Profiles (Station 2)

Dana Point (4 miles offshore, 5/15/73, 1 p.m.)
Bottom depth > 600 feet
Sun Zenith Angle: 15°

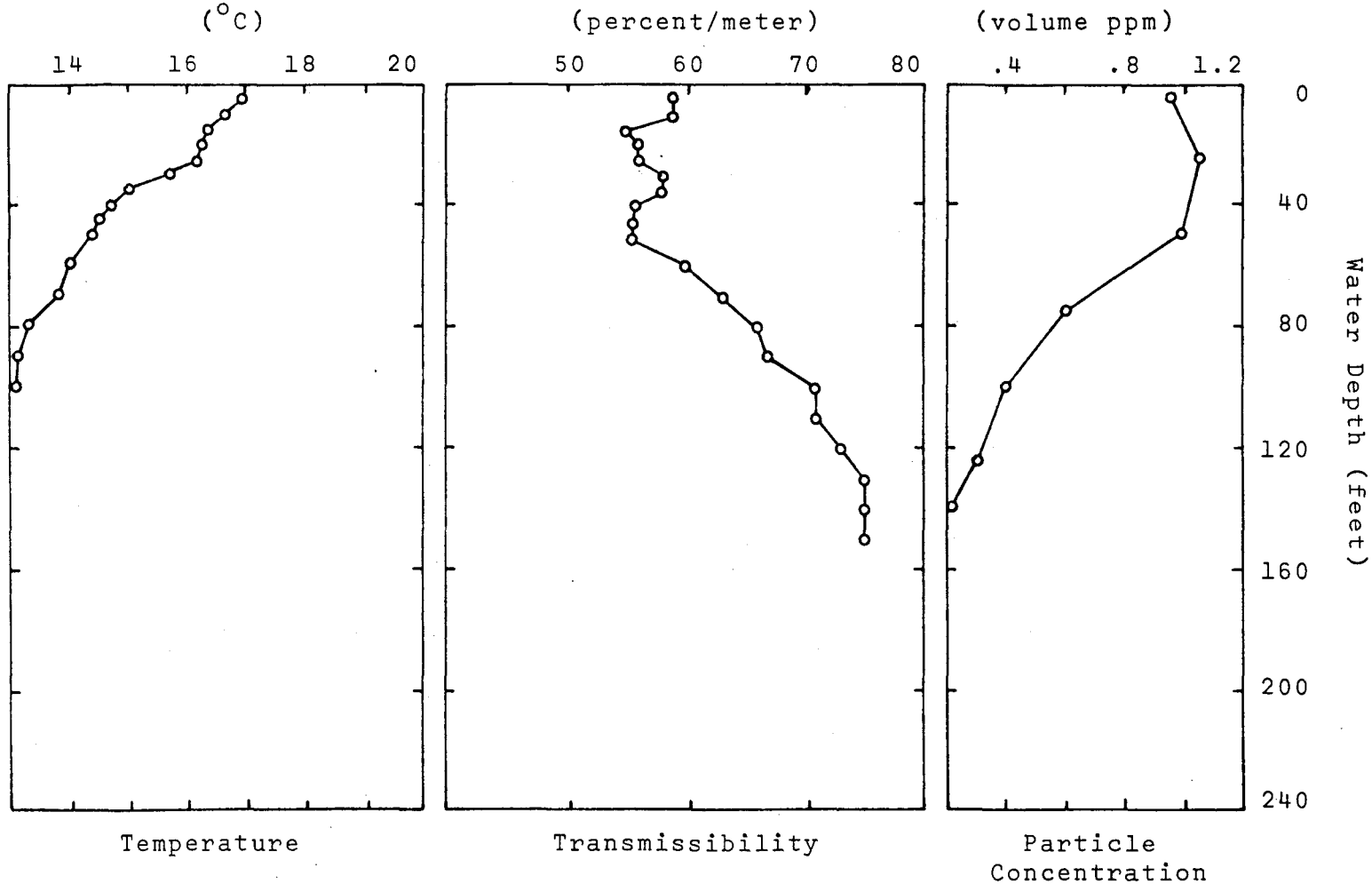

Figure 4-5. Temperature, Transmissibility and Particulate Volume Profiles. Station 2, Dana Point, 5/15/73.

a sharp transition from blue-green to blue at a depth of 75 feet. Visibilities exceeded 100 feet below the transition.

Station 3: Rocky Point, 11/29/72, bottom depth: 100 feet (no thermocline, uniform light turbidity, upwelling conditions), Figures 4-6 and 4-7.

By the end of November the summer thermocline had disappeared at Rocky Point. Both the transmissometer and temperature profiles were fairly uniform. Transmissibility increased slightly with depth. Suspended particulates caused slightly higher turbidity in the upper layers,presumably due to phytoplankton or suspended bottom sediments.

The fraction of suspended load due to non-living particulates was greater than experienced at Stations 1 and 2. There were strong Santa Ana (off shore) winds during the study period,possibly causing upwelling or introducing particulates of terrestrial origin. The temperature profile was typical for upwelling conditions (cold and uniform). Seas were calm and underwater visibility uniformly good. Suspended particulates gradually increased below 50 feet, indicating bottom entrainment. Reduced attenuance in the blue and violet relative to green suggested a lower fraction of chlorophyll pigmented plant material .

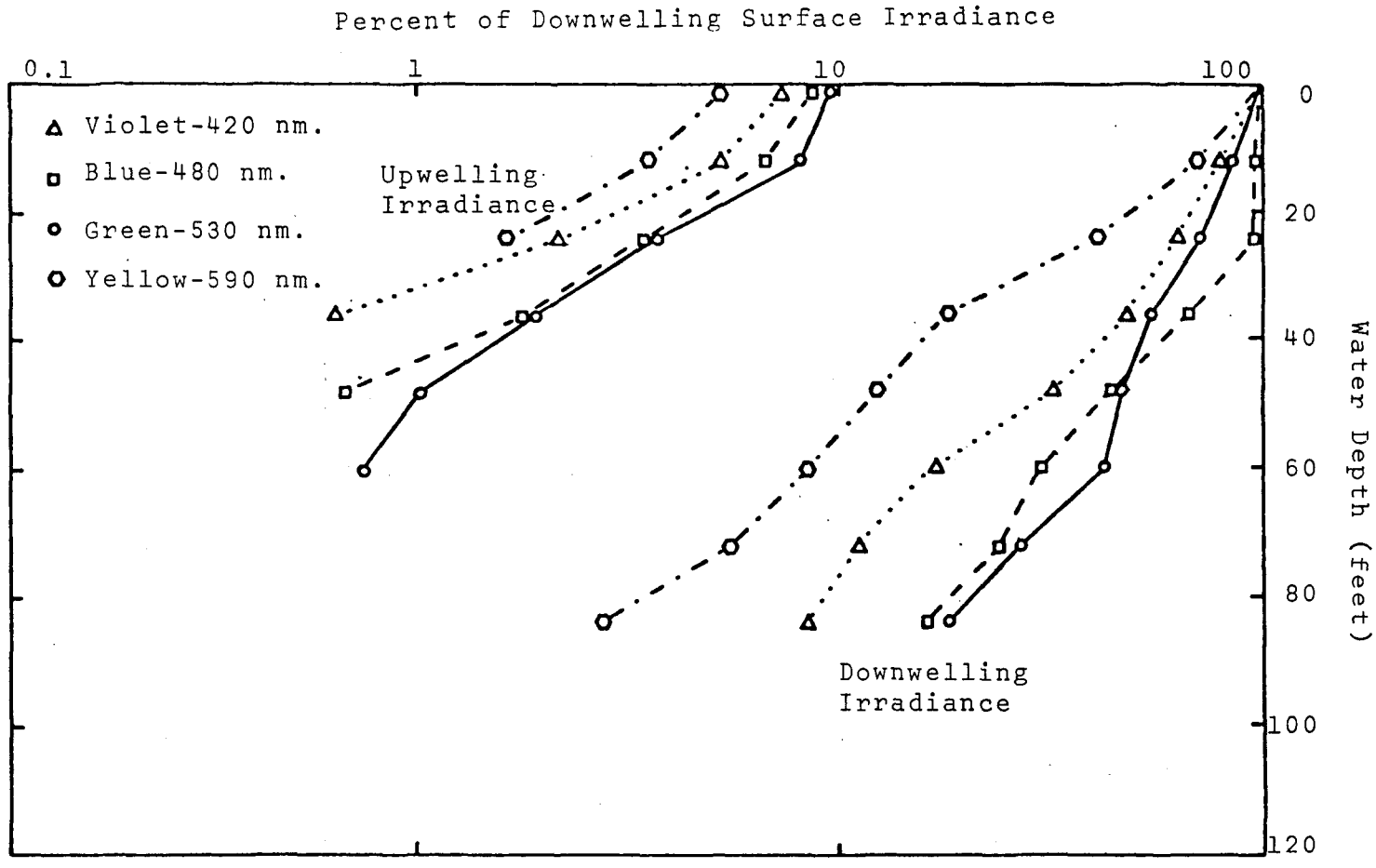

Figure 4-6. Downwelling and Upwelling Irradiance Profiles (Station 3)

Rocky Point (1 mile offshore, 11/29/72, 11 a.m.)
Water Depth: 100 feet
Sun Zenith Angle: 55°

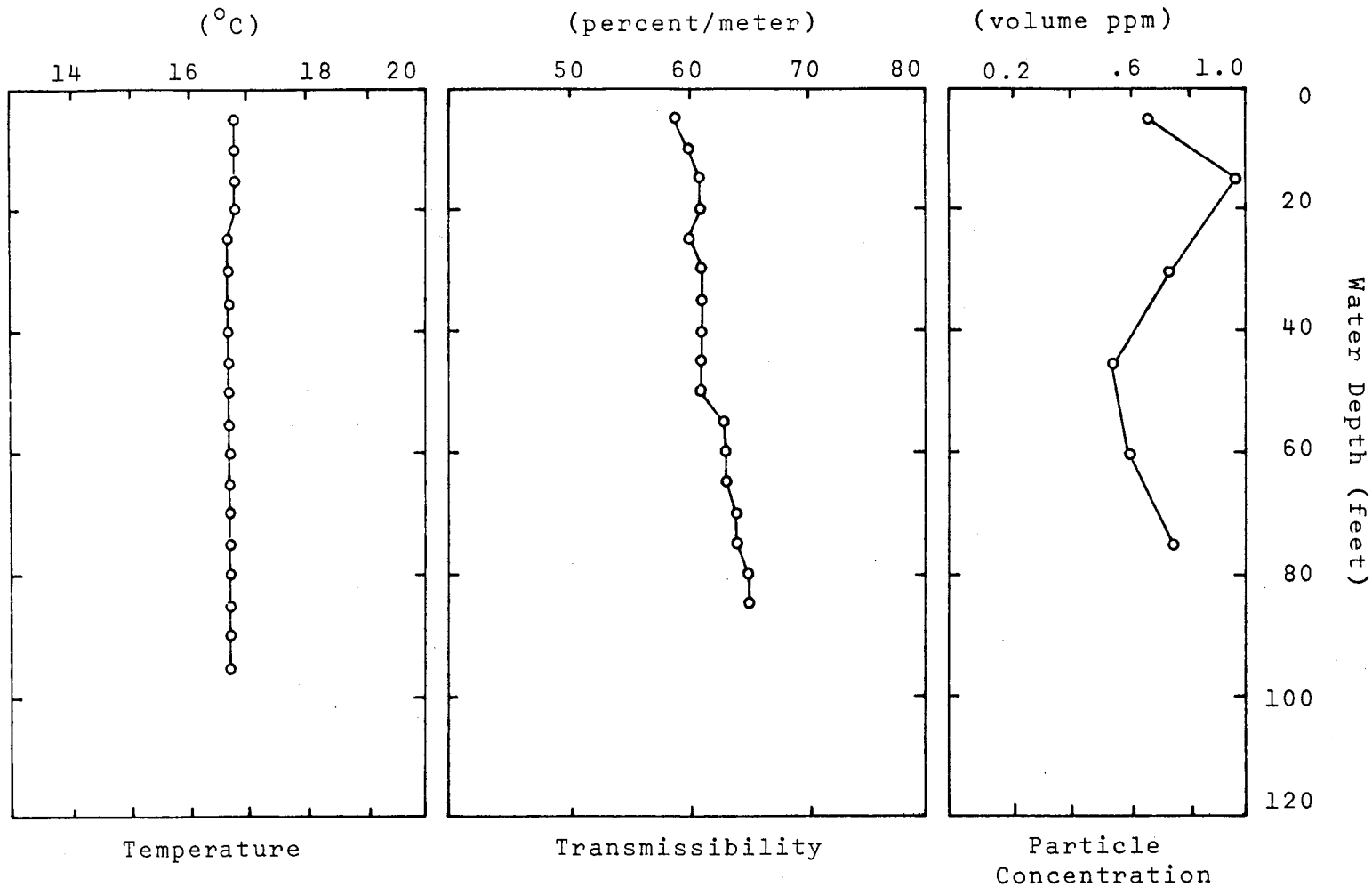

Figure 4-7. Temperature, Transmissibility and Particulate Volume Profiles. Station 3, Rocky Point, 11/29/72.

Station 4: Bunker Point, 10/12/73, bottom depth: 125 feet (strong thermocline, turbid sewage field held beneath thermocline), Figures 4-8 and 4-9.

There was a typical late-summer, strong thermocline. The transmissometer indicated moderately turbid waters above the thermocline and very turbid conditions in the sewage field below the thermocline. The suspended sediment profile peaked at 15 feet, suggesting a layer of phytoplankton material in the upper layers. The suspended load was greatest in the upper layers. But the transmissometer indicated less attenuance in the upper layers than in the subthermocline sewage field. This suggests a large amount of light-absorbing dissolved material was present in the sewage field.

Blue and violet were enhanced in the top 20 feet. A transition to green occurred from 20 to 50 foot depths due to absorption by phytoplankton chlorophyll. Diffuse attenuance increased dramatically below 50 feet for all colors due to the sewage plume. Upwelling blue and green irradiance was fairly constant down to about 40 feet where the sewage field began. Most of the upwelling light at this station was thus due to backscattering by particulates in the sewage field (as if the sewage field was a diffuse reflector).

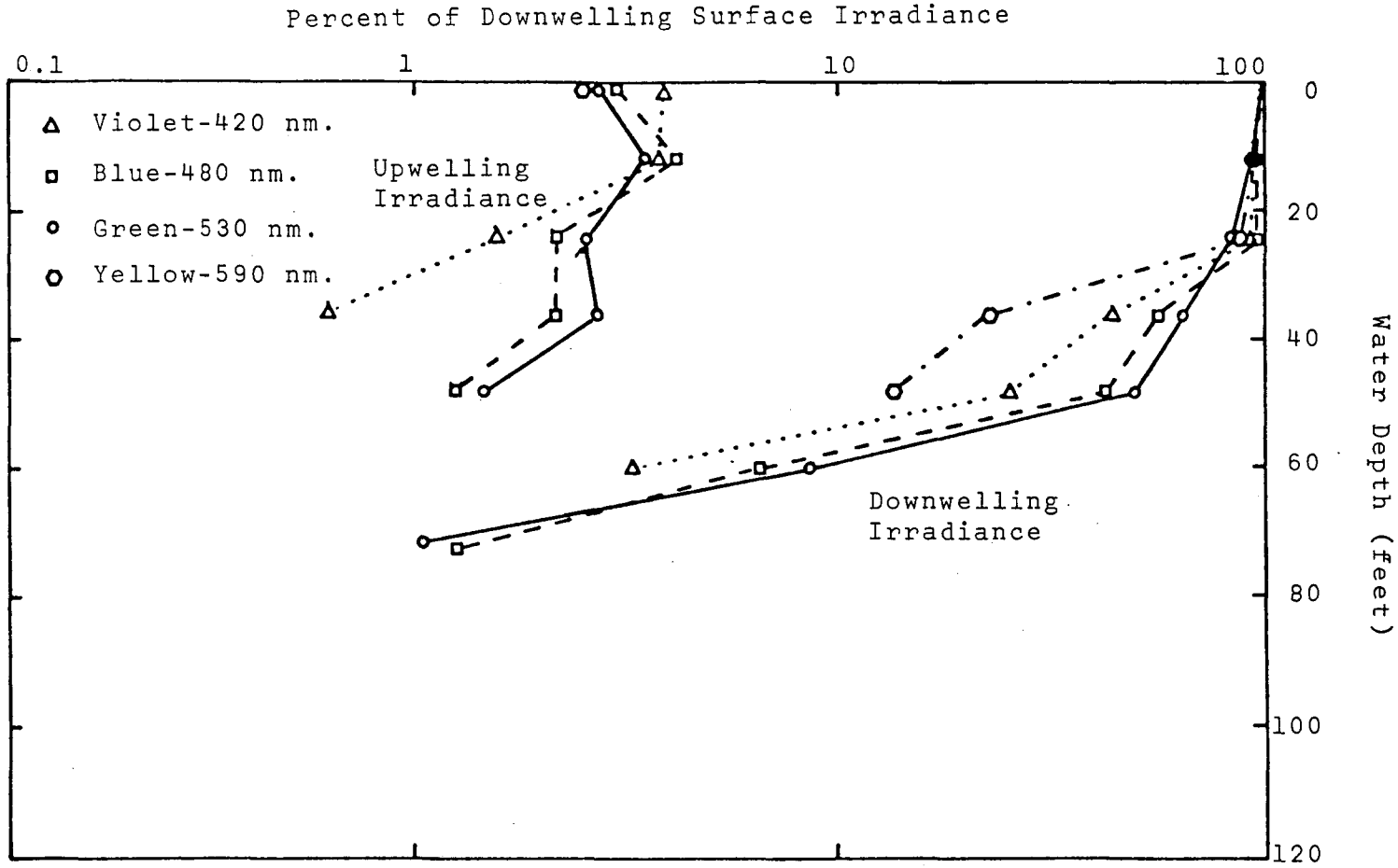

Figure 4-8. Downwelling and Upwelling Irradiance Profiles (Station 4)

Bunker Point (3/4 miles offshore, 10/12/72, 12 noon)
Bottom Depth: 125 feet
Sun Zenith Angle: 40°

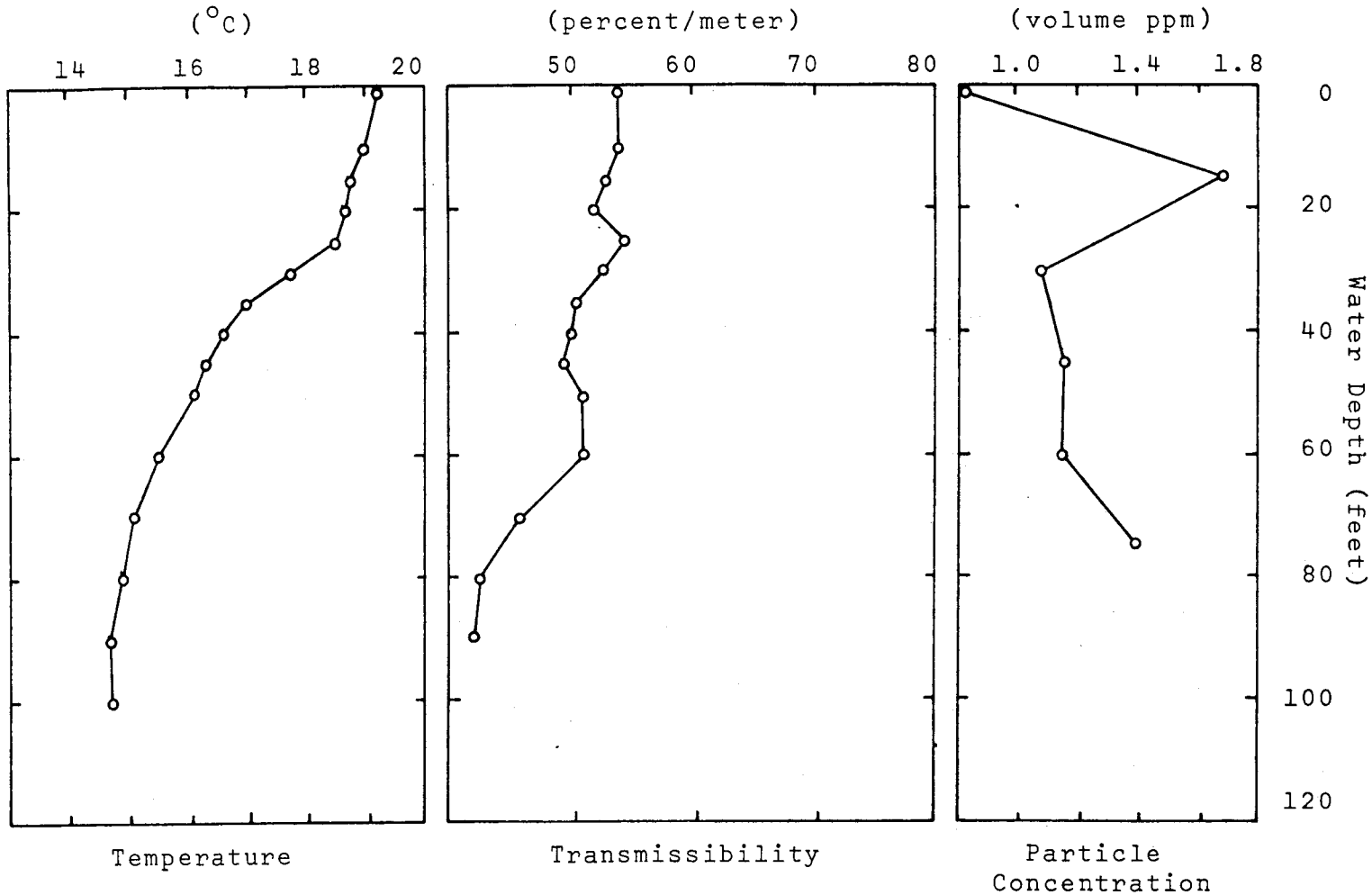

Figure 4-9. Temperature, Transmissibility and Particulate Volume Profiles. Station 4, Bunker Point, 10/12/72.

Diving observations revealed 15 to 20 foot visibilities above the sewage field and less than a few feet within the field. The dive was terminated at 70 feet because the light meters could no longer be read. Assuming that one percent of the surface irradiance represents compensation, the Station 4 data indicate the depth of the euphotic zone was about 60 to 70 feet. Compensation levels for the background stations were 150 feet to over 200 feet. Reduced intensity of upwelling light also differentiated Station 4 from the background stations. This implies the ratio of absorption to scattering was greater in the sewage field than in natural waters. The cause could be due either to increased dissolved material or to a difference in particle optics.

Station 5: Whites Point, 11/2/72, bottom depth: 140 feet (strong thermocline, moderate sewage field, clear surface waters), Figures 4-10 and 4-11.

By early November the surface waters had cooled to 18°C but the thermocline gradient resembled October data from Station 4. Transmissometer readings and low suspended particle measurements both indicated upper waters were very clear relative to other coastal measurements of this study. In the sewage field, below the thermocline, waters were moderately turbid. The data for both Stations 5 and 6 demonstrate how a strong thermocline effectively protects the surface waters against penetration by the sewage field.

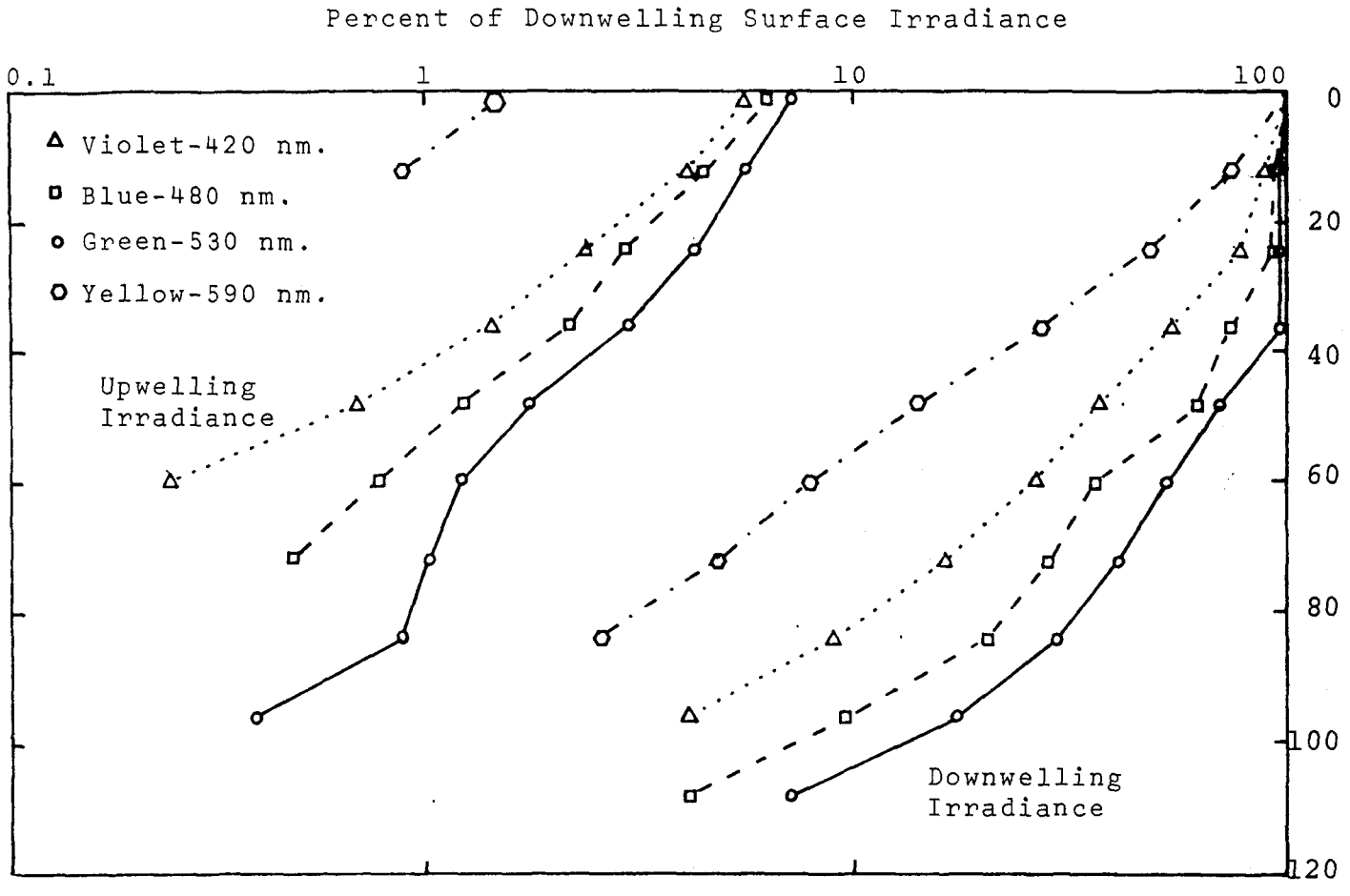

Figure 4-10. Downwelling and Upwelling Irradiance Profiles (Station 5)

Whites Point (1¼ miles offshore, 11/2/72, 12 noon)
Water Depth: 140 feet
Sun Zenith Angle: 45°

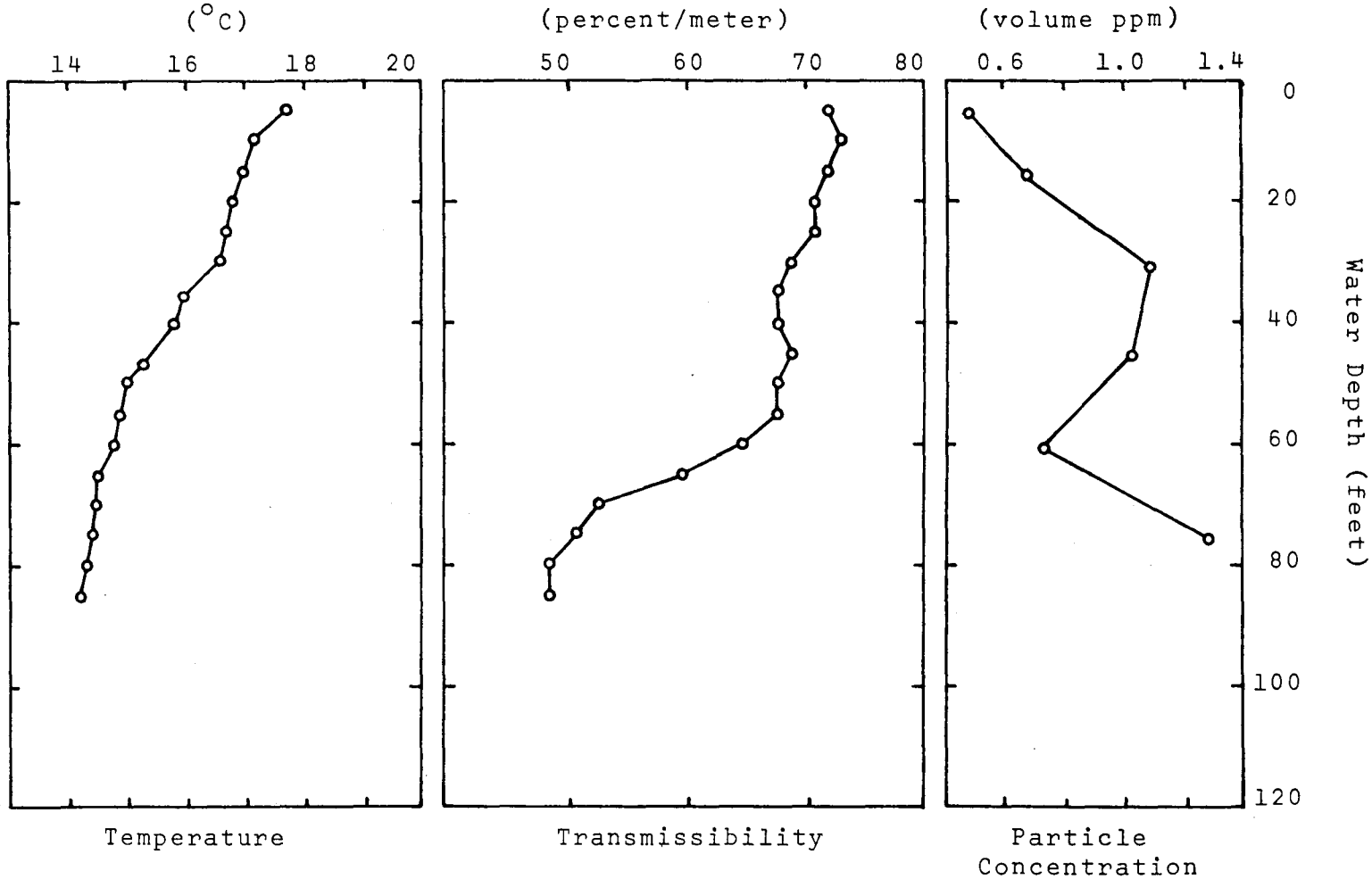

Figure 4-11. Temperature, Transmissibility and Particulate Volume Profiles. Station 5, Whites Point, 11/2/72.

Blue and green were equally enhanced in the surface layers where the particulate load was less than 0.8 ppm. From 20 feet to 40 feet the particle load increased, transmissometer values dropped below 70 percent/meter, and the downwelling irradiance became dominantly green. Below 70 feet the dense portion of the sewage field was reached. The diffuse attenuance (slope of the semi-log irradiance plots) increased in all colors except yellow. Upwelling irradiance values at the surface were low relative to the natural background stations and resembled the Station 4 data.

Diving observations yielded surface visibilities greater than 20 feet. Visibilities decreased to 5 feet as the sewage field was entered. The compensation depth extended below 100 feet. This was deeper than the other stations in the LACSD outfall area, but not sufficiently deep to reach the benthic zone (zone of bottom dwelling organisms).

Station 6: Whites Point, 2/27/73, bottom depth: 100 feet (weak thermocline, turbid surface waters, extremely turbid sewage field below thermocline), Figures 4-12 and 4-13.

The data, acquired in late February, showed a typical weak winter thermocline (less than $1^{\circ}C$ temperature difference between deep and surface waters). Transmissometer readings and measurements of suspended particulates both

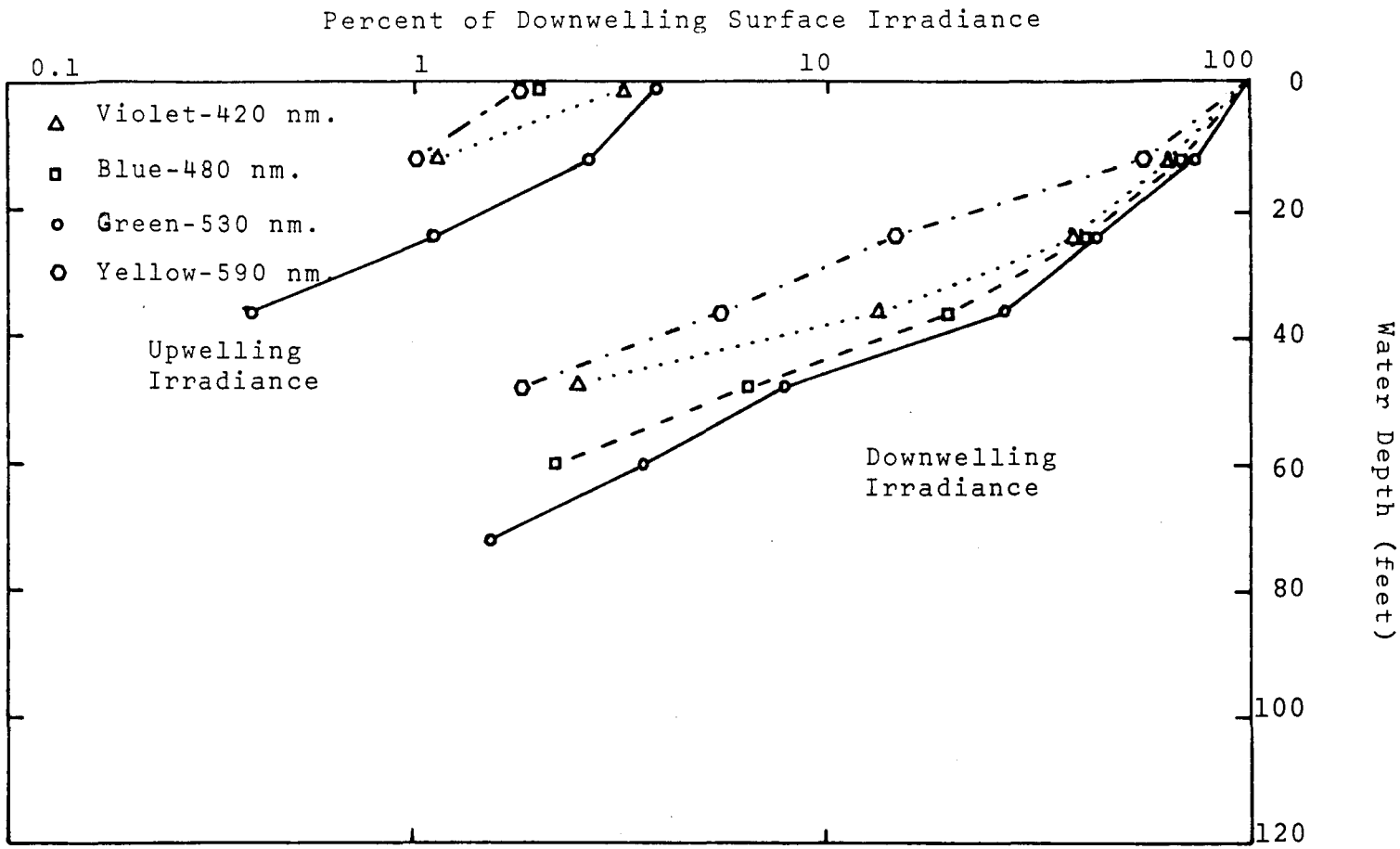

Figure 4-12. Downwelling and Upwelling Irradiance Profiles (Station 6)
Whites Point (3/4 miles offshore, 2/27/73, 11 a.m.)
Water Depth: 100 feet
Sun Zenith Angle: 40°

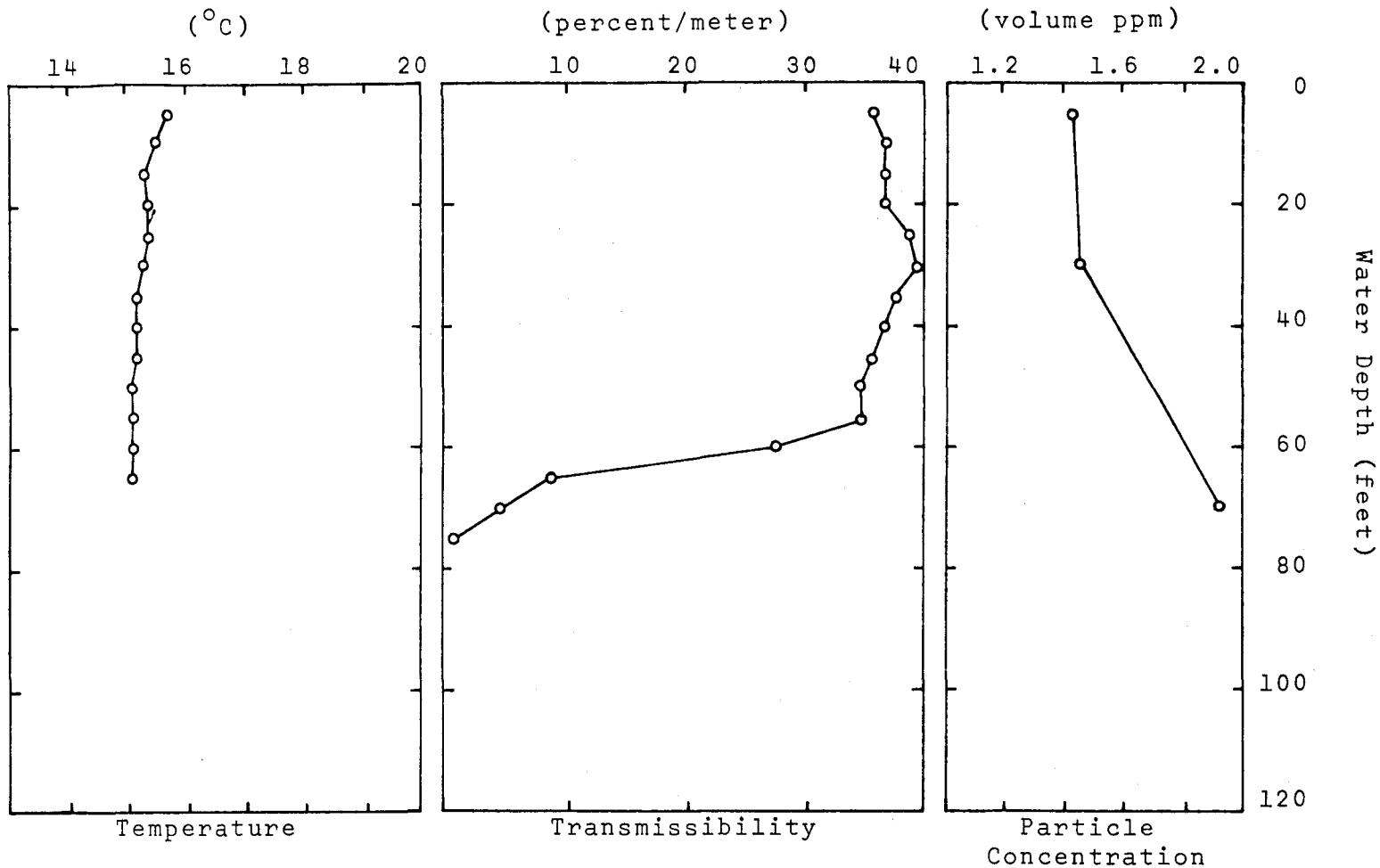

Figure 4-13. Temperature, Transmissibility and Particulate Volume Profiles. Station 6, Whites Point, 2/27/73.

demonstrated that the sewage field penetrated the thermocline to the surface waters. However, even this weak thermocline apparently prevented the majority of the pollutants from reaching the surface waters. Data given below (Section 4.3.2) show that typical natural values for particle concentrations along the California coast are 1.0 ppm above the thermocline and 0.8 ppm below the thermocline. Assuming such values represent background, we can speculate that 0.4 ppm above the thermocline and 1.0 ppm below the thermocline were particulate additions attributed to the outfall system. Surface values for stations 4 and 5 in the outfall area were similar to the 1.0 ppm background value, indicating that the sewage field did not significantly penetrate thermoclines where temperature differences between deep and surface waters were greater than $4^{\circ}C$.

All colors were attenuated rapidly at all depths. Attenuance increased sharply as light entered the sewage field. Resembling other stations in the sewage-affected areas, upwelled irradiance at the surface was lower than that found in natural background areas. Both upwelled and downwelled yellow irradiance was stronger relative to the other three colors in the polluted water data compared to the natural background data.

Underwater visibilities were about 10 feet in the top layers, decreasing to 2 to 3 feet in the sewage field. The dive was discontinued at 70 feet. The depth of the euphotic zone was approximately 60 feet.

For the above presentation of the field data, depths are reported in feet. Metric units are assumed for the remainder of the data analysis.

4.2.3 Depth of the Euphotic Zone

Using the downwelling irradiance data presented in Section 4.2.2 to estimate euphotic zone depths we find that euphotic depths extend to 20 to 35 meters in the Los Angeles County outfall area and 40 to 65 meters in the natural water areas (Figure 4-14). These values compare with an environmental range of 10 meters in very turbid coastal waters to 30 meters in clear coastal waters (Figure 2-8). Values of 70 to 80 meters are typical in the clearest ocean waters. This suggests euphotic zones in southern California are significantly deeper than most coastal environments reported in the literature.

As discussed in Chapter 2, 5 percent of surface irradiance is a better criterion for the bottom of the euphotic zone during the winter months. Using the 5 percent

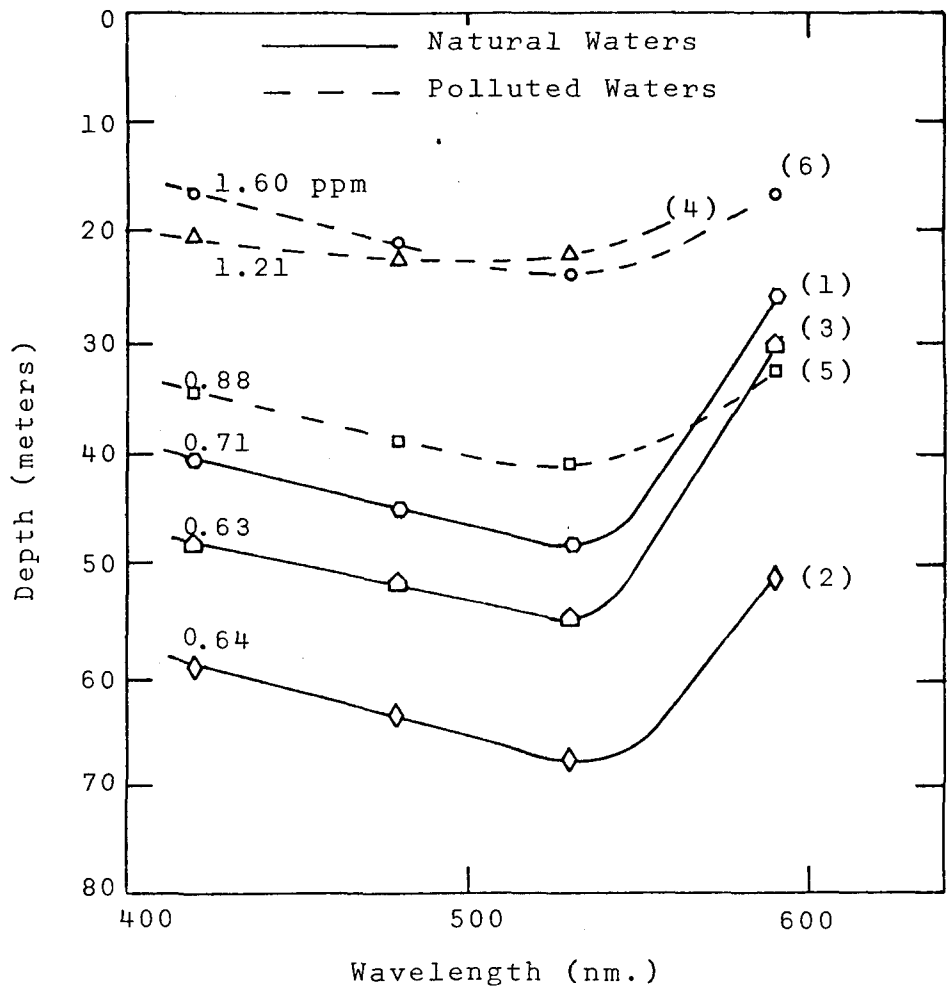

Figure 4-14. Depth at which the downwelling irradiance is one percent of surface values. Average particulate volume concentration given in ppm. Field station numbers (given in parentheses) correspond to locations depicted in Figure 4-1.

criterion, depth of the euphotic zone during winter varied from 15 to 25 meters in the outfall area and from 25 to 40 meters in the natural water areas. If energy requirements for the benthic plants (sea floor plants such as attached algae) were similar to plankton requirements outlined in Chapter 2, the pollution field would cause a 50 percent reduction in euphotic depth. Other effects such as flocculant deposition and toxicities may also be injurious so that light levels may represent only one factor limiting benthic plant survival.

For the six stations discussed in Section 4.2.2, average particulate concentrations ranged from 1.60 to 0.64 ppm (Figure 4-14). These values represent parts per million by volume as measured by the Coulter Counter over the size range of 0.65 microns to 20 microns (see procedures in Chapter 3). Increasing concentrations of particulates clearly reduces the euphotic depth.

The open symbols in Figure 4-15 depict the relationship between particulate concentrations (average values above the compensation depth) and the compensation depths for the green wavelength (530 nm.). The solid symbols are diffuse attenuance values calculated from the instantaneous slopes of the downwelling irradiance profiles (Figures 4-2, 4, 6, 8, 10, 12). Attenuance is plotted against the measured

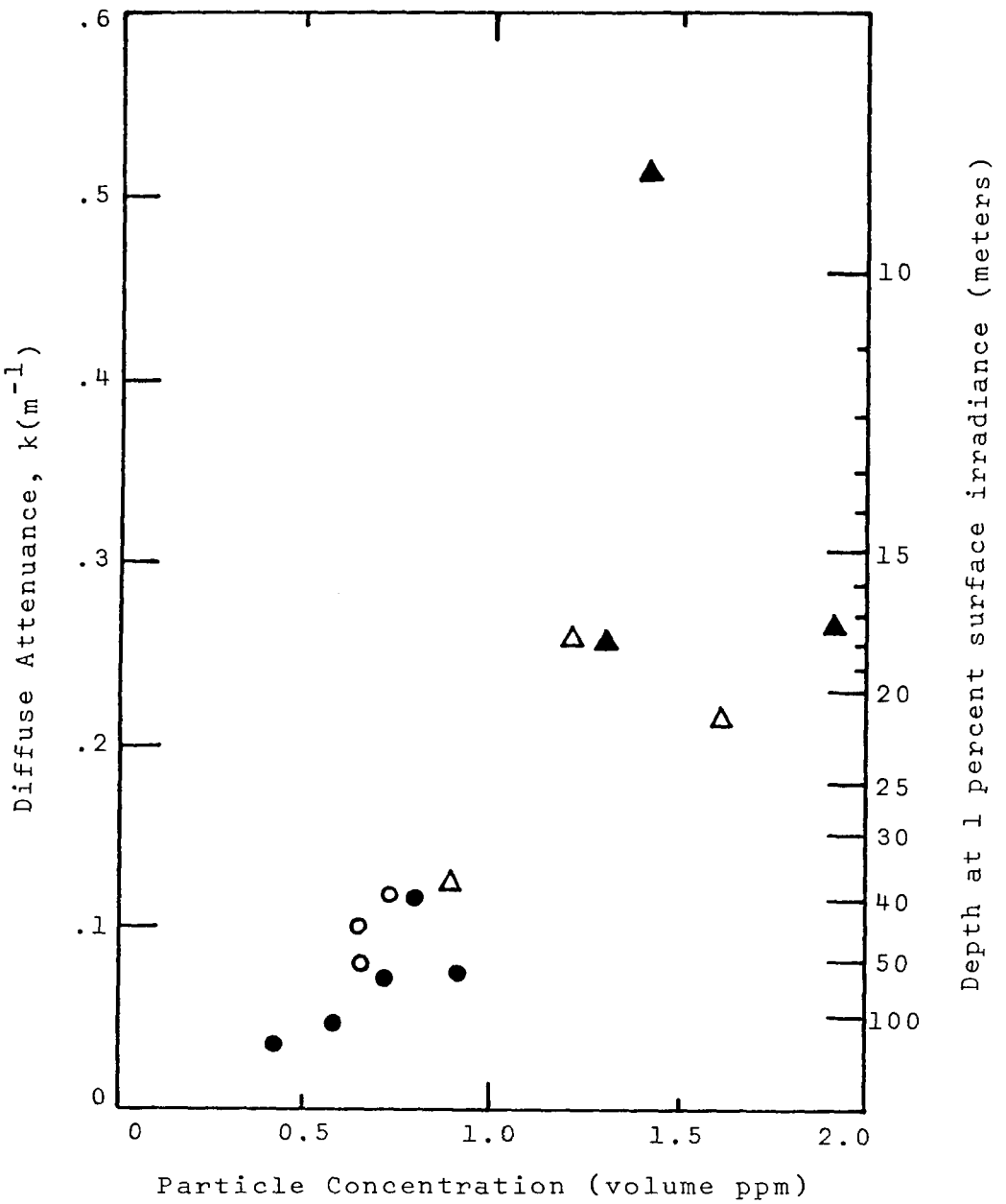

Figure 4-15. Diffuse attenuance and equivalent euphotic zone depths vs. particle concentration.

○ Natural waters, measured depth vs. average concentration
● Natural waters, calculated attenuance vs. concentration
△ Polluted waters, measured depth vs. average concentration
▲ Polluted waters, calculated attenuance vs. concentration

particle concentration at the depth of the attenuance calculation. The one percent euphotic depth, z_e, is related to the diffuse attenuance coefficient, k, by equation 2-2, Chapter 2.

Data from 10 field stations (Figure 4-24) show that average particle concentrations over the depth range 0-25 meters are 1.5 ppm in the polluted waters and 0.8 ppm in the natural waters of Southern California. This corresponds to projected average euphotic zone depths of 25 meters in polluted waters and 50 meters in natural waters (Figure 4-15). This is consistent with the light measurement determinations of polluted and natural water euphotic depths (Figure 4-14). Again, the compensation depth in polluted waters is approximately half that of natural waters.

4.2.4 Surface Ocean Color

The ratio of upwelling to downwelling irradiance just below the water surface was greater in natural waters than in polluted waters (Figure 4-16). The difference was most pronounced in the violet, blue, and green wavelengths. An apparent high absorption of these colors in the sewage field results in a yellow-brown surface color. One of the polluted water stations (station 5 at Whites Point) displayed the more natural blue-green color. Temperature and beam attenuance data for that day (Figure 4-11) showed a strong thermocline at 10 to 15 meters, a moderately turbid sewage field beneath the thermocline and clear waters above the thermocline.

Natural water ocean color appeared to be independent of particle concentration. Beam attenuance values were sufficiently high (0.4 to 0.7 m^{-1}) such that apparent surface color was more dependent upon particle type than particle concentration (Section 2.2.3). Catalina had the highest concentrations, yet the bluest water. Dana Point had the greenest water with strong chlorophyll absorption at 0.47 microns.

The Rocky Point spectrum was similar in shape to the spectrum at station 5 (Whites Point). Upwelling of bottom waters was suspected (see discussion, Section 4.2.2). The

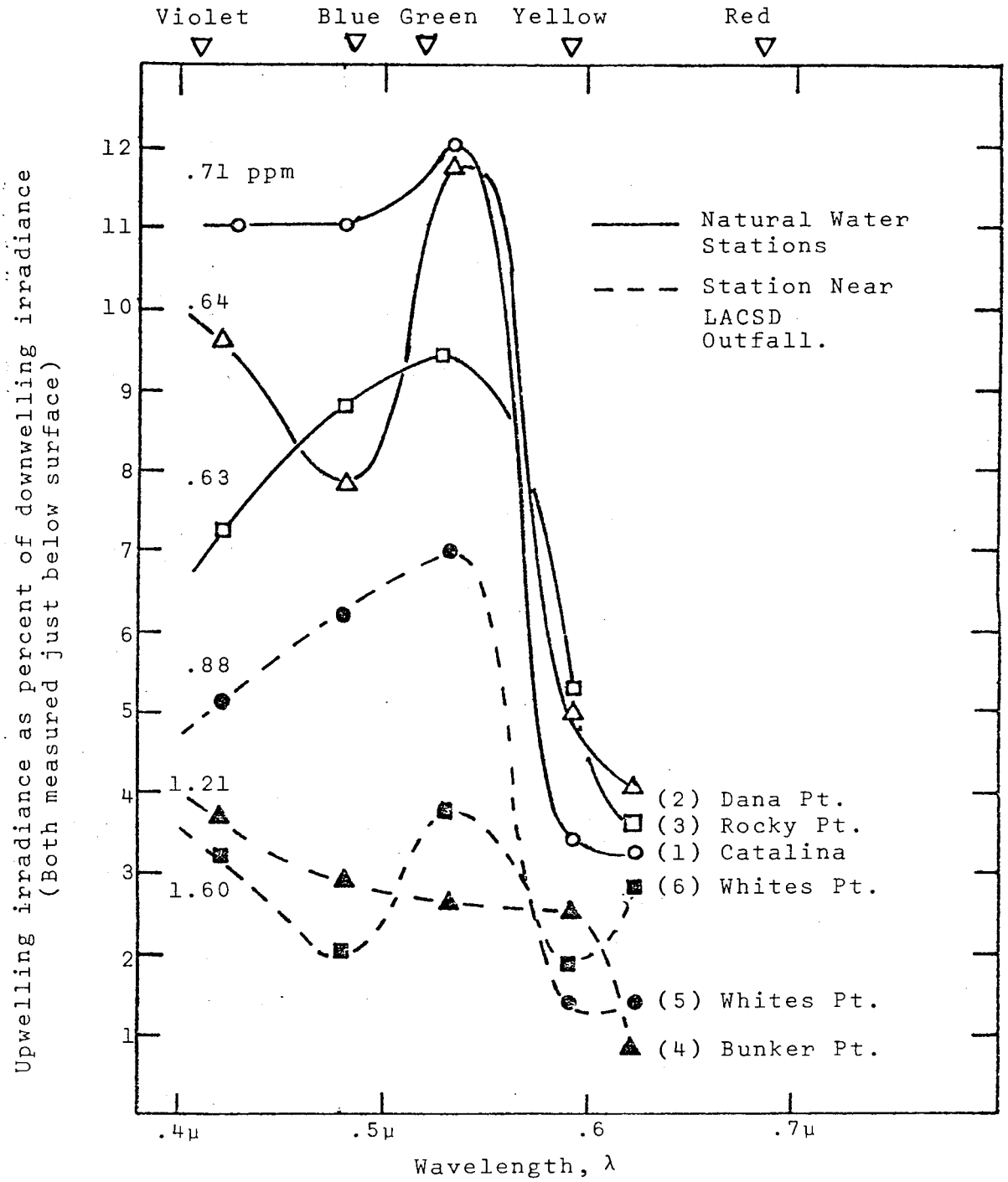

Figure 4-16. Ratio between upwelling and downwelling irradiance measured just below the water surface. Average particulate concentration given in ppm.

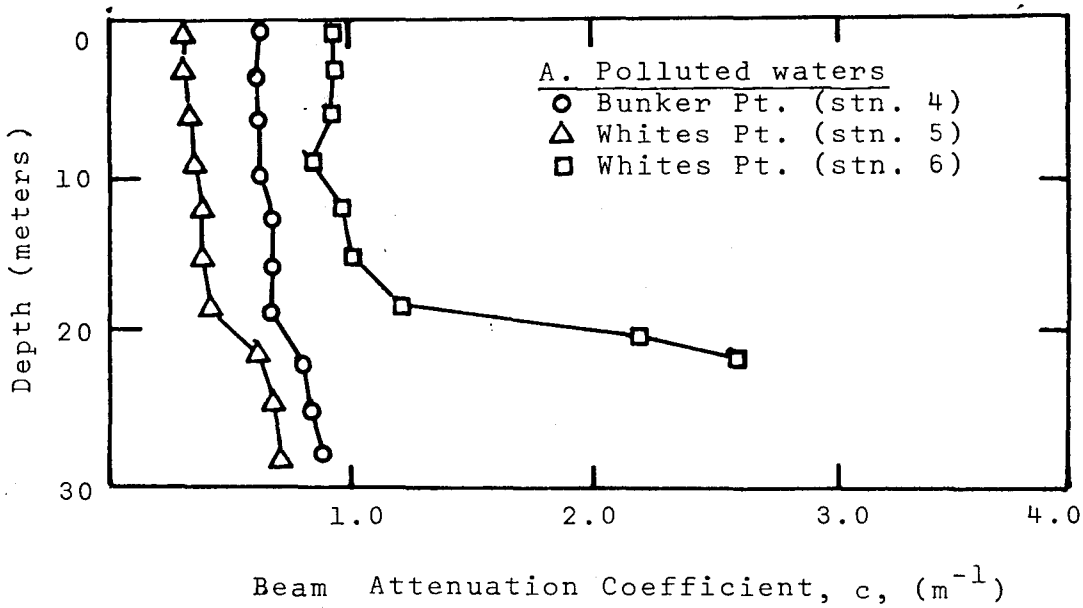

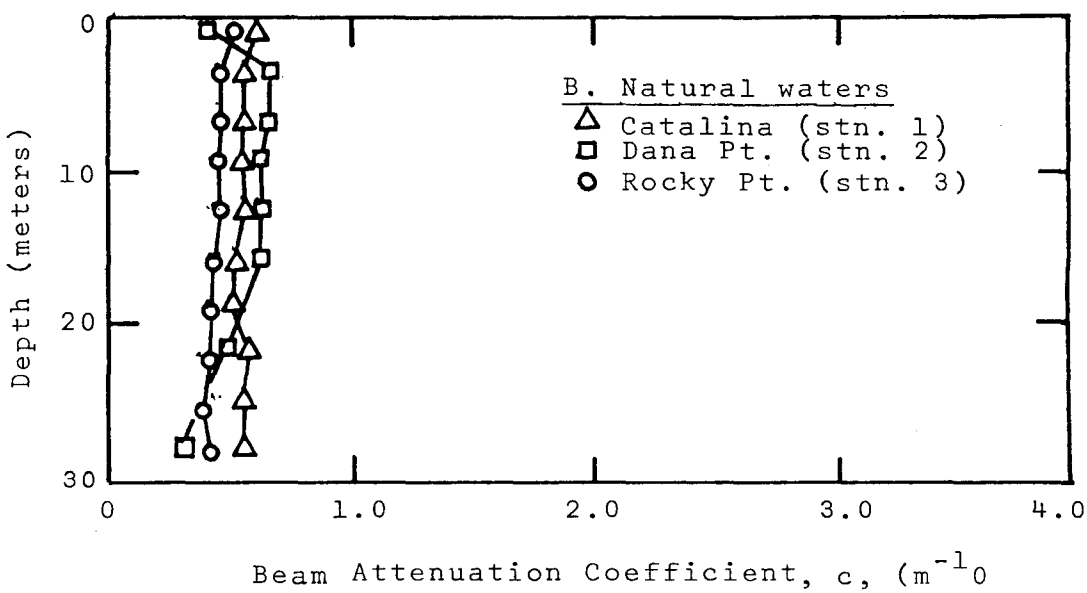

Figure 4-17. Beam attenuation profiles for polluted and natural water stations.

Rocky Point station was 8 nautical miles from the LACSD outfall (Figure 4-1). The bottom sediments at Rocky Point are affected by the effluents (41). Possibly upwelled bottom sewage particulates were affecting surface color.

In the polluted waters, the upwelling violet and blue irradiance was inversely related to particle concentration. The spectral character of polluted water reflected a mixture of natural and sewage particles with possible additions of dissolved effluent components. Assuming relatively constant background particle concentrations, the average particle characteristics in the dispersing sewage field, and therefore surface water color, will vary according to total particle concentration. Pollutants from the LACSD outfall apparently absorbed the violet and blue wavelengths strongly.

4.2.5 Sunlight Irradiance as a Function of Ocean Optical Depth

Sunlight is transmitted, scattered, or absorbed as it propagates from surface waters to deep waters. In ocean waters, 98 percent of light scattering is forward (See Appendix A). Therefore most of the scattered sunlight continues to propagate to deeper waters. Absorbed sunlight, however, is lost from the visible radiation spectrum and converted to other forms (e.g. heat or photo-chemical products).

An optical parameter for classifying ocean waters according to depth of sunlight energy penetration is the albedo, A. It is the ratio of the scattering coefficient to the beam attenuation coefficient.

(4-1) $$A = b/c = b/(a+b)$$

where b = scattering coefficient

c = attenuation coefficient

a = absorption coefficient

Given waters with equal values of beam attenuance, those waters with greater albedos have deeper euphotic zones. A lower fraction of the attenuated light is absorbed (more is scattered forward). Given waters with unequal attenuance, those waters with greater albedos will have deeper sunlight penetration as a function of optical depth (real depth weighted by attenuance).

Plotting the sunlight irradiance data as a function of ocean optical depth required conversion of real water depth, z (meters), to optical depth, τ. The beam attenuation coefficient (Figure 4-17) was integrated with respect to depth, z.

(4-2) $$\tau(z) = \int_0^z c(z')dz'$$

Four field stations were selected for contrasting conditions of natural versus polluted waters and strong versus weak thermoclines (Figure 4-18). The bandpass of the green irradiance filter (Figure 3-2) displayed best agreement with the transmissometer response (Figure 3-1). Calculations of optical depth were most accurate for that wavelength (530 nm).

Downwelling sunlight irradiance decayed more rapidly with optical depth in the sewage field than in natural waters. At station 6 the weak thermocline failed to keep the sewage field from reaching the surface waters resulting in rapid light attenuation at all depths. Attenuation above the strong thermocline at station 4 was similar to that of natural waters. There was a sharp transition to higher attenuation in the dense sewage field below the thermocline. Attenuation in natural waters appeared to be unaffected by the amount of thermal stratification.

Compared to polluted water, natural waters return to the atmosphere a greater percent of sunlight entering the ocean (high surface upwelling irradiances for natural waters in Figure 4-18). A greater percent also reaches the deep optical depths in natural waters. Therefore less of the light passing through an ocean layer of unit optical depth is absorbed in natural waters than in polluted waters.

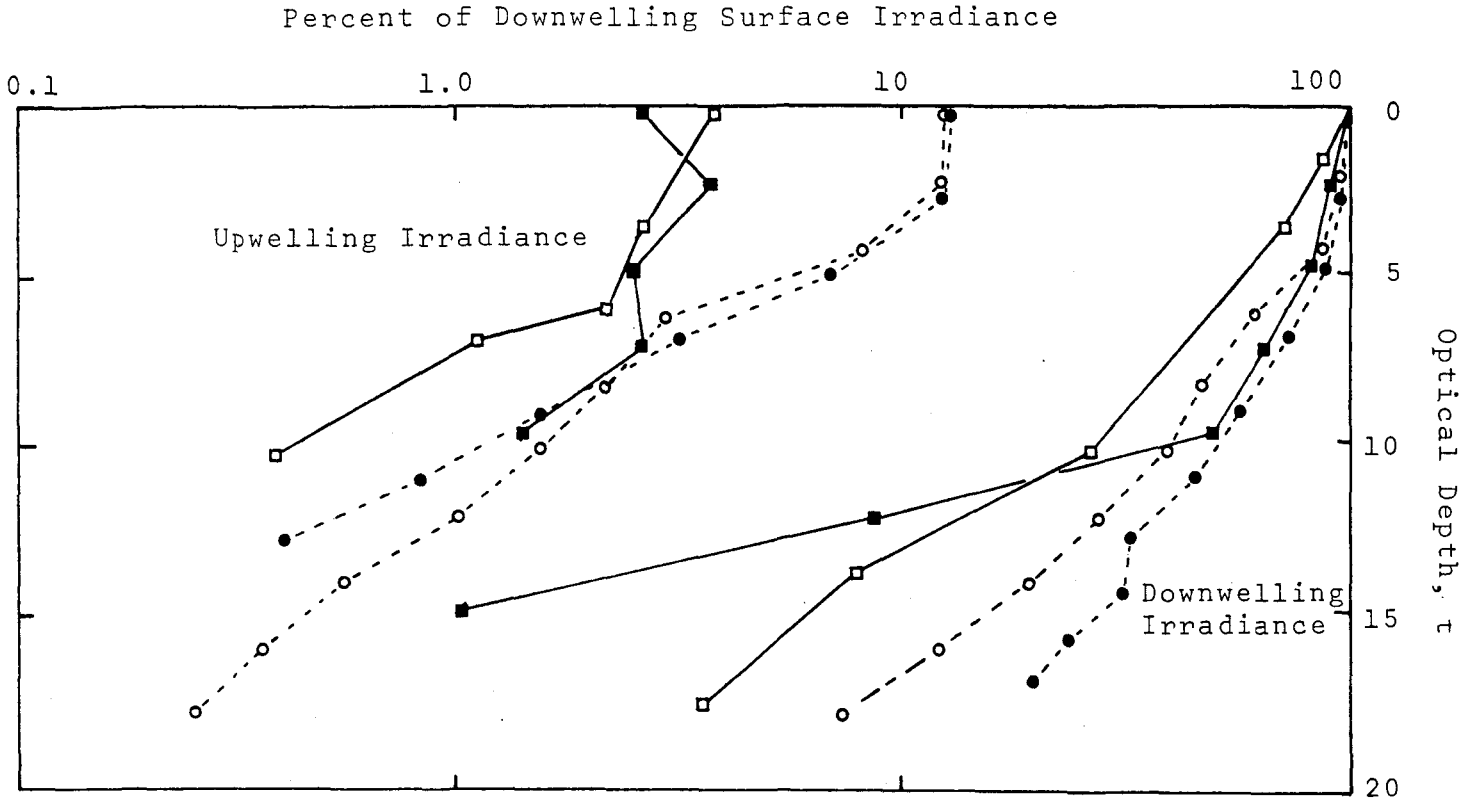

Figure 4-18. Downwelling and upwelling irradiance as a function of optical depth. (Green light, 530 nm.)

Station 6: Polluted waters--weak thermocline
Station 4: Polluted waters--strong thermocline
Station 1: Natural waters--weak thermocline
Station 2: Natural waters--strong thermocline

Hence, natural waters have lower ratios of absorption, a, to total attenuation, c, or higher albedos, A (since from equation 4-1, A = 1 - a/c).

Appendix A presents a sunlight propagation model. The model calculates upwelling and downwelling sunlight irradiance as a function of optical depth, z, and albedo, A. Results are compared with the field data in this section (Figure 4-18). Albedo values for the polluted and natural water stations are estimated. The results are preliminary. Further development of the model is required to increase confidence in the albedo estimates.

4.3 Particle Properties in Polluted and Natural Waters

4.3.1 Size Distributions

The particle size spectrum, dN/ds (N = number of particles per milliliter, s = particle diameter), varies approximately as the inverse fourth power of diameter in both polluted and natural waters (Figure 4-19). The slope of the polluted water spectrum increased to fifth power at diameters below 2 microns. There were ten times as many particles in very turbid polluted waters (samples from the sewage field at Whites Point) as in very clear natural waters (samples from below the thermocline at Corona Del Mar and Dana Point). Measurements of beam attenuation, c, show the same ten-fold difference. One sample, taken less than a meter from one of the discharge ports at the Laguna Beach outfall, had about twice as many particles as the Whites Point sewage field samples. Particle size spectra are presented in tabular form in Appendix B.

Comparison between sample size distributions is facilitated by conversion to the volume distribution:

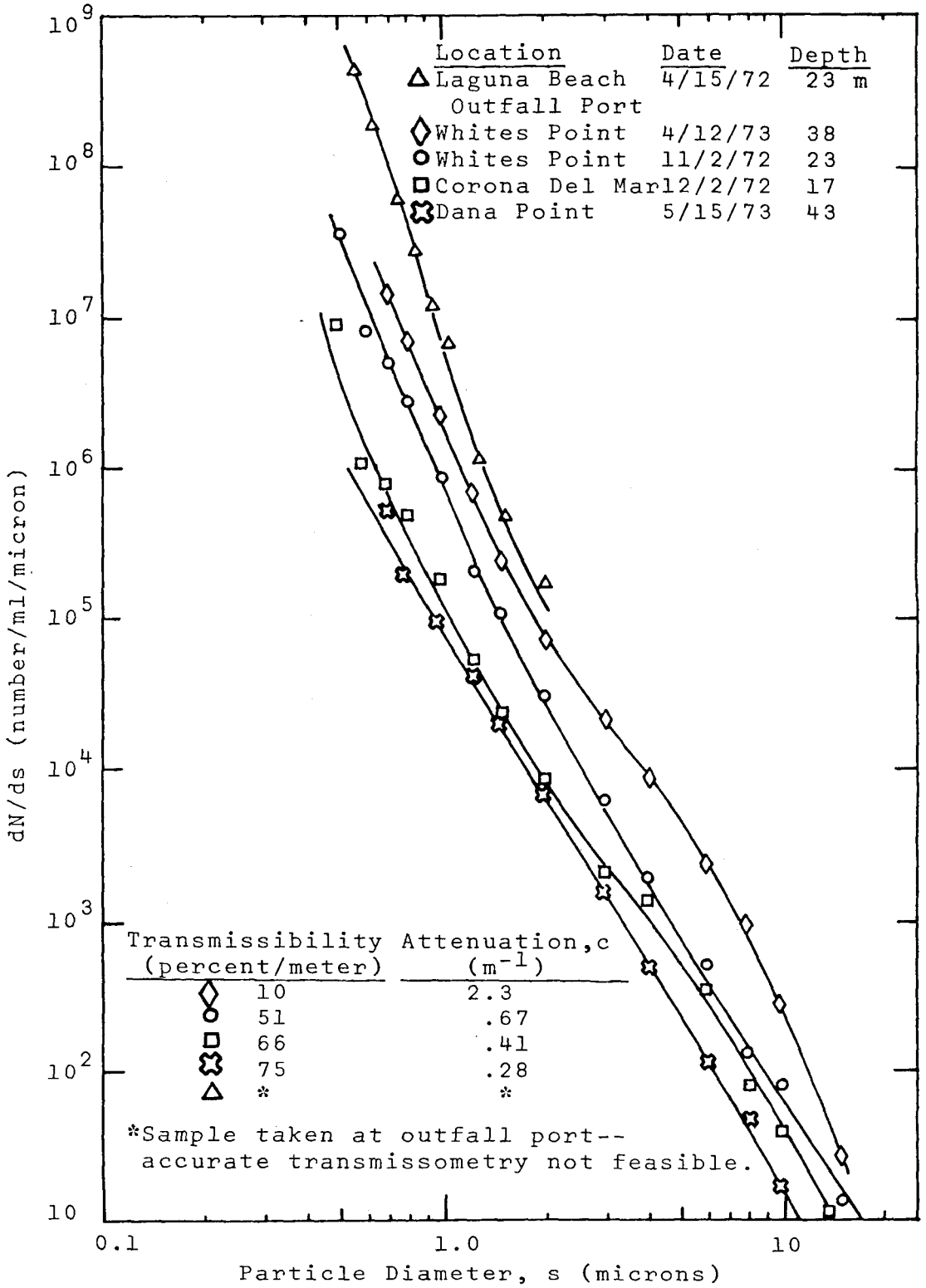

Figure 4-19. Particle size distributions--environmental range. Data include the most turbid and clearest waters measured.

(4-3) $$dV/d(\log s) = \left(\frac{dV}{ds}\right)\left(\frac{ds}{d(\log s)}\right)$$

$$= \left(\frac{\pi s^3 (dN/ds)}{6}\right)(s \ln s)$$

where V = volume concentration of particles (ppm)

ln s = natural logarithm of s

If dV/d(log s) is plotted as a function of log(s), the integrated area under the curve from s_1 to s_2 (any two diameters) represents the volume concentration of particulates between s_1 and s_2 (Figure 4-20).

Heavily polluted waters in the sewage field (classified as "turbid polluted" in Figure 4-20) have particle volume distributions that peak between 6 and 10 microns. Peak values may exceed 4 ppm. Phytoplankton activity in "turbid natural" waters produces distribution peaks in the same size range. However, peak values do not exceed 1 ppm except during intense blooms. The volume distribution for the clearest water sampled at Whites Point ("clear polluted") was similar to that of the turbid natural water. The volume distribution for the clearest natural water (sampled 43 meters deep at Dana Point) was less than 0.25 ppm throughout the measured size range.

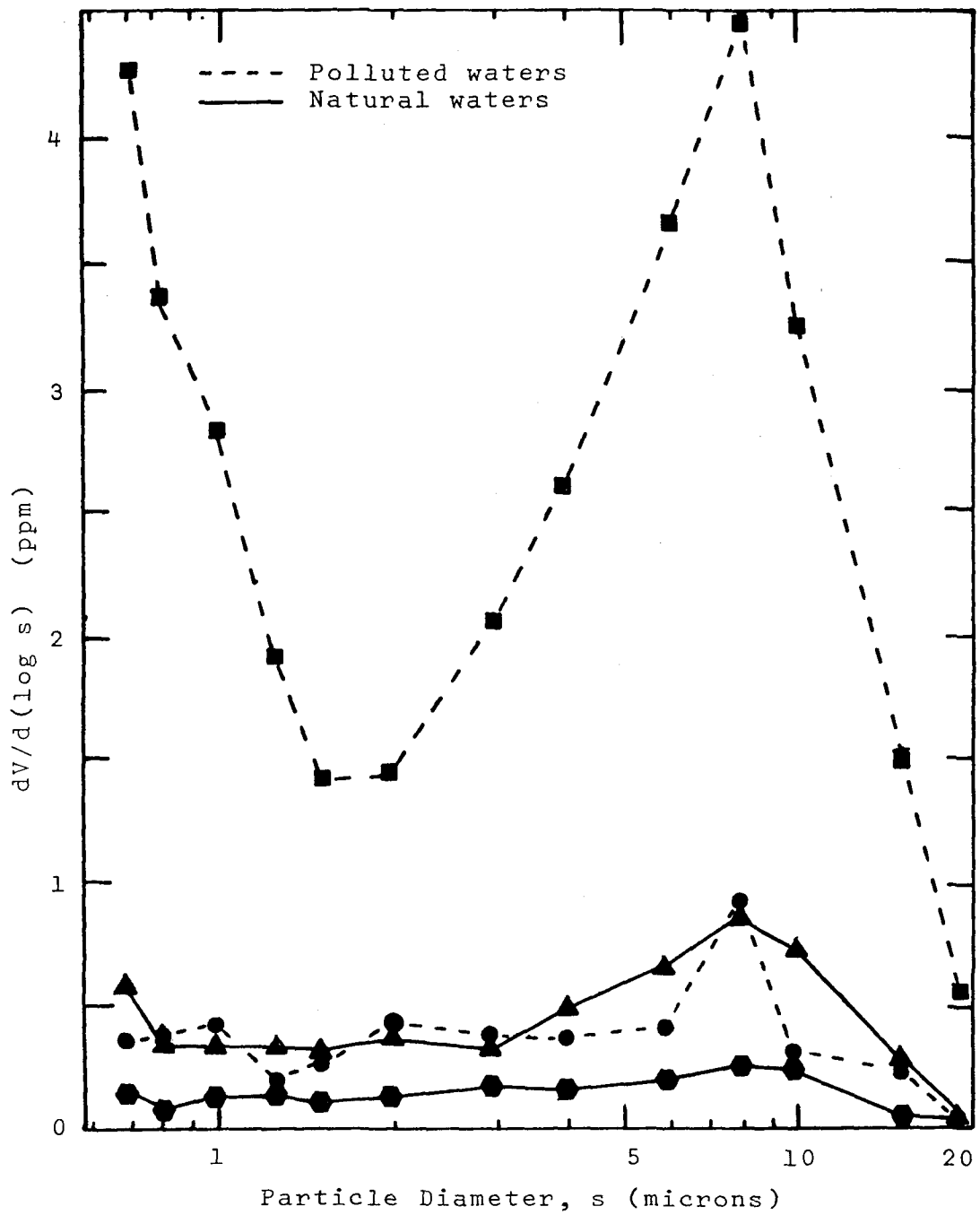

Figure 4-20. Particle size distributions by volume, V: environmental range for polluted and natural waters.

	Location	Date	Depth (m)	Water Type
■	Whites Pt.	4/12/73	38	Turbid polluted
●	Whites Pt.	11/2/72	0	Clear polluted
▲	Catalina	4/8/73	8	Turbid natural
⬢	Dana Pt.	5/15/73	43	Clear natural

Most water samples showed an increase in volume concentration with decreasing particle size below 1.5 microns. However, in the sewage field the increase was dramatic ("turbid polluted" in Figure 4-20) indicating that sub-micron particles are a major component in the discharge effluent. This is reasonable. Primary waste treatment (used by the LACSD prior to discharge) essentially removes particulates that settle or float. Sub-micron particles remain in suspension by Brownian motion.

Particle size distributions were routinely measured between 0.8 and 20 microns (the larger diameter representing the upper limit of optical significance, Section 2.3.2). This required the use of two Coulter counter apertures, 30 and 100 microns in diameter (Section 3.2). Using a third aperture, 11 microns in diameter, some samples were analyzed for particle diameters as small as 0.5 microns (Figure 4-19). A sub-micron maximum was never detected in any of the sewage field particle volume distributions.

The presence of a strong thermocline had a significant affect upon particle size distributions as a function of water depth. Two natural water stations had contrasting thermocline conditions (Figure 4-21). At Rocky Point the absence of a strong thermocline resulted in a relatively

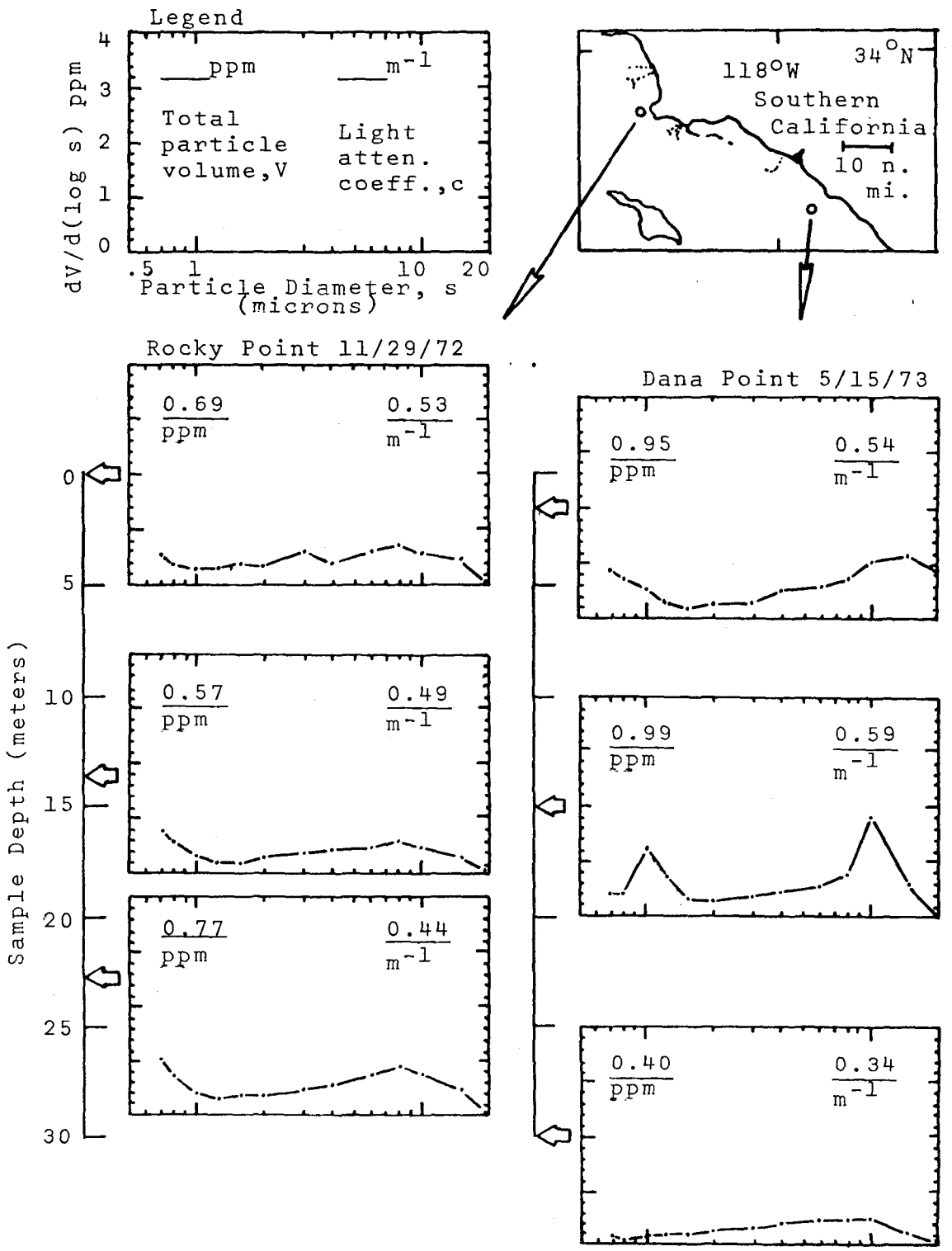

Figure 4-21. Particle size distributions at various depths for two natural water stations. Rocky Point had a weak thermocline. Dana Point had a strong thermocline.

constant particle size spectrum with sample depth. Light beam attenuation, c, and volume concentration, V (ppm), is given for each spectrum

$$V = \int_{s=0.65}^{s=20} \frac{dV}{d(\log s)} \, d(\log s) \qquad (4-4)$$

The shallow water spectra at Dana Point had more structure than the Rocky Point samples, indicating a higher level of phytoplankton activity. This would be expected when comparing May and November samples. For all depths, attenuance increased with concentration. Below the thermocline at Dana Point, the spectrum indicated a low level of productivity, volume concentration was very low, and the light attenuation was the lowest encountered for the duration of the study.

The effect of thermal stratification was dramatic in polluted waters (Figure 4-22). The strong thermocline at Bunker Point prevented most of the sewage field from reaching the surface. The volume concentration at the surface was typical for natural waters (see Figure 4-24). The surface particle size spectrum showed an absence of the small ($s < 1.5$ microns) sewage particles present in the sub-

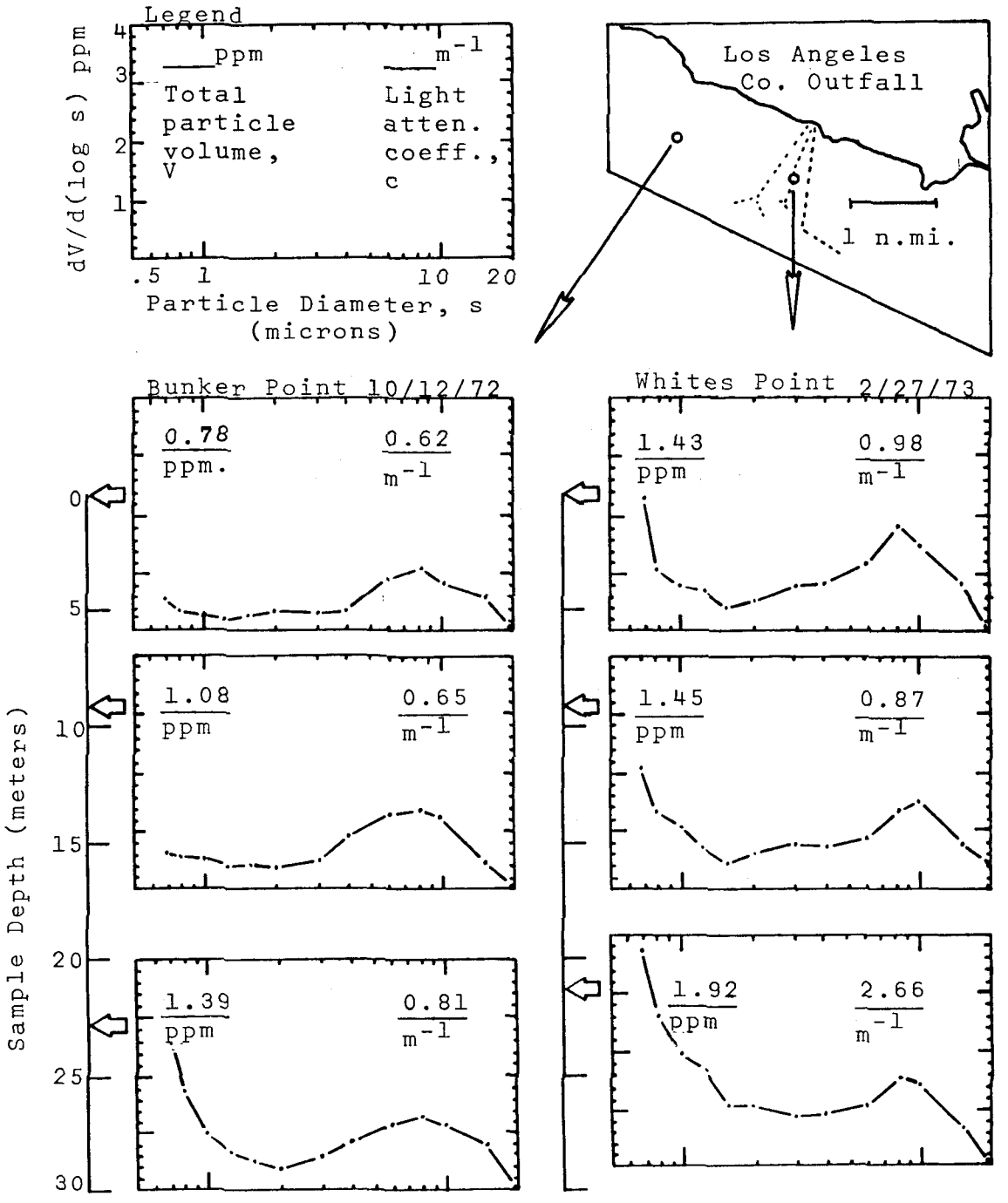

Figure 4-22. Particle size distributions at various depths for two polluted water stations. Bunker Point had a strong thermocline. Whites Point had a weak thermocline.

thermocline sewage field. Attenuance again increased with concentration, V.

Lack of a strong thermocline at Whites Point allowed the sewage field to penetrate to surface waters. The small sizes were abundant at all depths. A large increase in attenuance for a relatively moderate increase in concentration was noted for the deepest sample in the sewage field. This was attributed to instrument error. The transmissometer was not accurate in very turbid waters. Transmissibility was less than 5 percent per meter for the deep sample (Figure 4-13).

The size spectra for 70 water samples were categorized according to water depth (above thermocline or below thermocline) and water type (polluted or natural). The average size distribution was calculated (Figure 4-23A). Above the thermocline, the spectra for natural and polluted waters were remarkably similar. The difference between the polluted and natural water distributions (Figure 4-23B) represents the average addition of sewage particles as a function of size. The average addition clearly demonstrated a bimodal increase in particle numbers (a significant increase for particle diameters less than 1.5 microns and a secondary increase at 8 microns) below the thermocline.

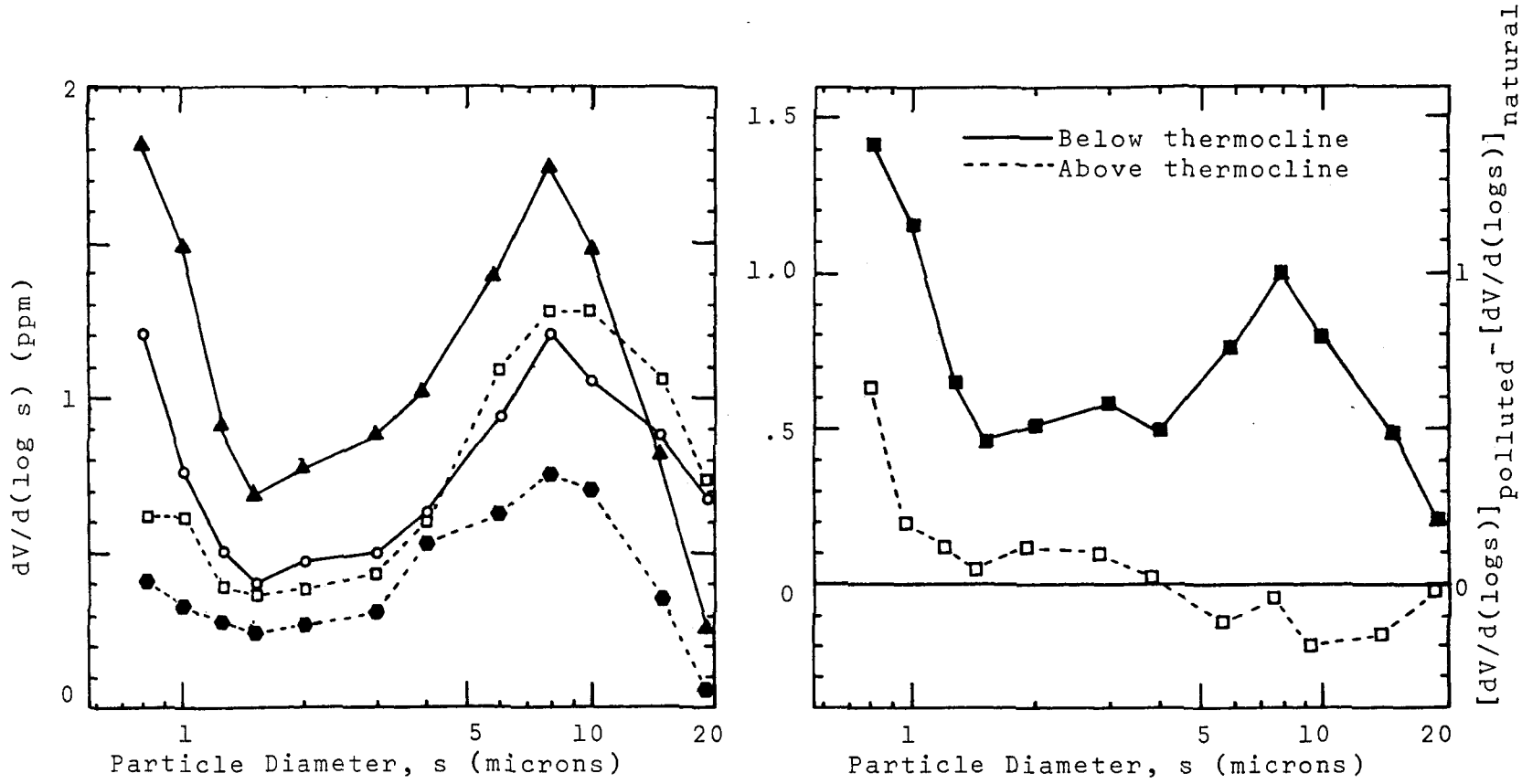

A. Average of 70 samples from 14 field trips.

- ○ Polluted waters--above thermocline
- ▲ Polluted waters--below thermocline
- □ Natural waters--above thermocline
- ⬣ Natural waters--below thermocline

B. Difference between polluted water and natural water distributions in A. Represents suspended particles due to Los Angeles County Outfall.

Figure 4-23. Average particle size distributions: Comparison between polluted water samples (Whites Pt. and Bunker Pt.) and natural water samples.

4.3.2. Vertical Distributions

The average particle concentration in polluted waters was twice that of natural waters (Figure 4-24). Average concentrations as a function of depth showed that concentrations increased with depth near the water surface due to an increase in phytoplankton productivity (stratification of phytoplankton is discussed in Section 2.2.2). After reaching a maximum, concentration decreased with depth as light for photosynthesis dwindled. The standard error of estimate was less than 0.2 ppm indicating the trends were statistically significant (an increase from 0.73 ppm at the surface to a maximum of 0.95 ppm and a decrease to 0.62 ppm at 22 meters).

In contrast, the variation of the polluted water data was too high for the average trend to be statistically significant. The standard error of estimate was 0.58 ppm, much greater than changes in the average curve with depth. However, the difference between the natural and polluted concentration profiles was significant at all depths.

4.3.3 Optical Densities

The measured light beam attenuation, c, was plotted as a function of particle volume concentration, V, for polluted and natural waters (Figure 4-25). The least squares linear fit was calculated for each water type, requiring

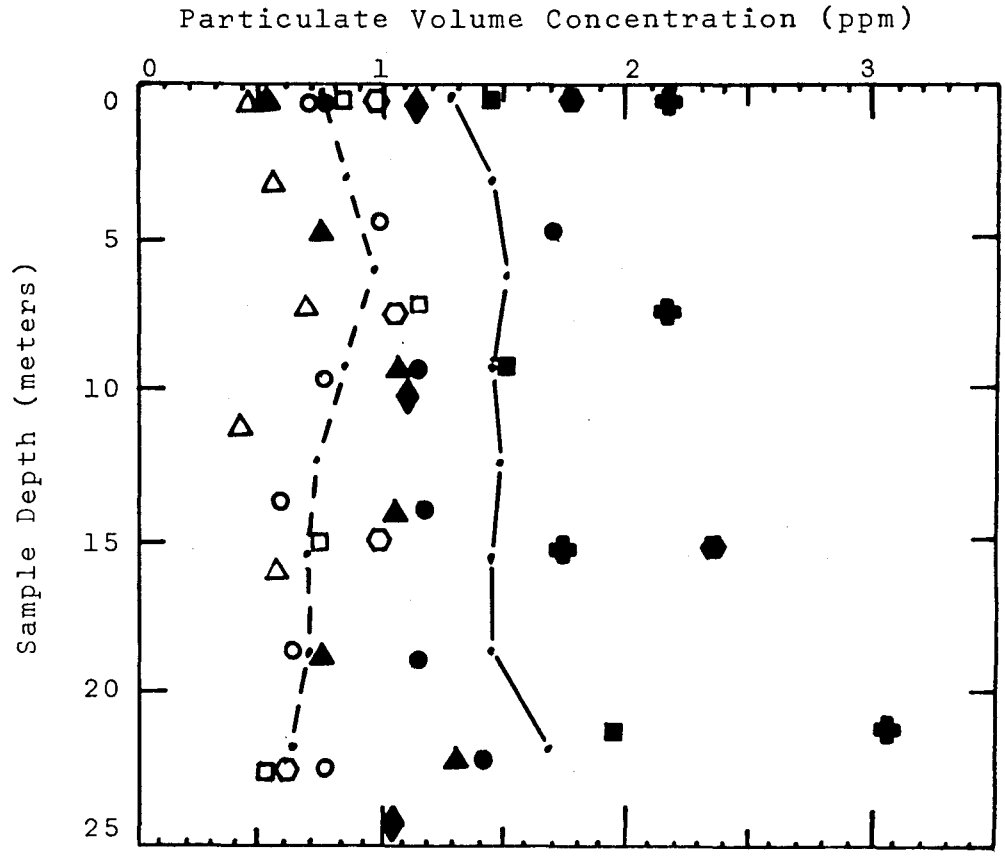

Figure 4-24. Vertical distribution of particles. Concentration values obtained by integrating particle size distributions over the diameter range 0.65 microns to 22.5 microns.

— — — Average concentration for natural waters. (standard error of estimate = 0.19 ppm.)

——— Average concentration for polluted waters (standard error of estimate = 0.58 ppm.)

Natural waters
- ○ Rocky Pt. 11/29/72
- △ Corona Del Mar 12/2/72
- □ Catalina 4/8/73
- ⬡ Dana Pt. 5/15/73

Polluted waters
- ● Bunker Pt. 10/12/72
- ▲ Whites Pt. 11/2/72
- ■ Whites Pt. 2/27/73
- ◆ Whites Pt. 3/29/73
- ✚ Whites Pt. 4/12/73
- ⬢ Whites Pt. 4/12/73

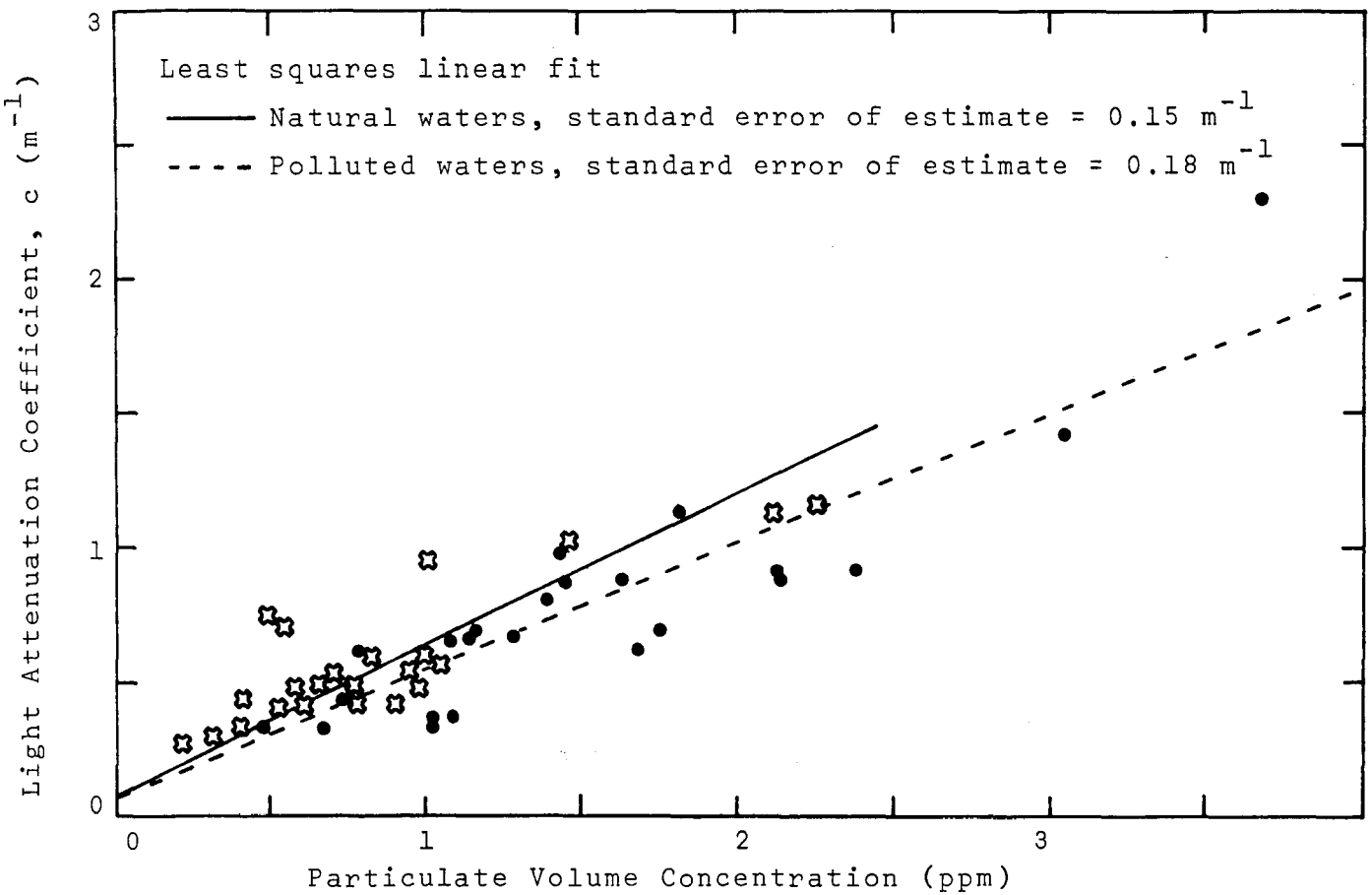

Figure 4-25. Correlation between light beam attenuation, c, and particulate volume concentration for stations listed in Figure 4-26.
- ✡ Natural waters
- ● Polluted waters

the attenuation coefficient be equal to the pure water value ($0.02m^{-1}$ at 500 nm., Figure 2-10) for zero particle volume concentration. On the average, the natural waters showed higher attenuation values for equal particle concentrations, but the standard error of estimates were greater than the difference between the least square fit lines between 0 and 2 ppm.

Assuming real refractive indices, the next section shows that natural particles have a higher average index than particles in the polluted waters. This would account for increased scattering by natural particles and hence increased attenuation. However, it will be shown that this conclusion is not necessarily true if complex refractive indices are considered.

4.3.4 Scattering and Absorption

Scattering and absorption by particles were calculated assuming real and complex refractive indices. Water samples from 18 field stations were categorized according to water depth (above or below thermocline) and water type (natural or polluted). Assuming real refractive indices (the case for non-absorbing particles, see discussion in Section 2.3.1), the average refractive index for each category was calculated (Figure 4-26).

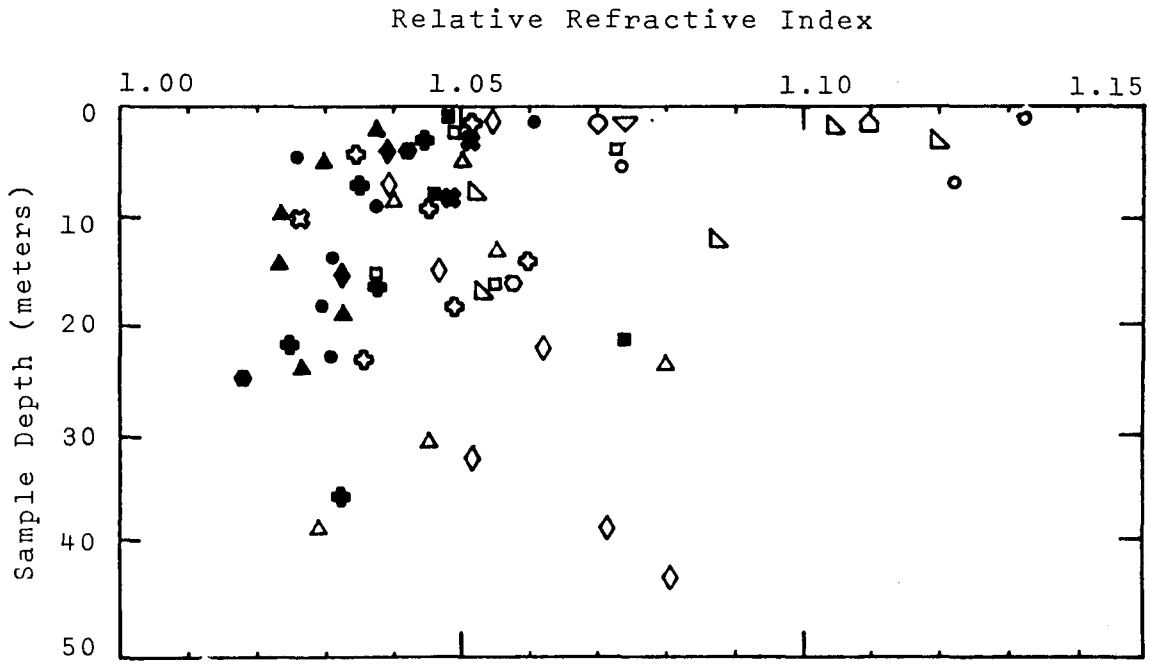

Figure 4-26. Calculated refractive index of particles (relative to water) for natural and polluted waters (assuming non-absorbing particles).

Natural waters	Polluted waters
Rocky Pt. 11/29/72	Bunker Pt. 10/12/72
Corona Del Mar 12/2/72	Whites Pt. 11/2/72
Catalina 1/19/73	Whites Pt. 11/29/72
Mid-Channel 1/20/73	Whites Pt. 2/27/73
Morro Bay 2/14/73	Whites Pt. 3/29/73
Humboldt Bay 3/18/73	Whites Pt. 4/12/73
Mid-Channel 4/12/73	Whites Pt. 4/12/73
Dana Pt. 5/15/73	
San Simeon 6/11/73	
Whalers Cove 6/11/73	
Cypress Pt. 6/11/73	

Average Indices (± standard deviations)

	Natural waters	Polluted waters
Above thermocline	1.069 (±.033)	1.039 (±.010)
Below thermocline	1.056 (±.016	1.034 (±.014)
All samples	1.064 (±.027)	1.037 (±.012)

This was accomplished by iterative calculations of particle scattering using different refractive indices (equation 2-5) and the particle size spectra (Appendix B). It was assumed that the measured attenuance, c, was equal to the sum of scattering by particles, absorption by water, and absorption by dissolved material. Scattering by water molecules was assumed negligible. Albedo values from Appendix A were used to estimate the fraction of attenuance due to particle scattering.

At all depths the average refractive index of natural water particles was statistically greater than the average index for polluted water particles. Of special note was the large standard deviation for above thermocline natural waters. A large variation can be encountered in natural surface waters due to high index land runoff particles (high in minerals) and low index biological particles (due to plankton blooms, Section 2.3.1).

Using the average particle size distributions (Figure 4-23A) and the average real refractive indices (Figure 4-26), the average distribution of the particle scattering coefficient, b_p, as a function of particle diameter, s, was calculated (Figure 4-27). Results show that even though polluted waters had a large number of small particles ($s < 1.5$ microns), contribution to the total scattering coefficient by small sewage particles was small. This was

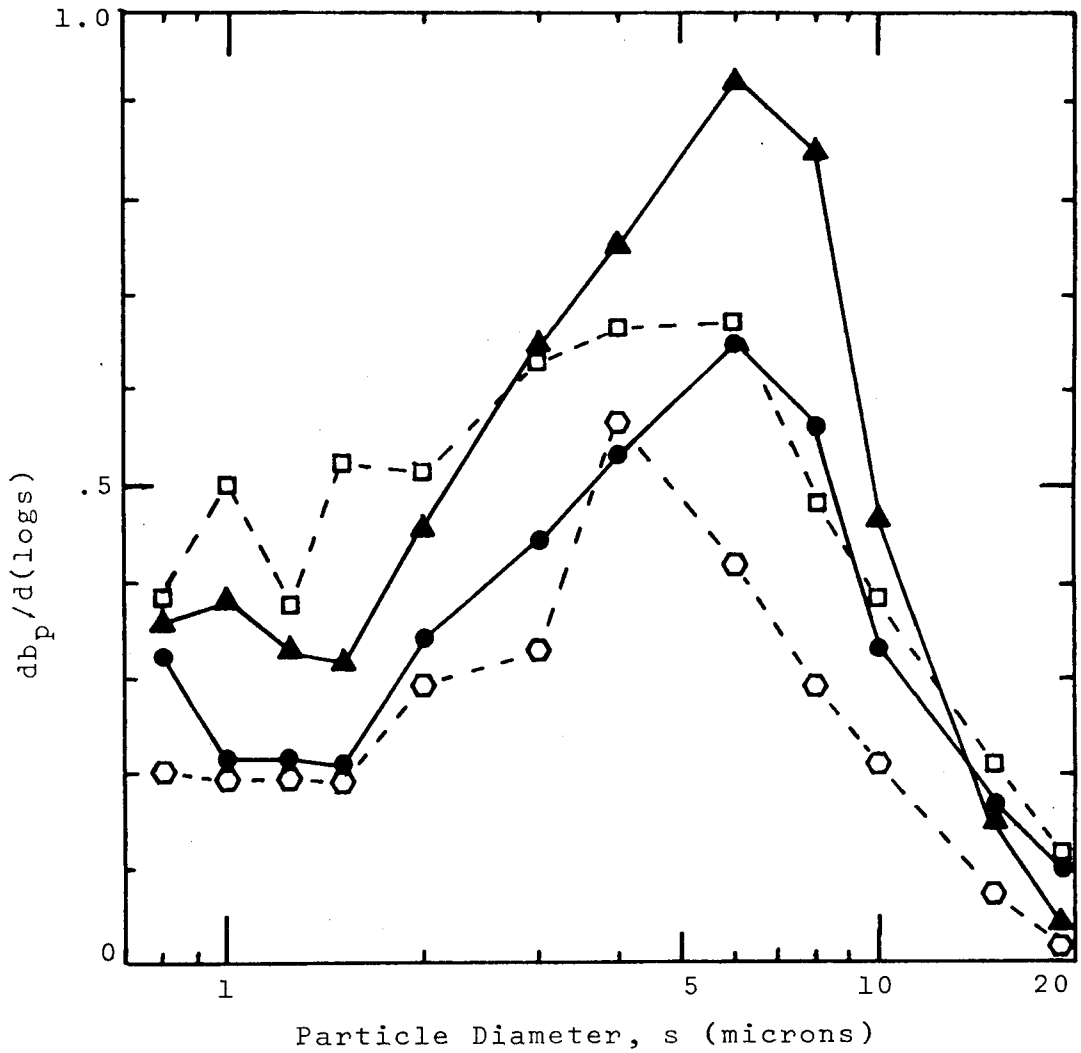

Figure 4-27. Distribution of scattering coefficient, b_p, with particle size. Calculations assumed green light (λ = 500 nm), average particle size distributions given in Figure 4-25 and nonabsorbing particle refractive indices from Figure 4-28).

Water type	Refractive index
Polluted, above thermocline	1.039
Polluted, below thermocline	1.034
Natural, above thermocline	1.069
Natural, below thermocline	1.056

attributed to the low refractive index (see Figure 2-12). Reduced scattering by particles larger than 10 microns was attributed to a smaller number of large particles in both natural and polluted waters.

Using the van de Hulst "anomalous diffraction" equations (2-10 and 2-11) and the correction factors by Moore, Bryant and Latimer (Section 2.3.1), the distribution of particle extinction (particle attenuation), c_p, and particle absorption, a_p, with particle diameter was calculated for two values of complex refractive indices (Figure 4-28). Low albedos in the sewage field (Section 4.2.5) suggested that sewage particles were most likely to be absorbing in character. Therefore, the below thermocline polluted water size distribution (Figure 4-23A) and the corresponding real index (n = 1.034, Figure 4-26) were used in the calculation.

As the complex part of the refractive index (n') was increased from 0.001 to 0.005, absorption and extinction by small particles ($s < 1.5$) became very significant and particle albedo decreased from 0.92 to 0.70. Hence, the low albedo of polluted waters could have been caused by either absorption due to dissolved pollutants or by absorption due to sewage particles.

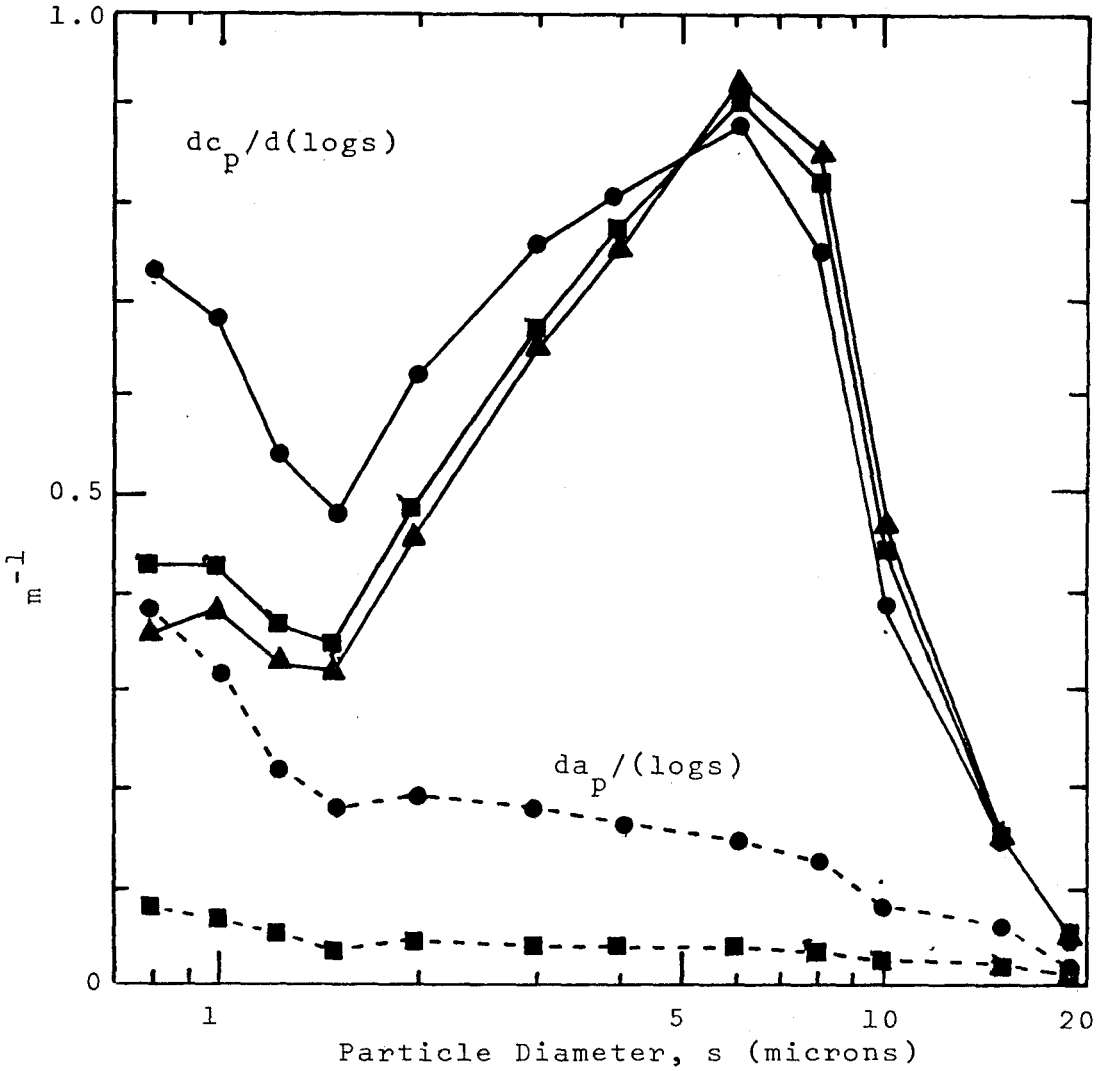

Figure 4-28. Distribution of particle extinction, c_p, and particle absorption, a_p, with particle diameter for below-thermocline polluted waters. Calculations assumed particle size distribution in Figure 4-25A, green light (λ= 500 nm), and three examples of refractive index.

Refractive Index, m = n-in'	Particle Albedo, $A = 1-a_p/c_p$
▲ 1.034	1.00
■ 1.034 - i(0.001)	.92
● 1.034 - i(0.005)	.70

4.3.5 Physical Density, Percent Organic Carbon, and Carbon Isotope Ratio

Water samples from three field stations were analyzed for carbon isotope composition, percent organic carbon, and mass concentration (mg/liter) of particulates. The laboratory work was performed by E. Myers (41). The organic carbon data indicated the fraction of material resulting from organic processes. The isotopic composition indicated whether the material was primarily of marine or terrestrial origin (Section 2.3.3). The particle volume concentration data (Figure 4-29A) were measured on the Coulter Counter. The particle density (specific gravity) was determined by dividing the mass data by the volume data (Figure 4-29B).

The data taken over the Y-diffuser at Whites Point (the most westerly diffuser in Figure 4-1) indicated that samples were taken above, in, and below a dense sewage field (particle concentrations exceeded 3 ppm). The data taken 4 nautical miles off-shore from Whites Point indicated a natural condition of high spring phytoplankton activity (high surface concentrations with decreasing concentrations below the thermocline). The Dana Point data were taken off the end of a submarine canyon that experiences a moderate amount of terrestrial runoff. Very high particle densities were noted (Figure 4-29B) indicating heavier mineral particles.

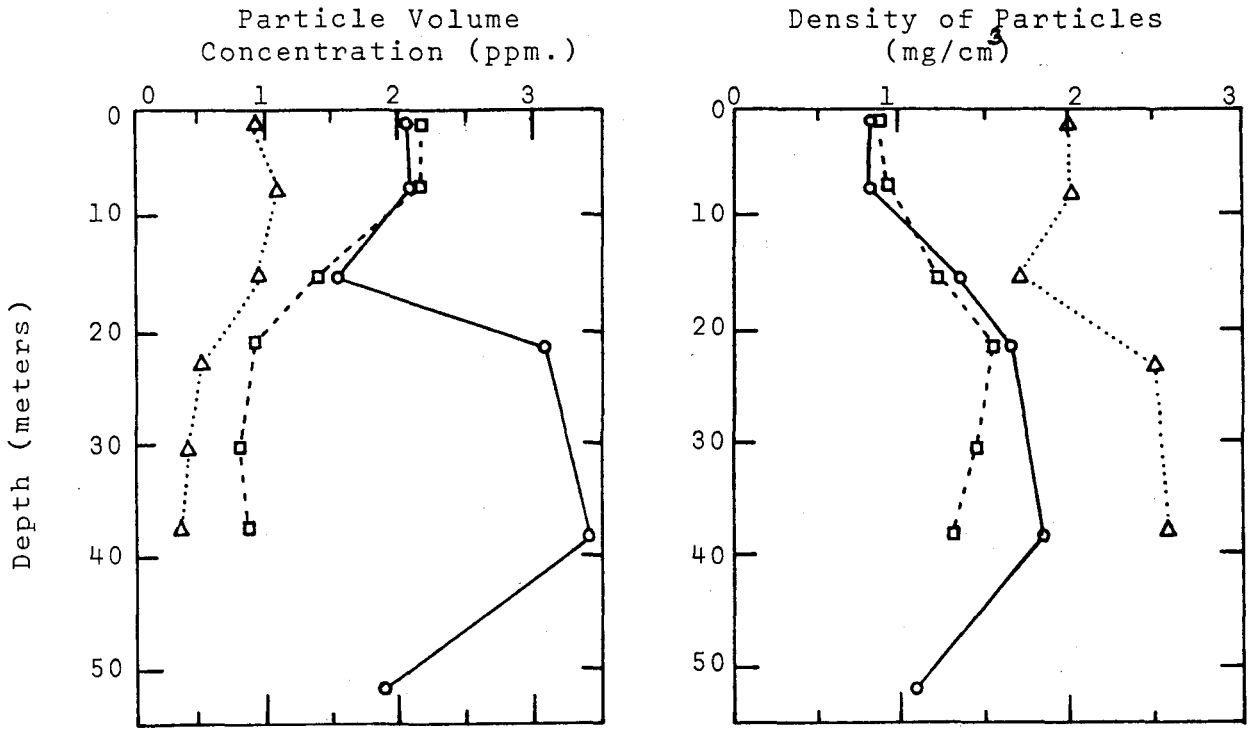

Figure 4-29. Physical characteristics of particles (volume concentration and density) at various depths. Data from three stations. Mass concentration measurements performed by E. Myers. Density calculated by dividing mass data (filtering and weighing) by volume data (Coulter counter measurements from 0.65 to 22.5 microns).

o——o	Whites Pt.	over Y-diffuser	4/12/73
□- - -□	Whites Pt.	4 n.mi. off shore	4/12/73
△·····△	Dana Pt.	4 n.mi. off shore	5/15/73

Low percent organic carbon and low isotope ratios (more negative δ_{PDB}, see Section 2.3.3) were found in the sewage field at Whites Point relative to surface waters (Figure 4-30, Y-diffuser data). The low isotope ratio reflected the terrestrial influence of the sewer outfall.

The high surface percent organic carbon at the off-shore Whites Point station was attributed to the high productivity. One suggestion was a transport of the sewer discharge by subsurface currents.

The low percent organic carbon and the low carbon isotope data from Dana Point were consistent with the high density data, indicating a high inorganic (mineral) terrestrial influence.

Particulate percent organic carbon and particulate carbon isotope ratio correlated with particle density (Figures 4-31 and 4-32). Percent organic carbon and carbon isotope ratio decreased with increasing particle density.

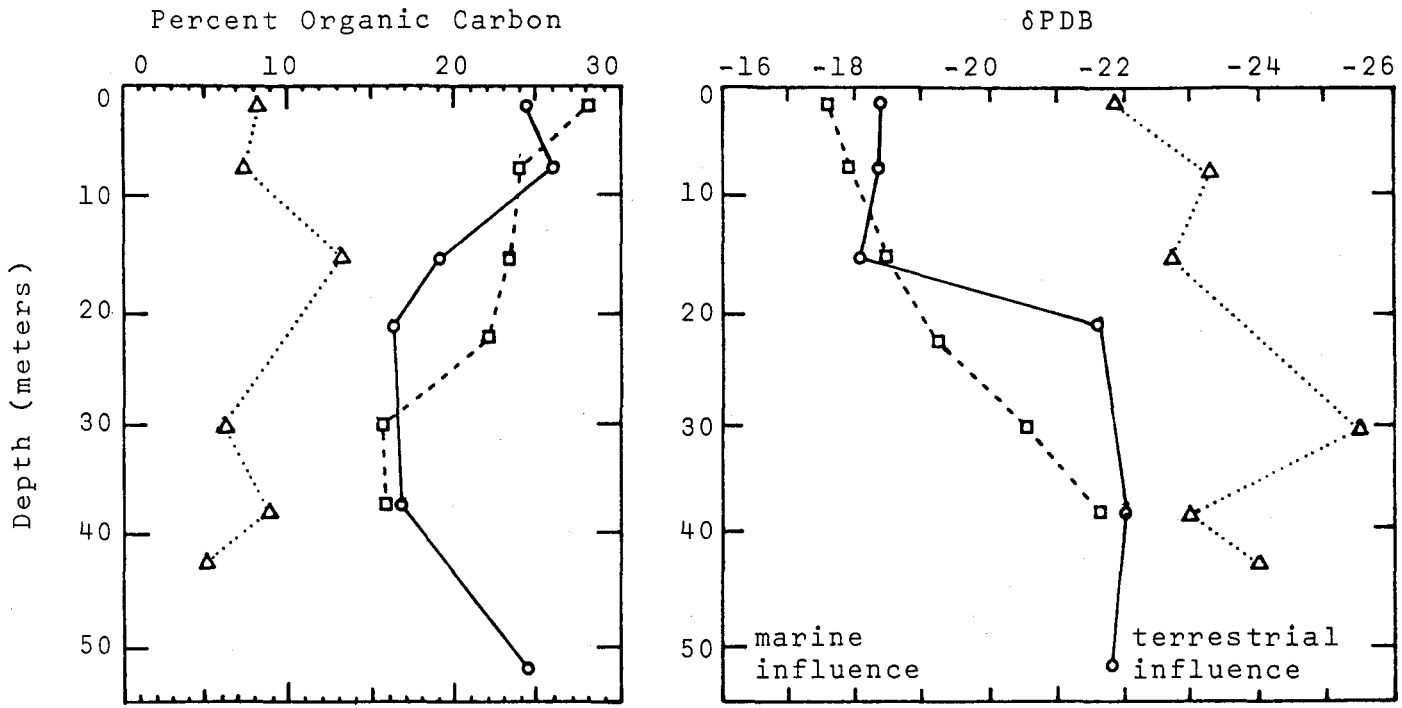

A. Particulate organic carbon vs. depth

B. Particulate carbon isotope ratio vs. depth

Figure 4-30. Particulate organic carbon and carbon isotope ratios at various depths. Measurements performed by E. Myers--see Myers (1974).

Whites Pt.	over Y-diffuser	4/12/73
Whites Pt.	4 n.mi off shore	4/12/73
Dana Pt.	4 n.mi. off shore	5/15/73

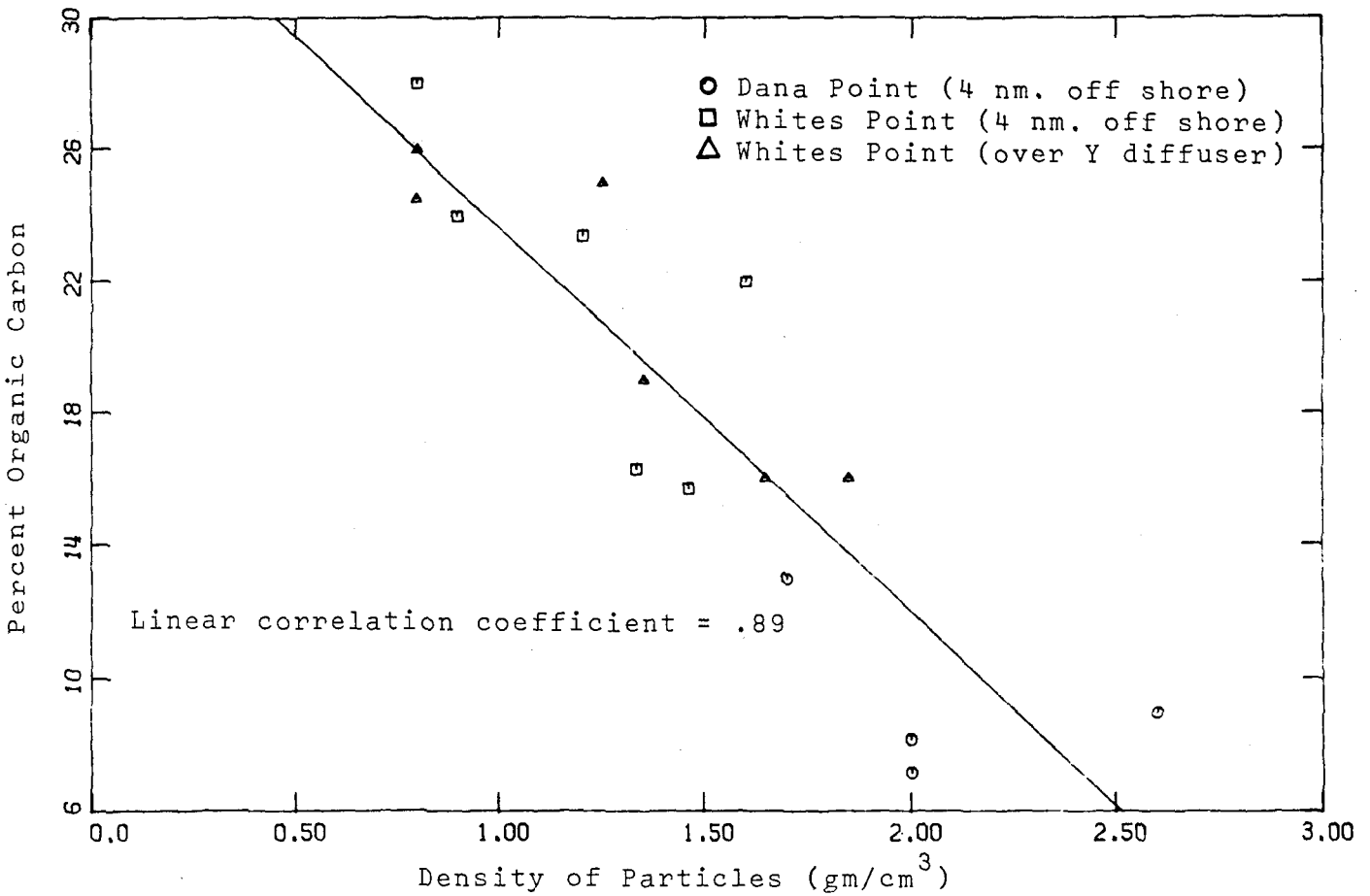

Figure 4-31. Particulate percent organic carbon vs. density of particles. Data from Figures 4-31 and 4-32. Line represents least squares fit.

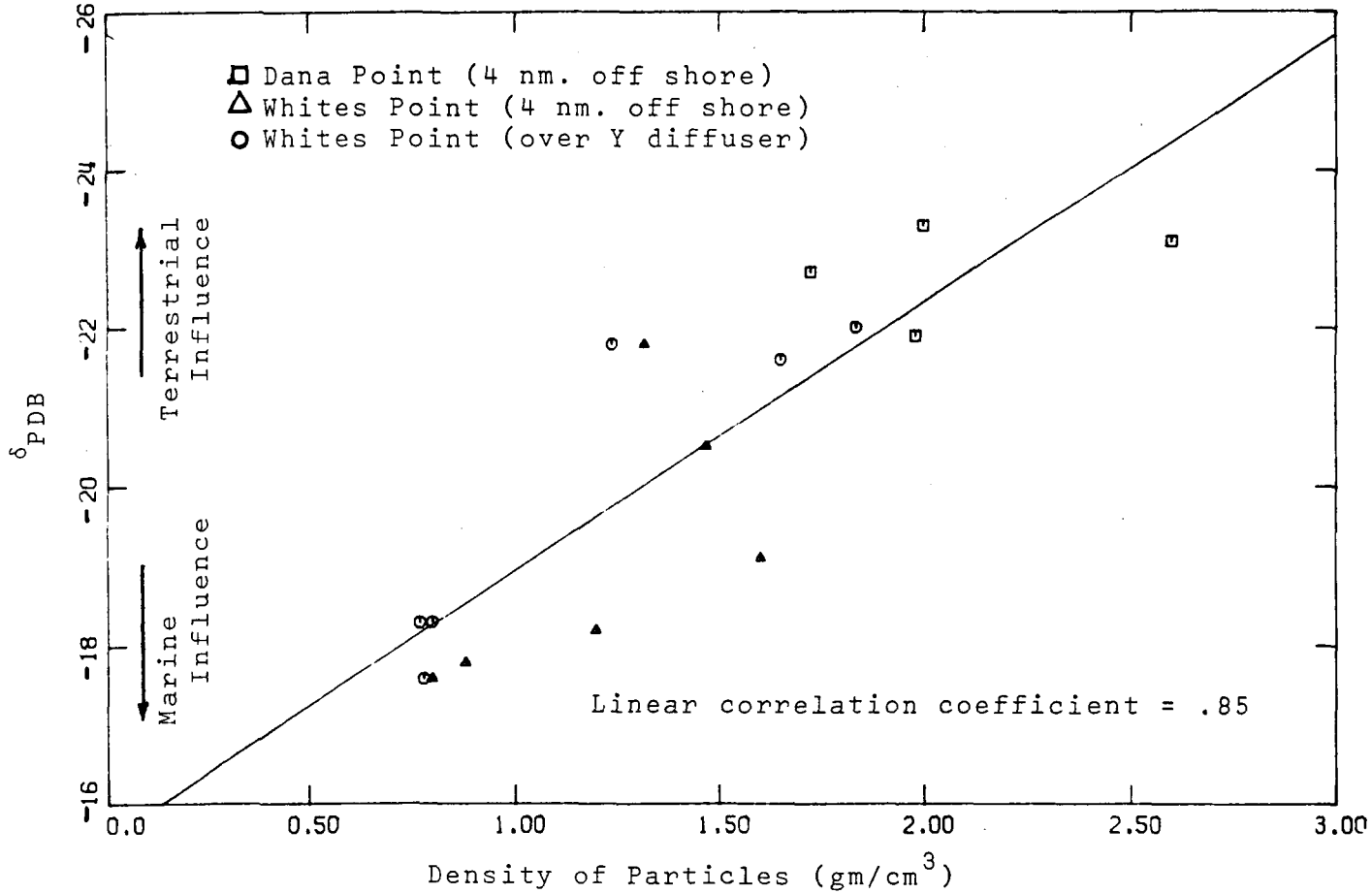

Figure 4-32. Particulate carbon isotope ratio vs. density of particles. Data from Figures 4-31 and 4-32. Line represents least squares fit.

CHAPTER 5

SUMMARY

Basic factors affecting the survivability and growth of marine plants are nutrients, tolerable temperatures, and sufficient sunlight. It has been suggested that increased turbidity in the vicinity of the LACSD sewer outfall decreases the amount of sunlight for photosynthesis. Another effect of the sewage discharge is a change in ocean surface color. Sophisticated remote sensing equipment could take advantage of relationships between color spectrum and pollution concentration for monitoring of dispersal. These considerations motivated a study of the effects of pollutants upon sunlight propagation in the ocean.

Sunlight irradiance, light beam attenuance, and particle size distributions were simultaneously measured as a function of depth. Temperature depth profiles were also measured to assess thermal stratification effects. Field stations in the vicinity of the LACSD outfall at Whites Point represented a dispersing sewage field. Background stations included Catalina, Dana Point, and Rocky Point.

A small boat was used to acquire the data. Sunlight irradiance in five colors was measured using SCUBA diving gear and a hand held bank of light meters. Each meter was fitted with a combination of interference filters

designed to transmit a narrow portion of the visible spectrum. A transmissometer and temperature probe were lowered from the boat. Light beam attenuance and temperature were recorded on deck. Water samples were taken to the Ocean Systems Laboratory at TRW Systems. There, a Coulter Counter was used to measure particle size distributions. The most significant result was that pollutants decreased the optical albedo of ocean water.

Changes in albedo have a significant effect upon ocean sunlight penetration. Light beam attenuation is the sum of light scattering and light absorption. Albedo is defined as the ratio of light scattering to light beam attenuation. Low albedo therefore means that the fraction of light beam attenuation due to scattering is small (i.e. the fraction due to absorption is high). Light scattering by ocean particles does not significantly alter sunlight penetration (98 percent is scattered in the forward direction). However, absorbed light is energy lost from the radiation field. Therefore, given waters with equal values of beam attenuance, waters with higher albedos allow deeper penetration of sunlight energy.

The euphotic zone is the portion of the ocean in which there is sufficient sunlight for plant photosynthesis to exceed plant respiration. It has been shown that one percent of surface irradiance is a reasonable estimate for the energy needs of phytoplankton. Using one percent of surface irradiance as a criterion, it was found that the average depth of the euphotic zone in natural waters was about 50 meters. Depending upon particle concentration, euphotic zone depths varied from 20 to 35 meters in the vicinity of the LACSD outfall, representing a 30 to 60 percent decrease from natural conditions.

Prior to the beginning of sewage discharge at Whites Point (1934) large kelp beds extended to water depths of 60 feet. Between 1940 and 1955, the kelp beds gradually disappeared as the rate of sewage discharge increased from an initial 17 MGD to 180 MGD. Large populations of sea urchins in the vicinity of destroyed kelp beds coupled with studies showing that dissolved organics from the waste discharge could be utilized by urchins indicate that increased predation is preventing the kelp beds from returning to their original state.

It is suggested that decreased light penetration is also a factor. Data from the natural water stations show that 60 feet (the depth to which the original kelp beds

grew) corresponds to 10 percent of surface illumination. Pollutants in the vicinity of the outfall have reduced the depth of 10 percent penetration to 30 feet.

Water surface color spectra indicated that pollutants increased light absorption at all wavelengths. Of the light entering the ocean, a smaller percent was returned to the atmosphere in polluted waters compared to natural waters. The difference between natural and polluted waters was most pronounced in the violet, blue, and green. A spectral dependence upon particle concentration was noted. High concentrations produced a yellow surface color.

The average particle concentration in polluted waters was twice that of background waters. The LACSD discharge caused a bimodal increase in particle numbers as a function of particle diameter: there was a significant increase for particles less than 1.5 microns and a secondary increase at 8 microns.

Scattering and absorption by particles were calculated assuming real and complex particle refractive indices. Assuming real refractive indices (the case of non-absorbing particles) the average refractive index for natural waters was calculated to be 1.064. The average refractive index for polluted waters was 1.037. (The average value was 1.034 in the most polluted waters below the thermocline.)

The lower index for polluted waters indicated that light scattering by small (less than 1.5 micron diameter) sewage particles was less significant than an equivalent concentration of natural particles. This effect should be taken into account if optical methods are used to measure sewage particle concentrations.

Assuming the above real particle refractive indices and the average particle size distributions for polluted and natural waters, scattering for both types of waters was maximum between particle diameters 3 and 8 microns. Calculations assuming complex refractive indices, $m = 1.034$, $1.034 - i(0.001)$, and $1.034 - i(0.005)$, showed that light absorption by sewage particles less than 1.5 microns in diameters became very significant as the complex part was increased. If sewage particles were absorbing in character, this would account for the lower albedo in polluted waters.

Water samples from three field stations were analyzed for carbon isotope composition, percent organic carbon, and mass concentration (mg/liter) of particulates. The laboratory work was performed by E. Myers, a fellow graduate student studying sewage discharge effects upon marine sediment carbon composition (41). Particles in a dense sub-thermocline sewage field had a lower percent organic carbon

and a lower carbon isotope ratio than surface water particles.

The organic carbon data indicated the fraction of material resulting from organic processes. The isotope composition indicated whether the material was primarily of marine or terrestrial origin. The carbon composition data were correlated with the particle size and mass data. Particles with a higher terrestrial influence and particles with lower percent organic carbon had a higher specific gravity. Correlation in each case was statistically significant.

APPENDIX A

Sunlight Propagation Model--Preliminary Results

This appendix presents a sunlight propagation model that calculates upwelling and downwelling irradiance as a function of optical depth, τ, and albedo, A. Results were compared with the field data reported in Section 4.2.5. This afforded quantitative estimates of A for the polluted and natural water stations. The results are preliminary. Further development of the model will increase confidence in the albedo estimates. Dr. W. H. White provided guidance in developing the model and wrote the computer program for the IBM 370/155 computer (72).

Sunlight is transmitted, scattered, or absorbed as it propagates from surface waters to deep waters. In ocean waters, 98 percent of light scattering is forward (28). Therefore most of the scattered sunlight continues to propagate to deeper waters. Absorbed sunlight is lost from the visible radiation spectrum and converted to other forms (e.g. heat or photo-chemical products).

An optical parameter for classifying ocean waters according to depth of sunlight energy penetration is the albedo, A. It is the ratio of scattering coefficient to beam attenuation coefficient.

(A-1) $A = b/c = b/(a+b)$

where b = scattering coefficient
c = attenuation coefficient
a = absorption coefficient

Given water with equal values of beam attenuance, those waters with greater albedos have deeper euphotic zones. A lower fraction of the attenuated light is absorbed (more is scattered forward). The following is a sunlight radiative transfer model that predicts attenuance of downwelling and upwelling sunlight irradiance as a function of ocean optical depth (real depth weighted by attenuance) for various albedos (72). The sunlight irradiance data from Chapter 4 will be compared with the model results for estimating the albedo differences between polluted and natural waters.

If $L(z, \gamma, \phi)$ represents the radiance (watt/m^2-steradian) at depth z (meters) in the direction defined by the azimuth angle ϕ and the zenith angle γ (Figure A-1),

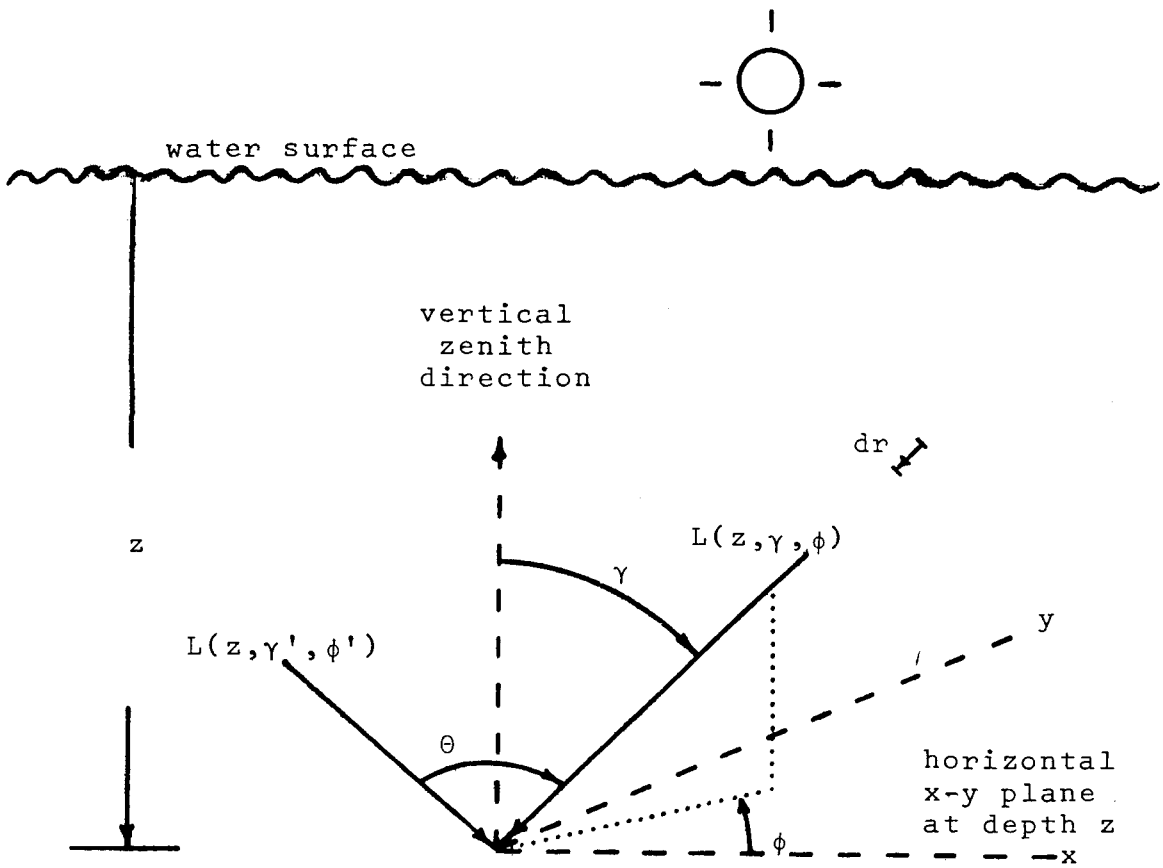

Figure A-1. Coordinate system for sunlight propagation model.

ϕ, ϕ' = azimuth angles

γ, γ' = zenith angles

$L(z,\gamma,\phi)$ = radiance in direction (γ,ϕ) at depth, z, below water surface.

θ = scattering angle between the directions of $L(z,\gamma',\phi')$ and $L(z,\gamma,\phi)$

dr = incremental distance in direction (γ,ϕ)

the change in radiance, dL, over the distance, dr is given by the radiative transfer equation (28, 49):

$$\text{(A-2)} \qquad \frac{dL}{dr} = -cL + L^*$$

where $L = L(z,\gamma,\phi$

$$L^* = \int_0^{2\pi}\int_0^{\pi} \beta(\gamma,\phi;\gamma',\phi')L(z,\gamma',\phi')\sin\gamma' d\gamma' d\phi'$$

$\beta(\gamma,\phi;\gamma',\phi') = \beta(\theta)$

= volume scattering function

θ = angle between the directions (γ,ϕ) and (γ',ϕ').

c = beam attenuation coefficient (m^{-1})

The first term on the right of equation A-2 represents loss by attenuation. The second term, L*, is the path radiance (49) and represents gain by scattering from all directions into the direction (γ,ϕ). The scattering coefficient is the integral over ϕ of the volume scattering function:

$$\text{(A-3)} \qquad b = 2\pi \int_0^{\pi} \beta(\theta)\sin\theta d\phi$$

To introduce the parameters albedo and optical depth into the basic transfer equation, an angular albedo function, $p(\phi)$, is defined such that

(A-4) $$\beta(\phi) = cp(\phi).$$

Since $A = b/c$,

(A-5)

$$A = 2\pi \int_0^{\pi} \sin\theta p(\theta) d\theta$$

Dividing both sides of equation 2-6 by c (assuming isotropic beam attenuance) and using equation A-4, the radiative transfer equation can be expressed as

(A-6) $$\frac{dL}{d\rho} = -L + L^{**}$$

where $L = L(\tau, \gamma, \phi)$

$$L^{**} = \int_0^{\pi} \int_0^{\pi} p(\gamma, \phi; \gamma', \phi') L(\tau, \gamma', \phi') \sin\gamma' d\gamma' d\phi'$$

$d\rho$ = incremental optical distance (cdr)

τ = ocean optical depth

$$= \int_0^z c(z')dz'.$$

$c(z)$ = beam attenuance as a function of water depth

Equation A-6 was solved numerically for the angular radiance distribution as a function of ocean optical depth. The problem was first converted to one of azimuth symmetry by assuming a symmetrical radiance boundary condition just below the ocean surface (Figure A-2). The sun was simulated by an annular ring. This was assumed permissible since the model results were to be compared to field irradiance data measured on a horizontal plane.

Zero reflectance for upwelling irradiance was assumed at the water surface. Near-surface comparisons between model results and field data would therefore be inaccurate. The boundary condition at $z = \infty$ was that solutions monotonically decrease in value with depth.

The angular albedo function, $p(\theta)$, is proportional to the volume scattering function, $\beta(\theta)$ (equation A-4). To save computation time, a single exponential was used to approximate the shape of the volume scattering data (Figure A-3). Similarly,

$$p(\theta) = K \exp\left(B_1(\cos(\theta) + B_2)^N\right), \tag{A-7}$$

where values for B_1, B_2, and N are given in Figure A-3. The value for K (a constant of proportionality) depends upon the albedo, A (equation A-5).

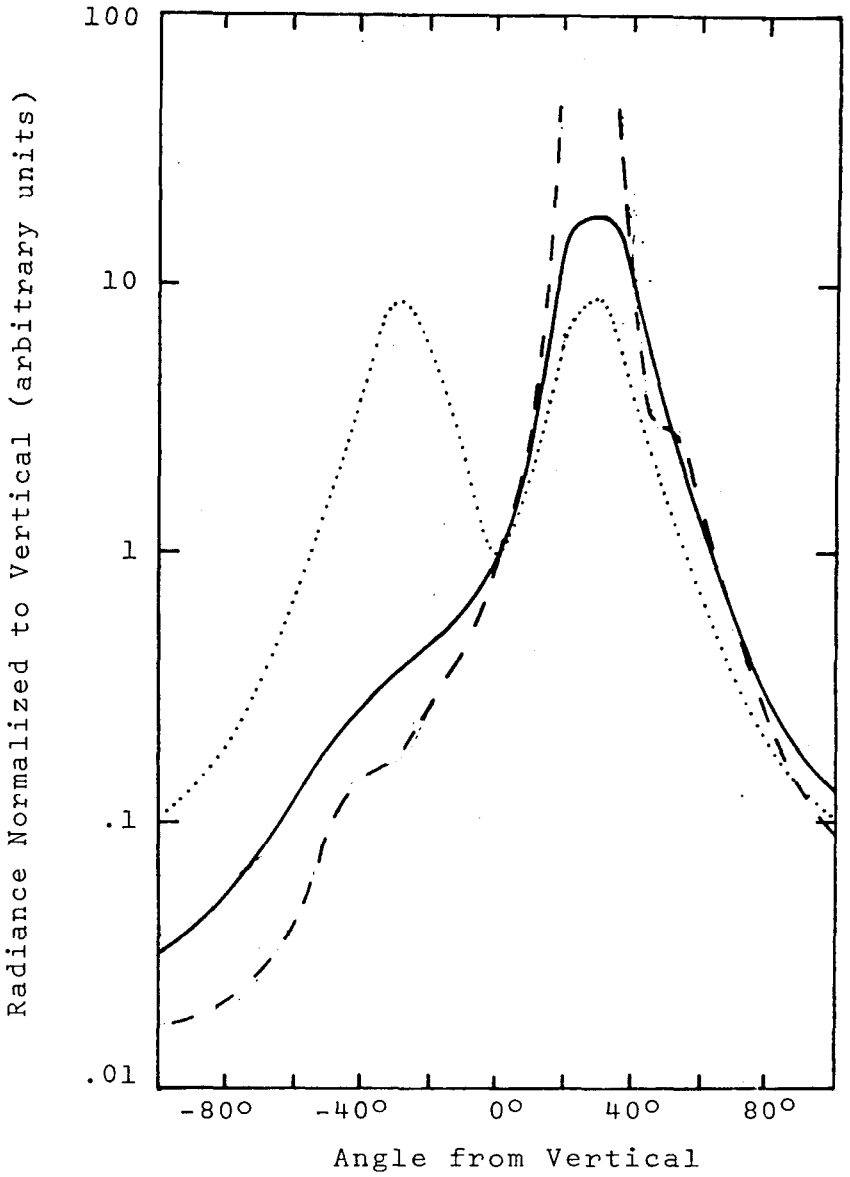

Figure A-2. Radiance distributions just below water surface.

Measurements in the vertical plane of the sun, Jerlov (1968).

——— Baltic Sea: green light, 5 meters deep

– – – Gullmar Fjord: green light, 1.9 meters deep

Surface boundary condition for sunlight propagation model.

····· Simulates sun as an annular ring for azimuth symmetry. Effective sun zenith angle = 30° below water surface (corresponding to ~40° above the water surface).

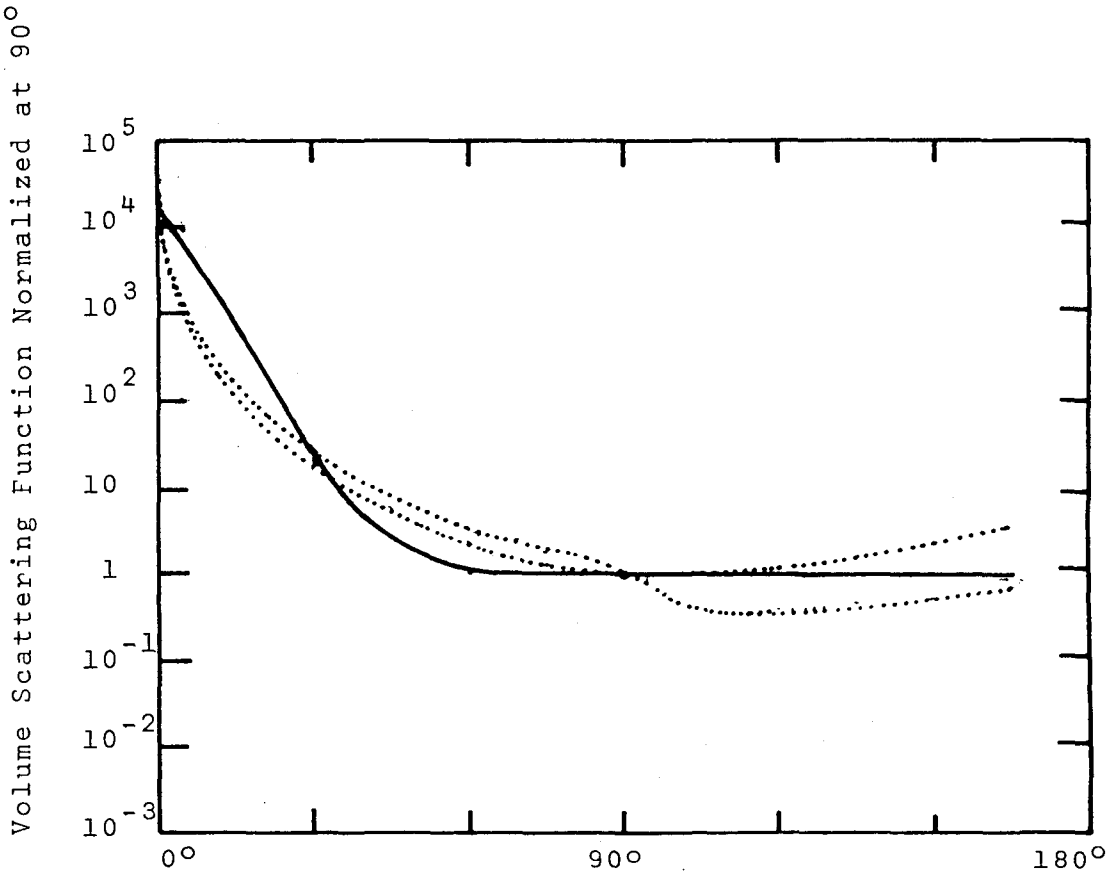

Figure A-3. Volume scattering function for sunlight propagation model.

:::::::::::: Range of scattering measurements by various investigators in different parts of the world, Duntley (1963)

——— Volume scattering used for sunlight propagation model represented by the function

$$\beta(\theta) = \exp\left(B_1(\cos(\theta) + B_2)^N\right)$$

$$B_1 = .05$$

$$B_2 = .5$$

$$N = 13$$

Using the method of discrete ordinates, after Chandrasekhar (12), the angular radiance distribution at optical depth, τ, was represented by 30 radiance "streams" (one stream for each six degrees of zenith between 0 and 180^{o}). This resulted in a set of integro-differential equations (one for each stream) amenable to standard numerical solutions (18). The upwelling irradiance, E_u, and the downwelling irradiance, E_d, were then obtained by integrating the radiance distributions at each optical depth.

$$(A\text{-}8) \qquad E_u(\tau) = \int_{\pi}^{\pi} L(\tau,\gamma)\sin\gamma d\gamma$$

$$(A\text{-}9) \qquad E_d(\tau) = \int_{0}^{\pi/2} L(\tau,\gamma)\sin\gamma d\gamma$$

The problem was programmed on an IBM 370/155 computer (72) and results were obtained for albedo values from 0.4 to 0.99 (Figure A-4). The computed irradiance profiles were then compared with the measured profiles in Chapter 4 to estimate the albedo of polluted and natural waters.

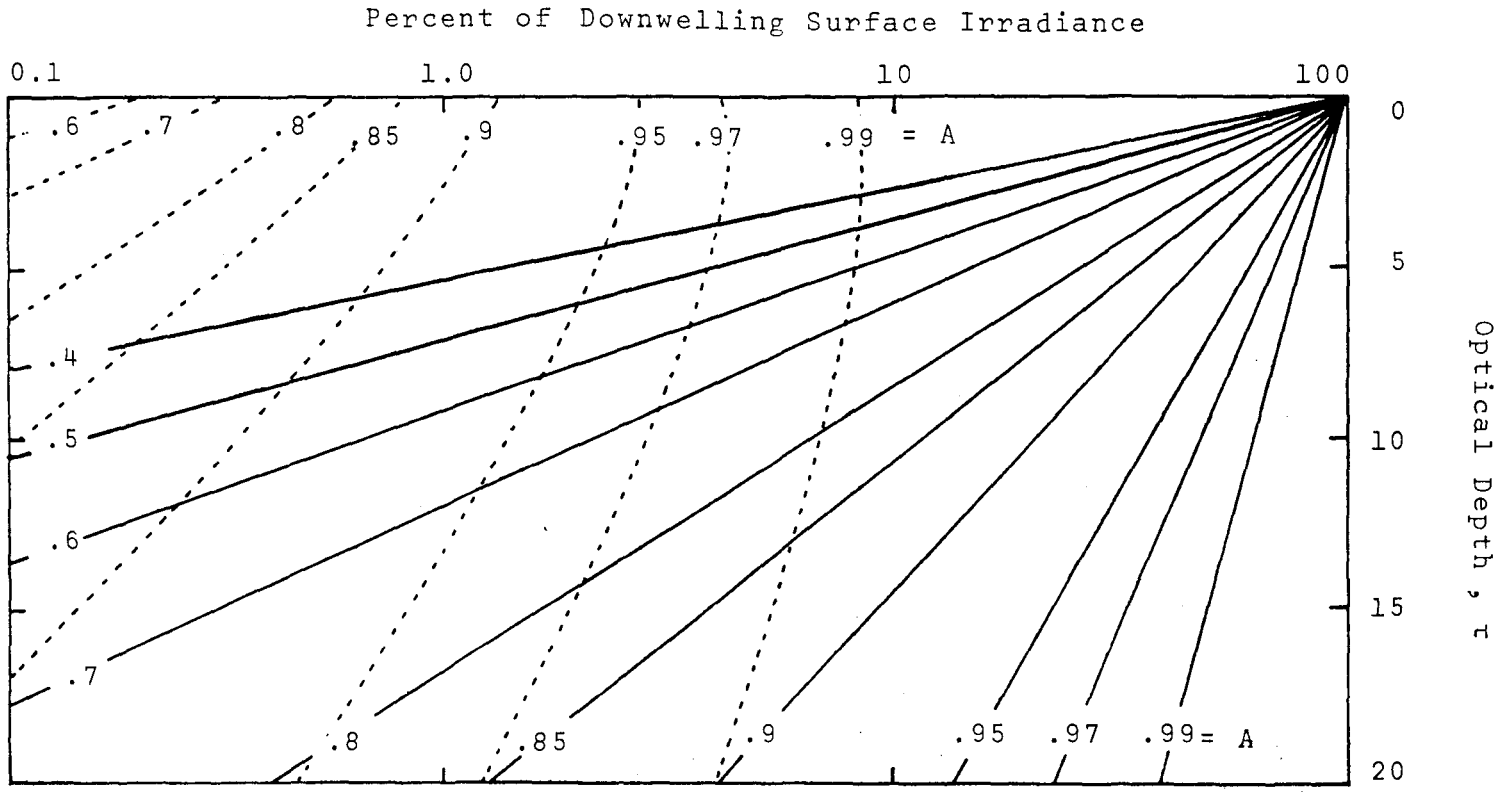

Figure A-4. Results of sunlight radiative transfer model (SEALIGHT) using the method of discrete ordinates with 30 streams. Numbers for each curve are albedo values (ratio of scattering coefficient to attenuation coefficient) White and Peterson (1973).

---- Upwelling Irradiance

——— Downwelling Irradiance

Comparing the results of the sunlight propagation model with the natural water irradiance profiles (Figure A-5), natural water albedos ranged from 0.7 to 0.9 for optical depths greater than 5 (estimates made by comparing attenuance values or slopes). Near-surface estimates were greater than 0.99.

At station 4 in the polluted waters (Figure A-6) A ranged from 0.9 above the strong thermocline ($5 < \tau < 10$) to 0.4 in the sewage field below the thermocline. For a weak thermocline (station 6) the field was distributed from surface to deep waters and the albedo was more uniform ranging from 0.7 to 0.9 (for $\tau > 5$). Near surface estimates were again high: 0.99 at station 4 and 0.95 at station 6.

The absorption coefficient for pure water at 530 nm. is 0.04 (attenuation less scattering, Figure 2-10). Near-surface total attenuation (Figure 4-17) ranged from 0.3 at station 5 to 0.9 at station 6. Maximum possible near-surface albedos (assuming a mixture of pure water and non-absorbing particles) would therefore range from 0.87 to 0.96 ($A = 1 - a/c$). Comparing field data with the model calculations results in significantly higher estimates for near-surface albedo. However, near-surface inaccuracies were

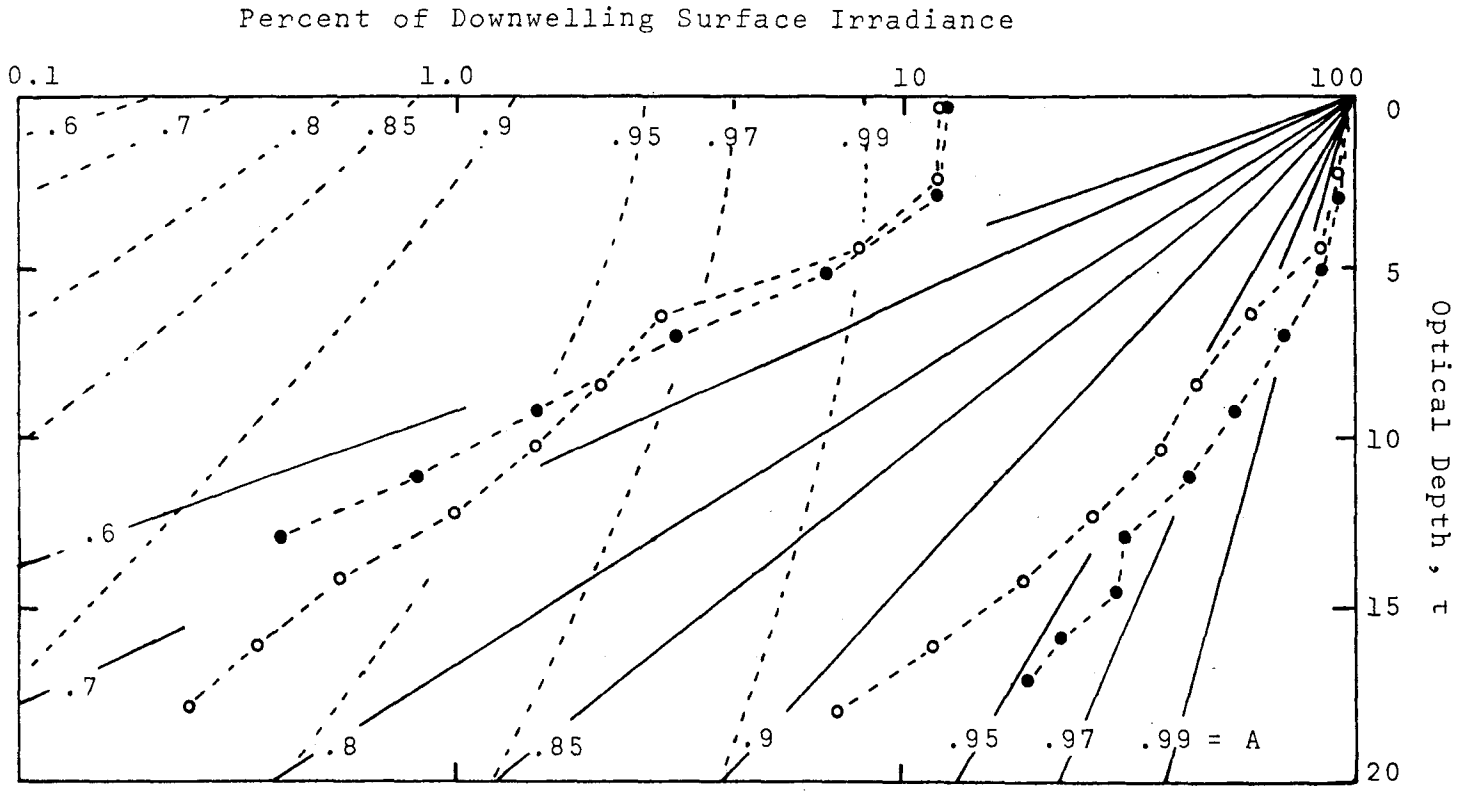

Figure A-5. Comparison of natural water irradiance data (Figure 4-18) with radiative transfer model (Figure A-4). Albedo values given for each model curve. (Green light, 530 nm.)

o---o Station 1: Natural waters--weak thermocline
●---● Station 2: Natural waters--strong thermocline
------ Upwelling irradiance model results
——— Downwelling irradiance model results

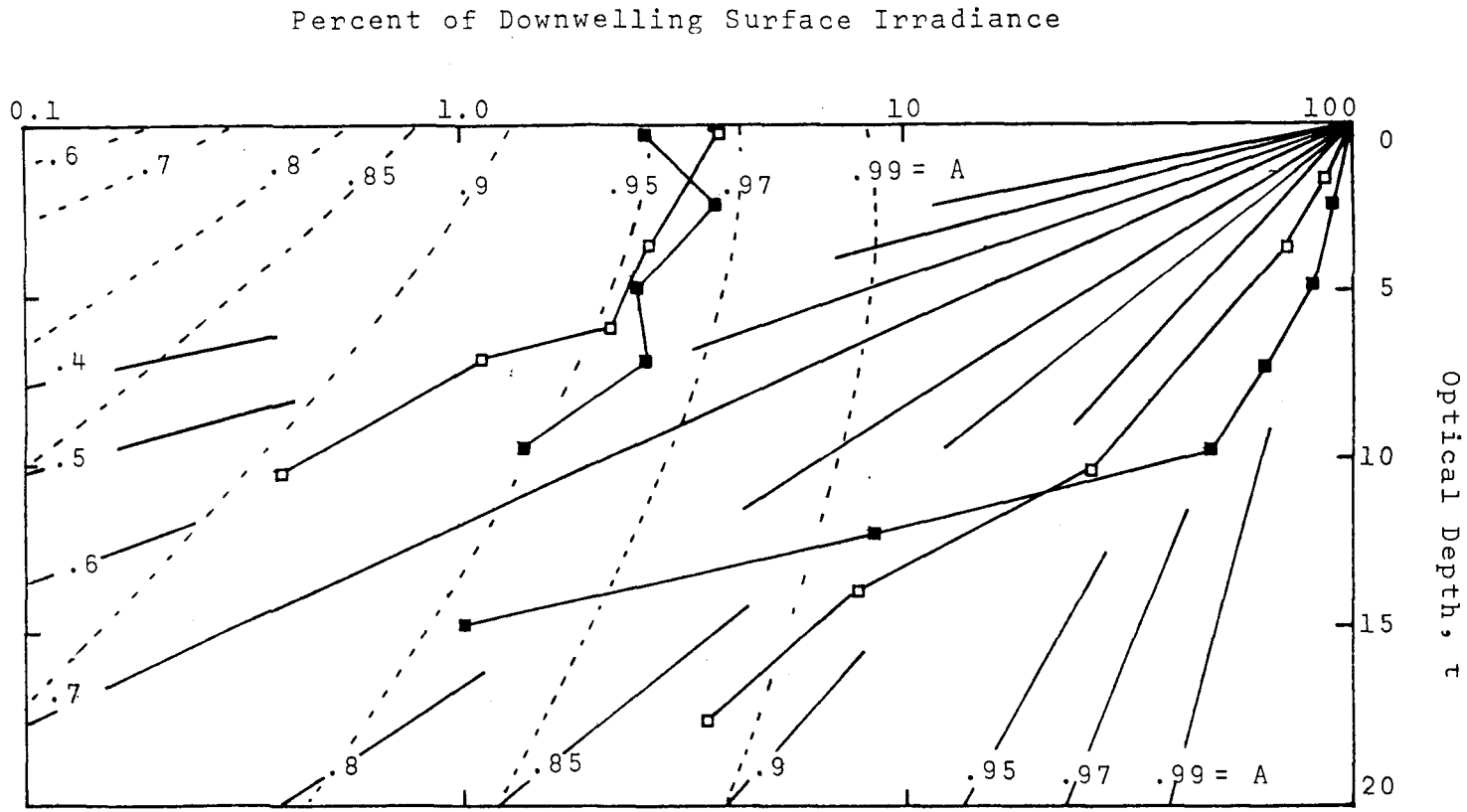

Figure A-6. Comparison of polluted water irradiance data (Figure 4-18) with radiative transfer model (Figure A-4). Albedo values given for each model curve. (Green light, 530 nm.)

Station 6: Polluted waters--weak thermocline
Station 4: Polluted waters--strong thermocline
-------- Upwelling irradiance model results
———— Downwelling irradiance model result

expected since the water surface boundary condition for the model calculations did not account for reflection of upwelling irradiance.

Again, the above model results are preliminary. Further effort is required in the following areas:

1) Zero reflectance was assumed for upwelling irradiance at the water surface. Reflectance should be accounted for or the resulting errors analyzed.

2) The single exponential fit for $\beta(\theta)$ (solid curve, Figure A-3) should be improved to better fit the volume scattering measurements (dotted curves, Figure A-3).

3) Effects of varying sun zenith angle should be analyzed. The 40° assumption for the model calculations (Figure A-2) agrees with the field data for two of the stations (stations 4 and 6, Figure A-6). However, the sun zenith for stations 1 and 2 (Figure A-5) were 50° and 15° respectively. The small sun zenith angle (γ in Figure A-1) might account for the increased sunlight penetration at Station 2.

4) Possible errors due to the azimuth symmetry assumption for the surface boundary condition (Figure A-2) should be investigated.

APPENDIX B

PARTICLE SIZE SPECTRA

This Appendix presents the particle size distribution data in tabular form. Each table gives the station location, date of sampling, and depths of samples (feet). The sizes of Coulter Counter apertures (microns) used to make the measurements are also included (see discussion in Section 3.2). The data are presented in chronological order.

TABLE B-1 PARTICLE SIZE SPECTRA, dN/ds (number/ml/micron)

STATION: Laguna Beach Outfall* DATE: 4/15/72

Coulter Aperture (micron)	Particle Diameter (micron)	dN/ds (number/ml/micron
	0.5	480,000,000
	0.6	210,000,000
	0.7	65,000,000
	0.8	30,000,000
	0.9	13,000,000
	1.0	7,000,000
	1.25	1,100,000
	1.5	530,000
	2.0	200,000

* Sample taken directly in front of outfall discharge part at water depth 75 feet.

TABLE B-2 PARTICLE SIZE SPECTRA, dN/ds (number/ml/micron)

STATION: Bunker Point DATE: 10-12-72

Coulter Aperture (microns)	Particle Diameter (microns)	WATER SAMPLE DEPTH (Feet)					
		0	15	30	45	60	75
30	0.7	200×10^4	240×10^4	220×10^4	350×10^4	580×10^4	860×10^4
	0.8	87×10^4	120×10^4	120×10^4	170×10^4	300×10^4	390×10^4
	1.0	26×10^4	45×10^4	48×10^4	52×10^4	120×10^4	83×10^4
	1.25	10×10^4	16×10^4	14×10^4	17×10^4	24×10^4	24×10^4
	1.5	51,000	10×10^4	71,000	59,000	92,000	84,000
	2.0	28,000	47,000	28,000	13,000	20,000	21,000
	3.0	4,400	7,400	5,100	5,100	4,400	7,400
100	2	12,000	24,000	18,000	23,000	35,000	23,000
	3	2,800	7,100	6,600	5,600	5,000	6,000
	4	1,500	3,700	3,000	2,700	2,300	2,800
	6	590	1,100	870	750	610	780
	8	150	280	190	220	130	180
	10	68	130	110	120	70	96
	15	11	30	7	15	8	13
	20	0	6	0	0	0	0

TABLE B-3 PARTICLE SIZE SPECTRA, dN/ds (number/ml/micron)

STATION: Whites Point DATE: 11/2/72

Coulter Aperture (microns)	Particle Diameter (microns)	WATER SAMPLE DEPTH (Feet)					
		0	15	30	45	60	75
30	0.7	120 x 10^4	160 x 10^4	150 x 10^4	300 x 10^4	320 x 10^4	600 x 10^4
	0.8	52 "	86 "	79 x "	180 x "	180 x "	300 x "
	1.0	22 "	39 "	32 "	110 x "	55 x "	96 "
	1.25	64,000	13 "	12 "	27 "	15 x "	23 "
	1.5	40,000	68,000	51,000	11 "	74,000	12 "
	2.0	19,000	22,000	33,000	39,000	28,000	34,000
	3.0	5,100	6,600	6,600	10,000	3,700	8,100
100	2	28,000	*	*	23,000	23,000	33,000
	3	2,300	4,900	8,100	4,600	3,500	6,400
	4	1,100	2,300	2,300	2,200	1,700	2,100
	6	270	390	470	500	330	570
	8	99	99	99	110	71	150
	10	23	31	34	51	28	90
	15	4.1	3.7	3.7	7.5	9.4	15
	20	0	0	0	0	0	0

*Excess noise in measurement

0 No counts registered during count period

TABLE B-3 (cont'd) PARTICLE SIZE SPECTRA, dN/ds (number/ml/micron)

STATION: WHITES POINT Date: 11/2/72

Coulter Aperture (microns)	Particle Diameter (microns	WATER SAMPLE DEPTH (Feet)					
		0	15	30	45	60	75
11	0.5	870 x 10^4	170 x 10^5	*	520 x 10^5	680 x 10^5	410 x 10^5
	0.6	380 "	50 "	*	94 "	58 "	91 "
	0.7	120 "	16 "	153 x 10^4	30 "	32 "	60 "
	0.8	31 "	42 x 10^4	60 "	17 "	22 "	49 "
	1.0	48,000	14 "	20 "	56 x 10^4	76 x 10^4	23"

*Excess noise in counts

TABLE B-4 PARTICLE SIZE SPECTRA, dN/ds (number/ml/micron)

STATION: Rocky Point DATE: 11/29/72

Coulter Aperture (microns)	Particle Diameter (microns)	WATER SAMPLE DEPTH (Feet)					
		0	15	30	45	60	75
30	0.7	190 x 10^4	220 x 10^4	350 x 10^4	280 x 10^4	300 x 10^4	380 x 10^4
	0.8	77 "	120 "	180 "	120 "	150 "	140 "
	1.0	24 "	47 "	28 "	28 "	46 "	33 "
	1.25	11 "	16 "	14 "	92,000	11 "	11 "
	1.5	63,000	71,000	60,000	41,000	37,000	59,000
	2.0	22,000	29,000	17,000	18,000	10,000	20,000
	3.0	6,600	8,200	4,500	4,100	3,800	4,100
100	2	14,000	21,000	16,000	14,000	13,000	16,000
	3	6,600	5,100	2,500	3,600	3,500	4,000
	4	1,400	1,700	1,400	1,400	2,300	1,700
	6	360	640	400	300	260	450
	8	100	180	110	82	73	120
	10	54	90	56	41	36	61
	15	9	12	9	4.5	4.5	7.5
	20	0	0	0	0	0	0

0 No counts registered during count period.

TABLE B-4 (Cont'd.) PARTICLE SIZE SPECTRA, dN/ds (number/ml/micron)

STATION: ROCKY POINT Date: 11/29/72

Coulter Aperture (microns)	Particle Diameter (microns)	WATER SAMPLE DEPTH (Feet)					
		0	15	30	45	60	75
11	0.5	100×10^5	210×10^5	340×10^5	79×10^5	95×10^5	160×10^5
	0.6	23 "	41 "	63 "	46 "	39 "	45 "
	0.7	14 "	22 "	36 "	26 "	26 "	31 "
	0.8	77 "	12 "	18 "	12 "	15 "	14 "
	1.0	15 "	42×10^4	39×10^4	23×10^4	50×10^4	45×10^4

TABLE B-5 PARTICLE SIZE SPECTRA, dN/ds (number/ml/micron)

STATION: Whites Point DATE: 11/29/72

Coulter Aperture (microns)	Particle Diameter (microns)	WATER SAMPLE DEPTH (Feet)					
		10'	30[2]				
30	0.7	270×10^4	140×10^4				
	0.8	180 "	62 "				
	1.0	94 "	20 "				
	1.25	25 "	58,000				
	1.5	82,000	25,000				
	2.0	27,000	9,300				
	3.0	5,300	1,800				
100	2	27,000	9,000				
	3	6,300	2,200				
	4	2,800	930				
	6	990	270				
	8	340	56				
	10	140	36				
	15	7.5	4.5				
	20	3.3	0				

0 No counts registered during count period

1 Sample taken in surfacing sewage plume

2 Sample taken in apparently clear water adjacent to surfacing sewage plume

TABLE B-6 PARTICLE SIZE SPECTRA, dN/ds (number/ml/micron)

STATION: Corona Del Mar DATE: 12/2/72

Coulter Aperture (microns)	Particle Diameter (microns)	WATER SAMPLE DEPTH (Feet) 0	10	25	40	55	
30	0.7	110 x 10^4	74 x 10^4	94 x 10^4	89 x 10^4	92 x 10^4	
	0.8	69 x "	47 "	52 "	62 "	54 "	
	1.0	33 "	24 "	23 "	35 "	25 "	
	1.25	11 "	58,000	77,000	58,000	60,000	
	1.5	46,000	31,000	34,000	24,000	27,000	
	2.0	13,000	10,000	9,100	8,000	8,100	
	3.0	4,900	1,700	2,200	1,300	2,000	
100	2	12,500	16,000	18,000	11,000	11,000	
	3	2,900	2,900	4,200	2,000	3,000	
	4	1,000	1,600	1,700	1,100	1,500	
	6	260	430	480	280	400	
	8	56	100	120	62	88	
	10	29	59	63	32	43	
	15	7.5	4.5	7.5	4.5	7.5	
	20	0	0	1.1	0	0	

0 No counts registered during count period

TABLE B-6 (Cont'd) PARTICLE SIZE SPECTRA, dN/ds (number/ml/micron)

STATION: Corona Del Mar Date: 12/2/72

Coulter Aperture (microns)	Particle Diameter (microns)	WATER SAMPLE DEPTH (Feet)					
		0	10	25	40	55	
11	0.5	79×10^5	115×10^5	81×10^5	89×10^5	96×10^5	
	0.6	15 "	16 "	11 "	13 "	12 "	
	0.7	98×10^4	70×10^4	68×10^4	75×10^4	76×10^4	
	0.8	69 "	47 "	52 "	62 "	54 "	
	1.0	23 "	17 "	17 "	22 "	15 "	

TABLE B-7 PARTICLE SIZE SPECTRA, dN/ds (number/ml/micron)

STATION: CATALINA DATE: 1/19/73

Coulter Aperture (microns)	Particle Diameter (microns)	WATER SAMPLE DEPTH (Feet) 55'					
30	0.7	666 x 10^4					
	0.8	330 "					
	1.0	180 "					
	1.25	40 "					
	1.5	60,000					
	2.0	18,000					
	3.0	2,200					
100	2	7,600					
	3	1,200					
	4	310					
	6	37					
	8	14					
	10	5.6					
	15	0					
	20	0					

0 No counts registered during count period

1 Sample taken 100 yards off White's Landing. High counts for diameters less than 2 microns probably due to bacteria growth during sample storage (~8 hours).

TABLE B-8 PARTICLE SIZE SPECTRA, dN/ds (number/ml/micron)

STATION: Mid-Channel DATE: 1-20-74

Coulter Aperture (microns)	Particle Diameter (microns)	WATER SAMPLE DEPTH (Feet)					
		30					
30	0.7	440 x 10^4					
	0.8	230 x 10^4					
	1.0	145 "					
	1.25	38 "					
	1.5	52,000					
	2.0	19,000					
	3.0	3,700					
100	2	5,600					
	3	1,500					
	4	1,000					
	6	47					
	8	14					
	10	5.6					
	15	0					
	20	0					

0 No counts

1 Sample taken midway between Catalina Island and Los Angeles Harbor. High counts for diameters less than 2 microns probably due to bacteria growth during sample storage (~ 6 hours)

TABLE B-9 PARTICLE SIZE SPECTRA, dN/ds (number/ml/micron)

STATION: MORRO BAY[6] DATE: 2-14-74

Coulter Aperture (microns)	Particle Diameter (microns)	WATER SAMPLE DEPTH (Feet)					
		0[1]	0[2]	20[3]	20[4]	0[5]	
30	0.7	280 x 10^4	270 x 10^4	160 x 10^4	308 x 10^4	250 x 10^4	
	0.8	160 "	150 "	70 "	34 "	130 "	
	1.0	100 "	98 "	42 "	22 "	71 "	
	1.25	58 "	55 "	25 "	12 "	39 "	
	1.5	26 "	29 "	14 "	58,000	16 "	
	2.0	96,000	10 "	42,000	17,000	52,000	
	3.0	21,000	19,000	7,300	4,000	8,400	
100	2	33,00	38,000	15,000	6,500	25,000	
	3	9,000	9,900	3,400	1,000	4,800	
	4	3,100	3,400	1,000	340	1,500	
	6	710	520	240	120	290	
	8	210	110	50	21	71	
	10	100	59	17	22	51	
	15	7.5	3.8	0	0	0	
	20	0	0	0	0	0	

0 No counts registered during count period
1 intake to power plant
2 power plant discharge canal
3 100 yds. offshore from discharge canal
4 1 mile offshore
5 channel entrance to Morro Bay
6 data taken after storm during heavy land runoff.

TABLE B-10 PARTICLE SIZE SPECTRA, dN/ds (number/ml/micron)

STATION: Whites Point (200' depth) DATE: 2/27/73

Coulter Aperture (microns)	Particle Diameter (microns)	WATER SAMPLE DEPTH (Feet)					
		0	30	70			
30	0.7	800 x 10^4	720 x 10^4	1300 x 10^4			
	0.8	250 "	270 "	530 "			
	1.0	72 "	94 "	160 "			
	1.25	23 "	29 "	58 "			
	1.5	73,000	81,000	17 "			
	2.0	33,000	33,000	62,000			
	3.0	9,200	11,000	9,100			
100	2	29,000	30,000	52,000			
	3	6,900	7,100	9,100			
	4	2,800	2,600	3,000			
	6	780	560	700			
	8	260	180	210			
	10	120	130	120			
	15	14	13	11			
	20	0	2.4	0			

0 No counts registered during count period.

TABLE B-11 PARTICLE SIZE SPECTRA, dN/ds (number/ml/micron)

STATION: Humboldt Bay DATE: 3/18/73

Coulter Aperture (microns)	Particle Diameter (microns)	WATER SAMPLE DEPTH (Feet)					
		50	0[1]	0[2]			
30	0.7	120×10^4	350×10^4	380×10^4			
	0.8	72 "	210 "	130 "			
	1.0	42 "	140 "	68 "			
	1.25	22 "	82 "	34 "			
	1.5	97,000	37 "	21 "			
	2.0	31,000	15 "	77,000			
	3.0	7,200	40,000	15,000			
100	2	28,000	120,000	120,000			
	3	4,700	32,000	28,000			
	4	2,200	13,000	10,000			
	6	440	3,300	2,500			
	8	105	750	640			
	10	28	320	340			
	15	0	7.6	13			
	20	0	0	0			

0 No counts registered during count period
1 Sample taken at entrance channel to Humbolt Bay
2 Sample taken at power plant cooling water discharge site

TABLE B-12 PARTICLE SIZE SPECTRA, dN/ds (number/ml/micron)

STATION: WHITES POINT (200' depth) DATE: 3/29/73

Coulter Aperture (microns)	Particle Diameter (microns)	WATER SAMPLE DEPTH (Feet)					
		0	80				
30	0.7	630×10^4	270×10^4				
	0.8	340 "	260 "				
	1.0	125 "	180 "				
	1.25	35 "	45 "				
	1.5	92,000	78,000				
	2.0	25,000	22,000				
	3.0	6,400	5,900				
100	2	27,000	23,000				
	3	4,800	4,000				
	4	1,800	1,500				
	6	440	350				
	8	130	94				
	10	73	67				
	15	5.7	3.8				
	20	0	0				

0 No counts registered during count period

TABLE B-13 PARTICLE SIZE SPECTRA, dN/ds (number/ml/micron)

STATION: WHITE S POINT (150' depth) DATE: 4/12/74

Coulter Aperture (microns)	Particle Diameter (microns)	WATER SAMPLE DEPTH (Feet)					
		5	50				
30	0.7	1500 x 10^4	2300 x 10^4				
	0.8	470 "	740 "				
	1.0	72 "	120 "				
	1.25	23 "	21 "				
	1.5	11 "	62,000				
	2.0	28,000	26,000				
	3.0	7,900	6,800				
100	2	40,000	58,000				
	3	4,300	4,400				
	4	2,100	2,400				
	6	480	840				
	8	170	300				
	10	100	180				
	15	25	25				
	20	6.1	9.1				

TABLE B-14 PARTICLE SIZE SPECTRA, dN/ds (number/ml/micron)

STATION: WHITES POINT (200' depth) DATE: 4/12/73

Coulter Aperture (microns)	Particle Diameter (microns)	WATER SAMPLE DEPTH (Feet)					
		5	25	50	70	125	70
30	0.7	1000 x 10^4	2100 x 10^4	3400 x 10^4	1100x 10^4	1500 x 10^4	652 x 10^4
	0.8	350 "	710 "	263 "	470 "	680 "	290 "
	1.0	87 "	85 "	69 "	180 "	230 "	110 "
	1.25	21 "	17 "	15 "	54 "	66 "	33 "
	1.5	88,000	64,000	47,000	17 "	23 "	13 "
	2.0	28,000	31,000	14,000	71,000	52,000	54,000
	3.0	13,000	5,800	3,200	22,000	21,000	11,000
100	2	23,000	25,000	25,000	69,000	93,000	57,000
	3	4,600	4,400	3,600	14,000	21,000	14,000
	4	1,800	2,200	2,700	6,300	8,300	4,700
	6	530	760	1,300	2,200	2,300	980
	8	210	240	280	490	610	300
	10	150	160	170	240	270	150
	15	41	25	15	21	25	8
	20	18	9.1	2.8	3	3	0

0 No counts registered during count period

TABLE B-15 PARTICLE SIZE SPECTRA, dN/ds (number/ml/micron)

STATION: Mid Channel (4 miles off White's Point) DATE: 4/12/73

Coulter Aperture (microns)	Particle Diameter (microns)	WATER SAMPLE DEPTH (Feet)					
		5	25	50	75	100	125
30	0.7	890 x 10^4	2100 x 10^4	320 x 10^4	420 x 10^4	230 x 10^4	300 x 10^4
	0.8	250 "	270 "	89 "	92 "	80 "	94 "
	1.0	54 "	53 "	27 "	31 "	27 "	34 "
	1.25	14 "	17 "	76,000	98,000	98,000	11 "
	1.5	54,000	66,000	41,000	38,000	41,000	44,000
	2.0	22,000	30,000	17,000	14,000	17,000	24,000
	3.0	5,4000	6,000	3,200	3,200	3,200	4,700
100	2	27,000	25,000	22,000	14,000	15,000	19,000
	3	4,900	5,600	5,700	4,100	4,000	5,100
	4	2,300	3,300	3,100	3,500	3,200	2,900
	6	870	1,300	1,200	680	540	730
	8	330	330	250	210	120	140
	10	130	200	160	100	81	73
	15	54	33	19	5.7	5.7	82
	20	15	15	5.6	1.5	1.4	0

TABLE B-16 PARTICLE SIZE SPECTRA, dN/ds (number/ml/micron)

STATION: Dana Point (4 miles offshore) DATE: 5/15/73

Coulter Aperture (microns)	Particle Diameter (microns)	WATER SAMPLE DEPTH (Feet)					
		5	25	50	75	100	140
30	0.7	306 x 10^4	170 x 10^4	146 x 10^4	92 x 10^4	49 x 10^4	58 x 10^4
	0.8	140 "	125 "	86 "	28 "	18 "	21 "
	1.0	45 "	100 "	110 "	26 "	12 "	10 "
	1.25	96,000	16 "	26	11 "	64,000	53,000
	1.5	26,000	80,000	55,000	31,000	31,000	22,000
	2.0	10,000	21,000	13,000	7,900	9,000	8,000
	3.0	2,100	3,800	3,100	2,100	1,900	2,200
100	2	12,600	30,000	19,000	10,000	15,000	6,300
	3	3,000	6,400	3,900	2,200	3,300	1,500
	4	1,600	2,400	1,500	1,000	1,200	450
	6	380	560	360	260	290	130
	8	100	140	170	95	60	30
	10	92	88	150	108	39	18
	15	20	9	10	4.3	4.1	0
	20	4.8	2.2	0	0	0	0

0 No counts registered during count period

NOTATION

A	=	albedo, ratio of scattering coefficient to beam attenuation coefficient
a	=	absorption coefficient (m^{-1})
a_p	=	particle absorption coefficient
b	=	scattering coefficient (m^{-1})
b_i	=	scattering by all the particles of diameter s_i
b_p	=	particle scattering coefficient
$\beta(\theta)$	=	volume scattering function
c	=	beam attenuation coefficient (m^{-1})
c_p	=	particle extinction coefficient
C^{13}/C^{12}	=	carbon isotope ratio
γ	=	zenith angle
δ_{PDB}	=	$1000\ (\frac{R_s}{R_o} - 1)$
E_d	=	downwelling irradiance at depth z
E_s	=	downwelling irradiance just beneath the water surface ($watts/m^2$)
E_u	=	upwelling irradiance at depth z
θ	=	scattering angle
i	=	square root of -1
k	=	diffuse irradiance attenuance (m^{-1})
K_{abs}	=	absorption efficiency

NOTATION (continued)

K_{ext}	=	extinction efficiency
K_{sca}	=	scattering efficiency
L	=	radiance (watts/m^2-steradian)
L*	=	path radiance
LACSD	=	Los Angeles County Sanitation District
λ	=	wavelength of scattered light (nm.)
m	=	complex refractive index
MGD	=	million gallons per day
N	=	number of particles per milliliter
n	=	particle refractive index (relative to water)
n'	=	imaginary part of m
N_i	=	number of particles per unit volume with diameter s_i
$p(\theta)$	=	angular albedo function
ppm	=	parts per million
R_o	=	C^{13}/C^{12} of a reference sample prepared from a Cretaceous belemnite, Belemnitella americana, found in the Peedee formation of South Carolina (hence the subscript, "PDB")
R_s	=	C^{13}/C^{12} of a sample
s	=	particle diameter (microns)
ϕ	=	azimuth angle
T	=	beam transmissibility (percent/meter)

NOTATION (continued)

τ	=	ocean optical depth
V	=	volume concentration of particles (ppm)
z	=	depth in the water (meters)
z_c	=	compensation point depth (meters)

References

1. "An investigation of the effects of discharged wastes on kelp." State Water Quality Control Board, Pub. 26, 1964.

2. Bader, H., "The hyperbolic distribution of particle sizes." J. Geophys. Res., 75, 2822, 1970 .

3. Beardsley, G. F., H. Pak, K. L. Carder, "Light scattering and suspended particles in the eastern equatorial Pacific Ocean. J. Geophys. Res., 75, 2837-2845, 1970.

4. Boden, B. P., E. M. Kampa, and J. M. Snodgrass, "Underwater daylight measurements in the Bay of Biscay." Jour. Marine Biol. Assn. U.K., 39, 227-238, 1960.

5. Burt, W. V., "Interpretation of spectrophotometer readings on Chesapeake Bay waters." Jour. of Marine Research, 14, 33-46, 1955.

6. Burt, W. V., "Distribution of suspended materials in Chesapeake Bay." Jour. of Marine Research, 14, 47-62, 1955.

7. Burt, W. V., "A light scattering diagram." Jour. of Marine Research, 15, 76-80, 1956.

8. Burt, W. V., "Selective transmission of light in tropical waters." Deep Sea Research, 5, 51-61, 1958.

9. Carder, K. L., "Particles in the eastern Pacific Ocean: their distribution and effect upon optical parameters." Ph.D. Thesis, Oregon State University, 1970.

10. Carder, K. L., G. F. Beardsley, Jr. and H. Pak, "Particle size distributions in the eastern Equatorial Pacific." J. Geophys. Res., 76 (21), 5070-5077, 1971.

11. Carder, K. L., R. D. Tomlinson and G. F. Beardsley, Jr., "A technique for the estimation of indices of refraction of marine phytoplankters." Limnology and Oceanography, 17 (6), 1972.

12. Chandrasekhar, S., Radiative Transfer, New York: Dover, 1960. 393 pp.

13. Clarke, G. L. and H. R. James, "Laboratory analysis of the selective absorption of light by sea water. J. Opt. Soc. Am., 29, 43-55, 1939.

14. Clarke,G. L., "The significance of spectral changes in light scattered by the sea." Remote Sensing in Ecology, Athens, Georgia: Univ. of Georgia Press, 164-172, 1969.

15. Clarke, G. L., G. C. Ewing, and C. J. Lorenzen, "Spectra of backscattered light from the sea obtained from aircraft as a measure of chlorophyll concentration." Science, 167, 1119-1121, 1970.

16. Duntley, S. Q., "Optical properties of diffusing materials." J. Opt. Soc. Am., 32 (2), 61-70, 1942.

17. Duntley, S. Q., "Light in the sea." J. Opt. Soc. Am., 53, 214-233, 1963.

18. Franklin, J., Matrix Theory. New Jersey: Prentice Hall, 1968, 292 pp.

19. Gordon, Howard R., and Otis B. Brown, "A theoretical model of light scattering by Sargasso Sea particulates." Limnology and Oceanography, 17 (6), 826-832, 1972.

20. Grigg, R. W., and R. S. Kiwala, "Some ecological effects of discharged wastes on marine life." Unpublished report, University of Southern California, Scripps Institute of Oceanography.

21. Holmes, R. W., "The Secchi disk in turbid coastal waters." Limnology and Oceanography, 15 (5), 688-694, 1970.

22. Hulbert, E. O. "Propagation of radiation in a scattering and absorbing medium." J. Opt. Soc. Am., 33, 42-45, 1943.

23. Hulbert, E. O., "Optics of distilled and natural water." J. Opt. Soc. Am., 35 (11), 698-705, 1945.

24. Ivanoff, A., N. Jerlov and T. H. Waterman, "A comparative study of irradiance, beam transmittance and scattering in the sea near Bermuda." Limnology and Oceanography, 6, 129-148, 1961.

25. Jerlov, N. G., "Optical oceanography." Oceanog. Marine Biol. Ann. Rev., 1, 89-114, 1963.

26. Jerlov, N. G., "Factors influencing the colour of the ocean." Studies on Oceanography, 260-264, 1964.

27. Jerlov, N. G., "Optical classification of ocean water." Physical Aspects of Light in the Sea, Univ. of Hawaii Press, 1964.

28. Jerlov, N. G., Optical Oceanography. New York: Elsevier Pub. Co., 1968, 194 pp.

29. Johnson, G. F., A. Burbank and S. Pyke, "A study of the influence of certain biological parameters on the spectral chracteristics of light in the ocean." Unpublished Report, TRW Systems, Redondo Beach, 1969.

30. Kalle, K. "Über die gelösten organischen Komponenten im Meerwasser." Kieler Meeresforsch., 18: 128-131, 1962.

31. Kalle, K., "The problem of the Gelbstoff in the sea." Oceanog. Marine Biol. Ann. Rev., 4, 91-104, 1966.

32. "Kelp habitat improvement project--annual report." W. M. Keck Laboratory of Environmental Health Engineering, California Institute of Technology, 1967.

33. Kerker, M., The Scattering of light and other electromagnetic radiation. New York: Academic Press, 1969.

34. Kinney, J. S., S. M. Luria, and D. O. Weitzman, "Visibility of colors under water." J. Opt. Soc. Am., 57 (6), 802-809, 1967.

35. Latimer, P. and E. Rabinowitch, "Selective scattering of light by pigment-containing plant cells," Interscience, 1957.

36. Lepley, L. K., "Coastal water clarity from space photographs." Photogrammetric Engineering, 34 (7), 667-674, 1968.

37. Moore, D. M., F. D. Bryant and P. Latimer, "Total Scattering and absorption by spheres where m=1." J. Opt. Soc. Am., 58, 281, 1968.

38. Moore, J. G., "The determination of the depths and extinction coefficients of shallow water by air photography using color filters." Roy. Soc. Phil. Trans., 240A, 163-217, 1947.

39. Mullin, M. M., "Size fractionation of particulate organic carbon in the surface waters of the Indian Ocean." Limnology and Oceanography, 10, 459-462, 1965.

40. Mullin, M. M., P. R. Sloan and R. W. Eppley, "Relationship between carbon content, cell volume and area in phytoplankton." Limnology and Oceanography, 11, 307-311, 1966.

41. Myers, E. P., "The concentration and isotopic composition of carbon in marine sediments affected by a sewage discharge." Ph.D. Thesis, California Institute of Technology, Pasadena, California, 1974.

42. North, Wheeler J., "Effects of wastewaters on marine biota." Proceedings of 13th coastal engineering conference, American Society of Civil Engineers, 2099-2116, 1972.

43. Oster, R. H. and G. L. Clarke, "Penetration of red, green and violet components of daylight into Atlantic waters." J. Opt. Soc. Am., 25 (2), 84-91, 1935.

44. Pak, H., G. F. Beardsley, Jr., G. R. Heath, and H. Curl, "Light scattering vectors of some marine particles." Limnology and Oceanography, 15 (5), 683-687, 1970.

45. Pak, H., G. F. Beardsley, Jr., P. K. Park, "The Columbia River as a source of marine light scattering particles." J. Geophys. Res., 75 (24), 4570-4578, 1970.

46. Pak, H., J. R. V. Zaneveld, G. F. Beardsley, Jr., "Mie scattering by suspended clay particles." J. Geophys. Res., 76 (21), 5065-5069, 1971.

47. Plass, G. H. and G. W. Kattawar, "Monte Carlo calculations of radiative transfer in the earth's atmosphere --ocean system." Journal of Physical Oceanography, 2 (2), 139-145, 1972.

48. Poulet, S. A., "Grazing of Pseudocalanus minutus on naturally occurring particulate matter." Limnology and Oceanography, 18 (4), 564-573, 1973.

49. Preisendorfer, R. W., "A model for radiance distributions in natural hydrosols." Physical aspects of light in the sea, University of Hawaii Press, 1964.

50. Prewett, O. E., D. R. Lyzenga, and F. C. Polcyn, "Techniques for measuring light absorption, scattering and particle concentrations in water." Rep. #ERIM-190500-1-F, Environmental Research Inst. of Michigan, 1973.

51. Ramsey, Richard C., "Study of the remote measurement of ocean color." TRW Systems Group Report No. 08645-6001-R000, 1968.

52. Ryther, J. H., "Photosynthesis in the ocean as a function of light intensity." Limnology and Oceanography, 1 (61), 1956.

53. Scher, J. P., D. R. Graff, W. C. Boyle, "Photographic characteristics of water pollution." Photogrammetric Engineering, 1969.

54. Schuster, A. "Radiation through a foggy atmosphere." Astrophysical Journal, 21 (1), 1-22, 1905.

55. Sheldon, R. W., A. Prakash, and W. H. Sutcliffe, Jr., "The size distribution of particles in the ocean." Limnology and Oceanography, 17 (3), 327-340, 1972.

56. Sheldon, R. W. and T. R. Parsons, "A continuous size spectrum for particulate matter in the sea." Journal Fisheries Research Board of Canada, 24 (5), 909-915, 1967.

57. Sheldon, R. W. and T. R. Parsons, A practical manual on the use of the Coulter Counter in marine science. Toronto: Coulter Electronics, 1967.

58. Sheldon, R. W., T. P. T. Evelyn, and T. R. Parsons, "On the occurrence and formation of small particles in seawater." Limnology and Oceanography, 12, 367-375, 1967.

59. Smith, R. C. and J. E. Tyler, "Optical properties of clear natural water." J. Opt. Soc. Am., 57 (5), 589-595, 1967.

60. Stevenson, R. E., and W. Polski, "Water transparency of the southern California Shelf." Bulletin, So. Calif. Academy of Sciences, 60, Part 2, 77-87, 1961.

61. Stamm, G. L. and R. A. Langel, "Some spectral irradiance measurements of upwelling natural light off the east coast of the United States." J. Opt. Soc. Am., 51 (10), 1090-1094, 1961.

62. Strickland, J. D. H., "Solar radiation penetrating the ocean. A review of requirements, data and methods of measurement, with particular reference to photosynthetic productivity." Journal Fisheries Research Board of Canada, 15 (3), 453-493, 1958.

63. Strickland, J. D. H., "A comparison of continuous and discreet vertical sampling of chlorophyll." Limnology and Oceanography, 13 (2), 388-391, 1968.

64. Sutcliffe,W. H.,Jr., R. W. Sheldon, A. Prakash, and D. C. Gordon, Jr., "Relations between wind speed, Langmuir circulation and particle concentration in the ocean." Deep Sea Research, 18, 639-643, 1971.

65. Tyler, J. E., "In situ detection and estimation of chlorophyll and other pigments in the ocean." Proc. N.A.S., 47, 800-805, 1961.

66. Tyler, J. E., "Measurement of the scattering properties of hydrosols." J. Opt. Soc. Am., 51, 1289-1293, 1961.

67. Tyler, J. E., "In situ spectroscopy in ocean and lake waters." J. Opt. Soc. Am., 55 (7), 800-805, 1965.

68. Tyler, J. E. and R. C. Smith, "Spectroradiometric characteristics of natural light under water." J. Opt. Soc. Am., 57 (5), 595-600, 1967.

69. Tyler, J. E., R. C. Smith, W. H. Wilson, Jr., "Predicted optical properties for clear natural water." J. Opt. Soc. Am., 62 (1), 83-91, 1972.

70. Van de Hulst, H. C., Light Scattering by Small Particles. New York: Wiley, 1957, 470 pp.

71. White, Peter G., "Visible region remote spectroscopy of polluted water," unpublished TRW Report, 1970.

72. White, W. H. and L. L. Peterson, "SEALIGHT--N-stream computer model of sunlight propagation in a scattering and absorbing media." Unpublished program, California Institute of Technology, Pasadena, California, 1973.

73. Yentsch, C. S., "The influence of phytoplankton pigments on the color of seawater.: Deep Sea Research, 7, 1-9, 1960.

74. Yentsch, C. S., "Measurement of visible light absorption by particulate matter in the ocean." Deep Sea Research, 6, 207-217, 1962.

75. Zeitzschel, B., "The quantity, composition and distribution of suspended particulate matter in the Gulf of California." Marine Biology, 7, 305-318, 1970.